In vivo monosynaptic connectivity and network activity of neocortical interneurons

DISSERTATION

zur Erlangung des akademischen Grades

Doctor rerum naturalium

(Dr. rer. nat.)

im Fach Biologie

eingereicht an der

Lebenswissenschaftlichen Fakultät

der Humboldt-Universität zu Berlin

von

Dipl.-Biol. Anja Luise Dorrn

Präsidentin der Humboldt-Universität zu Berlin

Prof. Dr.-Ing. Dr. Sabine Kunst

Dekan der Lebenswissenschaftlichen Fakultät

Prof. Dr. Bernhard Grimm

Gutachter: 1. Prof. Dr. Matthew Larkum

2. Prof. Dr. Imre Vida

3. Dr. James Poulet

Tag der mündlichen Prüfung: 3. November 2016

Eidesstattliche Erklärung

Hiermit erkläre ich, die vorliegende Dissertation selbstständig und nur unter Verwendung der angegebenen Hilfen und Hilfsmittel angefertigt zu haben.

Ich habe mich anderwärts nicht um einen Doktorgrad beworben und besitze einen entsprechenden Doktorgrad nicht.

Ich erkläre die Kenntnisnahme der dem Verfahren zugrunde liegenden Promotionsordnung der Mathematisch-Naturwissenschaftlichen Fakultät I der Humboldt-Universität zu Berlin vom 27. Juni 2012.

Berlin, den 26.07.2016 Anja L. Dorrn

Abstract

GABAergic interneurons provide the source of inhibition in local neocortical networks, where they form inhibitory connections with nearby excitatory and other inhibitory neurons. In cortical circuits *in vivo* synaptic transmission is thought to emerge during depolarized active network states, when spontaneous spiking can occur. However, current knowledge is limited on the one hand to interneuron connectivity derived from brain slices and on the other hand to interneuron activity derived from mainly extracellular recordings in the living animal. Hence, it is not known how inhibitory interneurons transmit information to neighboring inhibitory cells during ongoing network activity. During active network states inhibitory monosynaptic transmission might affect membrane potential dynamics and spike timing of postsynaptic cells and thus enhance synchronicity of interneurons embedded in a subnetwork. The aim of this study was to identify monosynaptic inhibitory connections *in vivo* in order to relate interneuron connectivity to their spontaneous activity.

Therefore simultaneous two-photon targeted whole-cell recordings were made from two to three neighboring layer 2/3 GABAergic interneurons in the forepaw primary somatosensory cortex of urethane anesthetized mice. Two different mouse strains were used to record from genetically identified interneurons: GAD67-GFP animals allowed to examine interneurons without respect to their subtype. However, recordings mainly derived from non-fast spiking cells. In a parallel approach the interaction between SST- and VIP-expressing interneurons was investigated. Breeding of the triple transgenic mouse line GIN-VIPcre-Ai9 allowed to specifically target SST and VIP cells.

Monosynaptic inhibitory connections could be identified in both mouse lines, with higher connectivity rates of non-fast spiking interneurons recorded in GAD67-GFP animals than for SST and VIP cells. Overall, the ongoing state of the cortex powerfully modulated inhibitory synaptic transmission, with IPSPs increasing in amplitude in depolarized network states.

Subtype-specific correlations in the activity of neocortical interneurons could be observed and were reflected in the subthreshold and also spontaneous firing activity of cells. SST and VIP interneurons showed overall less correlated activity compared to cells recorded in GAD67-GFP animals. Neighboring interneurons recorded in these animals received common excitatory synaptic input around the time of a spontaneous spike in

one cell. Splitting data by connectivity revealed differences between synaptically connected and unconnected cells. The membrane potential of postsynaptic cells showed a fast and sharp hyperpolarizing slope during the decay phase of the excitatory input, which was locked to the presynaptic spike. This resulted in a reduction of firing rate compared to unconnected cells, suggesting that connections between non-fast spiking interneurons may regulate precise spike timing *in vivo*, thus enhancing firing synchrony.

Overall, it could be demonstrated that two-photon targeted whole-cell recordings are a powerful tool to investigate inhibitory monosynaptic transmission *in vivo*. By recording from identified interneurons this technique allowed to link interneuron connectivity to the network activity of cell-type specific subnetworks, which may fulfill different functions in maintaining ongoing cortical activity.

Zusammenfassung

In lokalen neokortikalen Netzwerken stellen GABAerge Interneurone die Quelle der Inhibition dar, wobei sie inhibitorische Verbindungen mit benachbarten exzitatorischen und anderen inhibitorischen Neuronen bilden. Man geht davon aus, dass synaptische Transmission *in vivo* als Folge spontaner Aktionspotentiale während aktiven depolarisierten Erregungszuständen des Netzwerks auftritt. Heutiges Wissen beschränkt sich jedoch einerseits auf die Konnektivität von Interneuronen, welches in Hirnschnitten erworben wurde. Andererseits konnten Erkenntnisse über die Aktivität dieser Zellen hauptsächlich durch extrazelluläre Ableitungen im lebenden Tier gewonnen werden. Daher ist es nicht bekannt, wie Information von inhibitorischen Interneuronen auf benachbarte inhibitorische Zellen während kontinuierlicher Netzwerkaktivität übertragen wird. Während aktiver Erregungszustände des Netzwerks könnte sich monosynaptische inhibitorische Übertragung auf die Dynamik des Membranpotentials und die zeitliche Koordinierung von Aktionspotentialen der postsynaptischen Zellen auswirken. Dadurch könnte die Synchronizität von Interneuronen, welche Teil eines Subnetzwerks sind, erhöht werden. Das Ziel dieser Studie war es monosynaptische inhibitorische Verbindungen *in vivo* zu detektieren um dadurch den Zusammenhang zwischen der Konnektivität kortikaler Interneurone und deren Spontanaktivität untersuchen zu können.

Dafür wurden von zwei bis drei benachbarten GABAergen Interneuronen gleichzeitig gezielte elektrophysiologische Ganz-Zell-Ableitungen unter visueller Kontrolle des Zwei-Photonen-Mikroskops gemacht. Die Ableitungen wurden an Zellen in Schicht 2/3 des primären somatosensorischen Kortex der Vorderpfote von Mäusen durchgeführt, welche mit Urethan narkotisiert waren. Hierbei wurden zwei unterschiedliche Mauslinien eingesetzt, um elektrophysiologische Ableitungen von genetisch identifizierten Interneuronen zu erhalten. GAD67-GFP Mäuse wurden genutzt, um Interneurone allgemein und unabhängig von ihrem Subtyp untersuchen zu können. Hierbei wurden die meisten Ableitungen jedoch von 'nicht-schnell' feuernden Zellen erzielt. In einem parallelen Ansatz wurde die Interaktion von SST- und VIP-exprimierenden Interneuronen untersucht. Hierbei erlaubte die Züchtung der dreifach transgenen Mauslinie GIN-VIPcre-Ai9 gezielte elektrophysiologische Ableitungen von SST und VIP Neuronen.

In beiden Mauslinien konnten monosynaptische inhibitorische Verbindungen zwischen Interneuronen detektiert werden, wobei die Konnektivitätsrate zwischen 'nicht-schnell' feuernden Interneuronen, welche in GAD67-GFP Mäusen untersucht wurden, höher war als für SST und VIP Neurone. Die inhibitorische synaptische Transmission wurde jeweils stark vom aktuellen Erregungszustand des Kortex moduliert wobei ein Anstieg der IPSP-Amplitude während depolarisierter Zustände des Netzwerks festgestellt wurde.

Es konnten subtyp-spezifische Korrelationen in der Aktivität neokortikaler Interneurone beobachtet werden, welche sich im unterschwelligen Membranpotential und auch der spontanen Feuerrate der Zellen zeigte. Insgesamt zeigten SST und VIP Interneurone weniger korrelierte Aktivität als Zellen, die in GAD67-GFP Mäusen untersucht wurden. Elektrophysiologische Ableitungen von benachbarten Interneuronen in diesen Tieren zeigten, dass die Neurone gemeinsamen exzitatorischen synaptischen Eingang erhielten, während eine der beiden Zellen ein spontanes Aktionspotential feuerte. Das aufteilen der Daten bezüglich der Konnektivität zeigte Unterschiede zwischen synaptisch verbundenen und unverbundenen Zellen auf. Das Membranpotential postsynaptischer Zellen wies eine schnelle und steil abfallende Hyperpolarisierung während der abklingenden Phase des exzitatorischen Eingangs auf. Diese war an den Zeitpunkt des präsynaptischen Aktionspotentials gekoppelt. Daraus resultierte eine Verringerung der Feuerrate im Vergleich zu unverbundenen Zellen. Somit lässt sich darauf schließen, dass synaptische Verbindungen zwischen 'nicht-schnell' feuernden Interneuronen das präzise zeitliche Auftreten von Aktionspotentialen *in vivo* regulieren und dadurch die Synchronisation der Spontanaktivität dieser Zellen erhöhen können.

Generell konnte gezeigt werden, dass gezielte elektrophysiologische Ableitungen unter visueller Kontrolle des Zwei-Photonen-Mikroskops eine hervorragend geeignete Methode sind, um inhibitorische monosynaptische Konnektivität *in vivo* zu untersuchen. Durch die Ableitung von identifizierten Interneuronen erlaubte diese Technik einen Zusammenhang zwischen der Konnektivität von Interneuronen und der Netzwerkaktivität zelltypspezifischer Subnetzwerke herzustellen. Diese können unterschiedliche Funktionen in der Aufrechterhaltung kontinuierlicher Netzwerkaktivität erfüllen.

TABLE OF CONTENTS

1 Introduction

Since the early days of Ramón y Cajal and the beginning of modern neuroscience over a century ago, researchers have tried to disentangle the brain's complex network of neurons and their synapses. They seek to understand how this network is built and how the different cells within the network communicate with each other. Numerous studies in various model systems have contributed to the knowledge that we have today about wiring patterns of neural circuits, about information processing within active neuronal networks and about synaptic transmission. Histological and brain slice electrophysiological approaches mainly described network anatomy and mechanisms of synaptic transmission, while *in vivo* extracellular recordings helped to understand information processing in the living brain. It is widely acknowledged that cortical activity is shaped by synaptic excitation and inhibition where the balanced interplay of excitatory and inhibitory cells play a fundamental role. While the basic principles of excitatory networks in the neocortex and their direct interaction with interneurons are already better understood, the importance of inhibition of inhibitory neurons, or disinhibition, in cortical processing has drawn its attention only recently. In particular it is unknown how synaptic transmission between cortical inhibitory interneurons is affected by network activity. Correlated activity of synaptically connected ensembles of neurons is thought to be important for cortical function, which has been a subject for various computational models. These often are based on assumptions on monosynaptic connectivity and signal transduction derived from slice physiology data, which typically lacks network activity. While *in vivo* monosynaptic excitatory transmission recently already has been a matter of research, it still remains to be determined how inhibitory synaptic transmission contributes to brain function. To answer these questions it is of great importance to record from monosynaptically connected inhibitory interneurons *in vivo* and investigate their synaptic input during ongoing network activity.

In the following chapter I will outline the principles of neocortical circuit organization, what function inhibitory interneurons have in this network and how they transmit information onto their postsynaptic partners. Finally I will give an overview of open questions in the field and the thereof resulting goals for the present study and approaches to resolve these questions.

1.1 Neocortical circuit organization

Neocortex is organized in 6 layers, with each layer having its distinct composition of different cell types and wiring schemes. About 80 – 90 % of neurons in the neocortex are excitatory pyramidal cells (PC), which represent a relatively homogenous group of cells, and are also known as principal cells; these are mainly projection neurons with long axons, connecting to the spinal cord, brainstem, basal ganglia, thalamus and other cortical areas (Harris and Shepherd, 2015). The other 10 – 20 % of neocortical neurons are interneurons (Ren et al., 1992; Beaulieu, 1993; Meyer et al., 2011), whereof the majority are inhibitory, that release GABA (γ-aminobutyric acid) as their neurotransmitter. Interneurons are short-axon cells that mainly connect to nearby cells. Although GABAergic interneurons only make up less than 20 % of the entire population of neurons in the neocortex, the diversity based on their morphology, connectivity schemes, gene expression patterns and intrinsic physiology is enormous. Clear classifications are difficult as many of their features mentioned above are heterogeneously distributed and overlap (Markram et al., 2004; Kepecs and Fishell, 2014). Nevertheless, great effort has been made by the Petilla Interneuron Nomenclature Group in order to establish a common terminology (Ascoli et al., 2008), followed by an attempt to define morphological taxonomy (Defelipe et al., 2013).

1.1.1 Three major subgroups of cortical GABAergic interneurons

Despite the diversity of interneuron cell types three distinct groups of interneurons based on their gene expression patterns have been identified, namely parvalbumin-, somatostatin- and 5HT3aR-expressing interneurons; these groups represent non-overlapping populations and are not evenly distributed across cortical layers (Lee et al., 2010; Rudy et al., 2011). However, these populations still can or cannot co-express other molecular markers such as calretinin, calbindin, cholecystokinin or reelin (Kubota et al., 1994; Xu et al., 2010; Zeisel et al., 2015). Also considering other parameters, such as the morphology there is still overlap, and a clear distinction can become difficult. In the following sections I will focus on the most evident details that characterize the three subgroups mentioned above.

Parvalbumin-expressing interneurons Interneurons expressing the Ca^{2+}-binding protein parvalbumin (PV) form the biggest subgroup of all cortical interneurons and represent 40 % of the total interneuron population. While in layer 2/3 (L2/3) they represent only 25 % of all interneurons they become more dominant in deeper cortical layers (Lee et al., 2010). Cortical PV interneurons derive from the medial ganglionic eminence (MGE) (Butt et al., 2005; Fogarty et al., 2007). Based on their firing patterns

PV cells were determined to be fast-spiking interneurons with thin action potential (AP) waveforms (Kawaguchi and Hama, 1987; Cauli et al., 1997; Kawaguchi and Kubota, 1997). Nonetheless, they again can be divided in two major subgroups: Basket cells represent a major subgroup of interneurons that is thought to provide a dominant source of inhibition in neocortex due to their basket-like structure of axons that target the soma and proximal dendrites of postsynaptic partners (Markram et al., 2004). Despite their characteristic basket-like appearance of axons they are still diverse in their anatomy that can vary in somata size and the extent of dendritic and axonal projections, as well as co-expression of molecular markers beside PV and also firing patterns (Wang et al., 2002; Rudy et al., 2011). Though representing only a small subgroup chandelier (or axo-axonic) cells are unique regarding their morphology and the effect on their target neurons. Their axons have a chandelier-like appearance and their characteristic presynaptic terminals ('axon cartridges') target the axon initial segment of the postsynaptic cell (Kawaguchi and Kubota, 1997; Woodruff et al., 2009). Although Glickfeld et al. (2009) demonstrated their hyperpolarizing effect on hippocampal PCs, there is evidence that in neocortex chandelier cells can also depolarize their postsynaptic partners (Szabadics et al., 2006; Molnár et al., 2008; Woodruff et al., 2009).

Somatostatin-expressing interneurons Like PV cells, also neocortical cells that express the neuropeptide somatostatin (SST) derive from the MGE (Butt et al., 2005; Fogarty et al., 2007). They account for about 30 % of the interneuron population and, like PV cells, get more abundant towards deeper layers (Lee et al., 2010; Rudy et al., 2011). The majority of SST cells are Martinotti cells with their characteristic ascending axons that arborize in L1, where they innervate distal dendrites of postsynaptic cells; they typically show regular adapting firing patterns but especially L5 Martinotti cells also show burst spiking (Kawaguchi and Kubota, 1996; 1997; Wang et al., 2004). Martinotti cells can further be distinguished whether they co-express calretinin or not and hence show distinct morphologies and spike shapes (Xu et al., 2006). However, beside Martinotti cells, McGarry et al. (2010) identified two more subtypes of SST-expressing cells, which showed short and asymmetric axons targeting L2/3.

5HT3aR-expressing interneurons Interneurons that express the ionotropic serotonin receptor 5HT3a account for the remaining 30 % of all cortical interneurons. They are primarily found in superficial layers 1-3, where they are the predominant subpopulation of interneurons (Lee et al., 2010; Rudy et al., 2011). The majority of 5HT3aR-expressing interneurons derive from the caudal ganglionic eminence (CGE) (Lee et al., 2010; Vucurovic et al., 2010). Due to the expression of 5HT3aR and also nicotinic receptors these cells get depolarized by neuromodulators such as serotonin and acetylcholine (Férézou et al., 2002; Lee et al., 2010). Despite these common features, 5HT3aR-expressing cells are still a very heterogeneous group, which can be subdivided into at least 9 different types based on their electrophysiological properties and morphologies

(Miyoshi et al., 2010). However, Miyoshi et al. (2010) also showed that 5HT3aR-expressing interneurons either co-express the vasoactive intestinal polypeptide (VIP) (40 %) or the glycoprotein reelin (< 60 %). Although further subgroups of 5HT3aR-expressing interneurons exist, they have not been characterized systematically due to the their high variability and the lack of further specific molecular markers (Rudy et al., 2011).

VIP neurons appear denser in L2/3 compared to other cortical layers (Bayraktar et al., 2000; Lee et al., 2010; Prönneke et al., 2015). VIP-expressing interneurons have been suggested to be involved in the regulation of metabolism in local neuronal networks (Magistretti, 1990). Based on the Petilla convention (Ascoli et al., 2008) the morphology and electrophysiological profile of these cells appear diverse. However, bipolar cells with small cell bodies and vertically oriented dendrites have been shown to express VIP and are associated with irregular spiking patterns (Cauli et al., 1997; Porter et al., 1998; Jiang et al., 2015). Bipolar cells also co-express calretinin (Cauli et al., 1997), and Bayraktar et al. (1997) could show that one third of bipolar VIP-expressing cells are co-localized with choline acetyltransferase (ChAT) and thus are part of cholinergic systems. Further (bi)tufted cells have been described as VIP-expressing cells, which also mostly have vertically oriented dendrites, but show various firing patterns (Jiang et al., 2015; Prönneke et al., 2015). Both studies also showed that VIP interneurons in L2/3 restrict their dendritic tree to superficial cortical layers and extensively branch in L1, while their axons spread across all layers often descending down to L6. Further, VIP interneurons have been described to have high input resistances (IRs) and to be highly excitable (Cauli et al., 2000; Lee et al., 2010; Miyoshi et al., 2010).

One important group among reelin expressing interneurons are neurogliaform cells (NGF), which mostly co-express the neuropeptide Y (Overstreet-Wadiche and McBain, 2015). Their dendritic branches have a characteristic spider web-like appearance that radially spreads around their small and round soma, whereas the dense axonal plexus is composed of many fine branches (Kawaguchi and Kubota, 1997; Oláh et al., 2007). NGF typically show late spiking firing patterns (Tamas et al., 2003; Miyoshi et al., 2010). Unlike in cortex, NGF in CA1 have low IRs and fast membrane time constants (Miyoshi et al., 2007; 2010; Tricoire et al., 2010).

1.1.2 General connectivity motifs to control cortical activity via inhibition

Different cell types in cortex not only differ in their anatomy, gene expression patterns and physiology but also show distinct connectivity patterns.

The fine-tuned interplay of synaptic excitation and synaptic inhibition shapes cortical activity during spontaneous activity and sensory processing (Wehr and Zador, 2003;

Okun and Lampl, 2008; Haider et al., 2013). Two generalized motifs have been suggested of how the output of cortical excitatory neurons can be regulated by inhibition (Isaacson and Scanziani, 2011). Feedback inhibition describes a reciprocal connectivity scheme where the same subclasses of interneurons that provide inhibitory input to PCs in return also get excited by local PCs (Yoshimura and Callaway, 2005; Kapfer et al., 2007; Silberberg and Markram, 2007). Feed-forward inhibition is generated when excitatory input to interneurons originates from long-range axons of distant PCs, that also innervate PCs, which are inhibited by those interneurons (Gabernet et al., 2005; Cruikshank et al., 2007).

However, interneurons not only receive excitation, but also get inhibited by other interneurons, leading to a disinhibition of the PCs they are innervating (Pfeffer, 2014). One approach to describe disinhibitory motifs among interneurons was done by Pfeffer et al. (2013), who described connectivity patterns between molecularly defined classes of interneurons in L2/3 and L5 of mouse visual cortex. Only recently the inhibitory microcircuits in the same brain region were assessed by classification based on the morphology of interneurons with a focus on the axonal projection patterns (Jiang et al., 2015).

1.1.3 Connectivity schemes of neocortical neurons

In the following paragraphs I will outline the basic principles of neocortical connectivity patterns. In doing so I will mainly focus on excitatory and inhibitory in- and output patterns to and from cells in L2/3 (**Fig. 1.1**).

Basic principles of excitatory pathways To study and grasp inhibitory circuits it is crucial to also have an understanding of the basic excitatory connectivity schemes of PCs in neocortex. PCs are sparsely interconnected in L2 of mouse somatosensory cortex with local connectivity rates reported between 7 and 17 % (Lefort et al., 2009; Avermann et al., 2012; Jouhanneau et al., 2015). Regarding translaminar projections, major excitatory input to L2 PCs comes from L4, while L2 PCs primarily project to L5 (Lefort et al., 2009; Hooks et al., 2011; DeNardo et al., 2015). In the primary sensory cortex (S1) thalamo-cortical input derives from two sources: while the thalamic posteromedial nucleus (POm) is thought to predominantly target L1 and L5A, the ventral posteromedial nucleus (VPM) mainly projects to L4 and also L5B (Wimmer et al., 2010; Harris and Shepherd, 2015). Within cortex L2 PCs in S1 project to motor cortex and S2, but also receive excitatory input from these regions (Chen et al., 2013; Yamashita et al., 2013; Harris and Shepherd, 2015).

Connectivity patterns between cortical PCs and interneurons Although reported connectivity rates may vary, several studies have demonstrated that both SST and PV interneurons receive local and distant excitatory input and inhibit local PCs.

L2/3 PV-expressing cells receive strong excitatory input from L4 PCs (Xu and Callaway, 2009; Adesnik et al., 2012) and also get strongly activated by thalamocortical projections (Cruikshank et al., 2007). Further, they receive strong excitatory input from local L2/3 PCs (Holmgren et al., 2003; Avermann et al., 2012; Pala and Petersen, 2015) with which they tend to form reciprocal connections (Yoshimura and Callaway, 2005). This is reflected in a dense inhibitory innervation of PCs from local PV interneurons (Holmgren et al., 2003; Packer and Yuste, 2011; Avermann et al., 2012; Jiang et al., 2015).

SST-expressing cells in L2/3 mainly get activated by PCs in the same layer (Xu and Callaway, 2009; Adesnik et al., 2012). Synaptic connections from PCs to SST interneurons have been described to facilitate (Kapfer et al., 2007; Silberberg and Markram, 2007; Pala and Petersen, 2015). In return SST cells also innervate local PCs (Fino and Yuste, 2011; Jiang et al., 2015), which can result in feed-forward disynaptic inhibition (Silberberg and Markram, 2009; Berger et al., 2009).

VIP-expressing cells in L2 receive strong excitatory input from local axons (Jiang et al., 2015) but also corticocortical axons target their dendrites in L1 (Lee et al., 2013; Zhang et al., 2014), while L1 interneurons of various subtypes are also targets of excitatory thalamocortical projections (Cruikshank et al., 2012). Further these interneurons can also get excited by neuromodulators such as acetylcholine (Letzkus et al., 2011) and serotonin (Férézou et al., 2002; Lee et al., 2010). L1 interneurons, including NGF that provide strong inhibition, have been shown to inhibit L2/3 PCs, while VIP cells do not target PCs in L2/3 (Wozny and Williams, 2011; Jiang et al., 2013; 2015).

Connectivity patterns between cortical interneurons While there already exists vast knowledge about excitatory and inhibitory connectivity schemes involving PCs, only little is known about connectivity patterns among interneurons themselves. However, during recent years several research groups have focused on disinhibitory neocortical circuits and shed light on them.

While PV interneurons mainly inhibit themselves and only provide little inhibition to other interneurons, SST cells show the opposite pattern and inhibit all interneuron subclasses, but never themselves (Gibson et al., 1999; Pfeffer et al., 2013). However, Jiang et al. (2015) only recently refined this view and demonstrated that only Martinotti cells but not other SST-expressing interneurons avoided contacting each other. They further found evidence that basket cells also tend to inhibit Martinotti cells. There is also evidence that L1 interneurons mainly get inhibited from SST-expressing Martinotti cells (Pfeffer et al., 2013; Jiang et al., 2013; 2015). NGF have been shown to provide strong inhibition to all cell classes, PCs and interneurons (Jiang et al., 2013; 2015).

There is clear evidence that VIP cells preferentially target SST interneurons, resulting in disinhibition of PCs: this has been shown for sensory cortices in the somatosensory (Lee et al., 2013), visual (Pfeffer et al., 2013; Fu et al., 2014; Zhang et al., 2014; Karnani et al., 2016a) and auditory system (Pi et al., 2013). Jiang et al. (2015) report that VIP-expressing bipolar cells in L2/3 selectively target L5 Martinotti cells, while L2/3 bitufted cells inhibit L2/3 Martinotti cells, bitufted and also bipolar cells. However, bitufted cells can express either SST or VIP (Jiang et al., 2015). Caputi et al. (2009) have shown that two different types of calretinin-expressing interneurons preferentially target other interneurons, although these types differed in other characteristics and therefore belong to different cell classes. Because both SST and VIP cells can also express calretinin (Cauli et al., 1997; Xu et al., 2006), it is likely that Caputi et al. (2009) have recorded these subgroups in their study, which would confirm the interconnectivity between these two cell types.

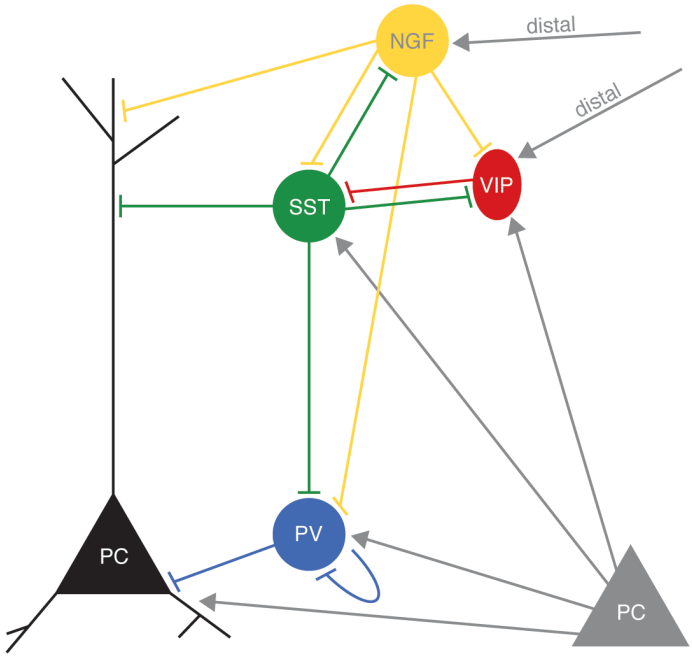

Figure 1.1: Basic principles of connectivity patterns between neocortical cells. PCs (black) receive inhibitory input from NGF (yellow), SST (green) and PV (blue) interneurons. While PV cells target the soma and proximal dendrites of PCs, SST cells innervate the distal dendrites. PCs provide excitatory input (grey) to SST, PV and also VIP (red) interneurons. VIP and NGF cells often get activated from long-range cortico-cortical projections. VIP cells provide inhibitory input mainly to SST cells, while SST cells inhibit all other interneuron classes, but not themselves. PV interneurons mainly inhibit themselves and NGFs provide strong inhibition to all classes of interneurons.

Unlike PCs, interneurons are not only connected via chemical synapses, but also form gap junctions with other interneurons which mediate electrical coupling (Galarreta and Hestrin, 2001a; Bennett and Zukin, 2004; Connors and Long, 2004). Anatomical and electrophysiological studies have shown that electrically coupled networks are highly specific and mainly built among interneurons of the same type: especially fast-spiking

PV-expressing cells (Galarreta and Hestrin, 1999; Tamás et al., 2000; Galarreta and Hestrin, 2001b), but also low-threshold-spiking SST-expressing cells (Gibson et al., 1999) build gap junctions with each other, respectively. However, NGF cells appear to establish electrical synapses with other NGF cells, but also basket cells, regular-spiking interneurons, axo-axonic cells and other interneurons (Simon et al., 2005).

1.2 Synaptic transmission

Signal transduction between neuronal cells happens at synapses, which are specialized structures that connect neurons either chemically or electrically. Chemical synapses can transmit either excitatory or inhibitory signals, allowing for complex communication patterns in neuronal networks. In the following I will give a brief overview about synaptic transmission in cortex with a focus on inhibitory signaling.

1.2.1 Excitatory synaptic transmission

Glutamate is the main excitatory transmitter in cortex. The arrival of an AP in the presynaptic axon terminal leads to opening of voltage-sensitive calcium (Ca^{2+}) channels, allowing Ca^{2+} influx that triggers the synaptic vesicles to release glutamate into the synaptic cleft. Glutamate can activate ionotropic AMPA, NMDA or kainate receptors on the postsynaptic side of the synapse, which generally mediate sodium (Na^{+}) and Ca^{2+} conductances. Na^{+} influx results in a depolarization of the postsynaptic membrane and therefore in excitatory postsynaptic potentials (EPSPs) (Jessell and Kandel, 1993).

1.2.2 Inhibitory synaptic transmission

In cortex GABA is regarded as the main inhibitory neurotransmitter, which is mostly mediated by GABA type A ($GABA_A$) and GABA type B ($GABA_B$) receptors, these get activated by two qualitatively different mechanisms, but can be expressed in the same neuron and even the same synapse (Mody et al., 1994).

Ionotropic $GABA_A$ receptors Spatially and temporally restricted phasic activation of ionotropic $GABA_A$ receptors results from a peak in GABA concentration in the synaptic cleft: the arriving AP in the axon terminal of the presynaptic cell leads to an influx of Ca^{2+}, which triggers synaptic vesicles to release GABA into the synaptic cleft (Farrant and Nusser, 2005). $GABA_A$ receptors, that are clustered opposite of the vesicle release site on the postsynaptic neuron are permeable to chloride (Cl^{-}): depending on the reversal potential of Cl^{-} in relation to the resting membrane potential (V_m), Cl^{-}-influx

or -efflux leads to hyper- or depolarizing postsynaptic potentials, respectively (Mody et al., 1994; Farrant and Nusser, 2005). During early developmental stages mainly depolarizing events of the V_m occur, while in the mature brain $GABA_A$-mediated responses are usually hyperpolarizing and are referred to as inhibitory postsynaptic potentials (IPSP) (Kaila, 1994; Ben-Ari, 2002). The concentration of Cl^- in the neuron is thought to be regulated by cation-chloride co-transporters, which are lacking in immature neurons (Payne et al., 2003). $GABA_A$ receptors are not only positioned in the center of the synaptic cleft of the postsynaptic neuron but can also occur at the presynaptic site of the axon terminal (Zhang and Jackson, 1993). Further they can be located extrasynaptically on somatodendritic compartments of neurons (Kullmann et al., 2005). The latter are thought to mediate tonic inhibition, which depends on the concentration of GABA in the extracellular space, for which the regulatory mechanisms are not fully understood (Farrant and Nusser, 2005; Kullmann et al., 2005).

When Cl^- channels are opened upon GABA activation, it further leads to an increase in the conductances across the cell membrane, which also affects excitatory inputs of the postsynaptic cell (Alger and Nicoll, 1979; Andersen et al., 1980). Thus not only hyper- or depolarizing postsynaptic potentials but also more complex phenomena can be observed referred to as shunting inhibition. The nature of this shunting effect depends on several factors: the reversal potential for GABA of the postsynaptic cell in relation to its resting V_m and the location and timing of the inhibitory in relation to the excitatory input (Gulledge and Stuart, 2003; Bartos et al., 2007; Paulus and Rothwell, 2016). If GABA receptor-mediated currents are equal to the resting V_m the local IR of the postsynaptic cell gets reduced. Thus the EPSP mediated of the subsequently activated adjacent excitatory synapse will get reduced in amplitude. When receptor-mediated synaptic currents are in between the resting V_m and the spiking threshold of the postsynaptic cell the dynamics of shunting inhibition are more complex. Two phases can be distinguished: based on the time course of the Cl^- conductances first the excitability of the cell is reduced followed by an increase in excitability due to an increase of the local IR. Further the strength of the shunting effect is much stronger for excitatory inputs located distally to the inhibitory input (Hao et al., 2009).

Metabotropic $GABA_B$ receptors Metabotropic $GABA_B$ receptors mainly mediate potassium (K^+) conductances, which generates slow and long-lasting IPSPs (Dutar and Nicoll, 1988). They are G-protein coupled receptors and upon GABA activation they release Gβγ subunits, which can activate K^+ channels but also inhibit Ca^{2+} channels. The mechanism depends upon the synaptic location of the receptor, whether they are sited on the pre- or postsynaptic site (Mody et al., 1994; Ulrich and Bettler, 2007; Chalifoux and Carter, 2011). Presynaptic $GABA_B$ receptors can modulate the amount of neurotransmitter release. Their function differs whether they are located on axon terminals of excitatory or inhibitory cells: on excitatory cells they are considered as

heteroreceptors leading to an inhibitory effect, whereas on inhibitory terminals they are considered as autoreceptors causing disinhibition of the postsynaptic cell (Ulrich and Bettler, 2007). Various mechanisms can be induced by the G-protein mediated signaling. Inhibition of voltage-sensitive Ca^{2+} channels leads to a decrease in Ca^{2+} influx, whereas the activation of K^+ channels can shunt the presynaptic AP (Chalifoux and Carter, 2011). Further it can reduce the vesicle recruitment in the synapse via lowering cyclic adenosine monophosphate levels (Sakaba and Neher, 2003). Postsynaptic $GABA_B$ receptors are mainly thought to induce G-protein mediated activation of Kir3 channels which leads to inward rectifying K^+ currents, usually resulting in a hyperpolarization of the membrane (Ulrich and Bettler, 2007).

Phenomena affecting both $GABA_A$ and $GABA_B$ receptors Spillover can act at both ionotropic $GABA_A$ and metabotropic $GABA_B$ receptors (Kullmann, 2000). It yields larger and slower IPSPs and occurs when multiple synaptic vesicles are released simultaneously or in short time intervals, which causes bigger and longer-lasting concentrations of GABA in the synaptic cleft and eventually also can activate perisynaptic receptors (Farrant and Nusser, 2005).

NGF cells play a unique role in inhibitory neurotransmission. They do not require synapses to produce inhibitory responses but can regulate cortical microcircuits by GABA-mediated volume transmission (Oláh et al., 2009). When NGF release GABA, $GABA_A$ and $GABA_B$ receptors can be activated at both the pre- and postsynaptic sites: activation at the presynaptic site allows to control the amount of neurotransmitter release (Tamás et al., 2003; Price et al., 2005; Oláh et al., 2009).

1.2.3 Electrical coupling

Electrical synapses function as reciprocal pathways, where ionic current and also small organic molecules can flow bidirectionally from one cell to the other; the strength of electrical coupling can be assessed by the coupling coefficient (Galarreta and Hestrin, 2001a; Bennett and Zukin, 2004; Connors and Long, 2004). In most cases electrical synapses are built by gap junctions that are channel-like structures, which are constructed of proteins called connexins (Evans and Martin, 2002). Connexin36 is an important gap junction protein, that is only is expressed in neurons and required for electrical coupling (Galarreta and Hestrin, 2001a; Connors and Long, 2004). Gap junctions mainly are built between two dendritic branches, but also occur between a dendrite and a soma (Galarreta and Hestrin, 2001a). Electrical synapses act as low-pass filters and depending on the afterhyperpolarization (AHP) of the spike the postsynaptic response can be biphasic and may lead to inhibition (Galarreta and Hestrin, 2001a; 2001b; Bennett and Zukin, 2004).

1.3 Interneuron function in neocortical circuits

Cortical activity is the result of the interaction of endogenously generated spontaneous rhythmic activity and responses to external stimuli (Ringach, 2009). In the living brain neurons in cortical circuits not only respond to sensory input but also show fluctuations of the V_m between hyperpolarized and depolarized episodes. During depolarized phases spontaneous APs can occur. The generation of an AP in a given cell depends on the specific excitatory and inhibitory synaptic input it receives at a given time. In order to understand how synaptic transmission affects spike timing *in vivo* one needs to understand how it is modulated by cortical activity, and what subtype-specific functions different neurons have to shape that cortical activity.

1.3.1 Cortical states

Oscillatory patterns or cortical states, also referred to as brain states, vary from low-frequency synchronized to high-frequency desynchronized states (Buzsáki and Draguhn, 2004; Harris and Thiele, 2011) and can be demonstrated at the level of electroencephalogram, local field potential and V_m recordings (Poulet and Petersen, 2008). Several oscillatory classes are distinguished and range from slow delta (1.5 - 4 Hz) to theta (4 - 10 Hz) and fast gamma (30 - 80 Hz) to ultrafast (80 - 200 Hz and higher) oscillations (Buzsáki and Draguhn, 2004). Cortical states can be determined by different levels of anesthesia, sleep, and changing arousal levels, which can vary between rest and awake behavior. Under anesthesia the V_m of neurons follows a slow rhythm (< 1 Hz) and fluctuates between periods of hyperpolarized DOWN-states and depolarized synaptically active UP-states (Steriade et al., 1993; Wilson and Kawaguchi, 1996). In the awake animal one can distinguish between quiet wakefulness with slow oscillatory neuronal activity, when the animal is awake but not behaving and active states with fast fluctuations of the V_m, when the animal is behaving (Crochet and Petersen, 2006; Reimer et al., 2014; McGinley et al., 2015). Dual whole-cell recordings of PCs in the awake animal showed that the V_m of nearby cells are highly correlated during quiet wakefulness but get desynchronized when the animal starts moving (Poulet and Petersen, 2008). A similar state change of the V_m from synchronous to active states with uncorrelated activity can be caused by sensory stimulation (Tan et al., 2014). On the one hand neuromodulators are important for the regulation of network activity (Zagha and McCormick, 2014). On the other hand interneurons are believed to play a crucial role in the control of brain states as their spike timing is coupled to different phases of oscillatory activity depending on their cell type (Buzsáki and Chrobak, 1995; Klausberger and Somogyi, 2008; Wester and McBain, 2014).

1.3.2 Cortical sensory processing

How cortical neurons process sensory input has been a long-standing question in neuroscience. It is evident that PCs are tuned to different parameters and selectively spike to certain sensory modalities such as the orientation and contrast of visual or the frequency and intensity of auditory stimuli. In the primary visual cortex (V1), it has been shown that PCs that are tuned to the same orientation are also more likely to be synaptically connected (Ko et al., 2011). Wertz et al. (2015) extended this view and demonstrated that postsynaptic PCs can receive and compute synaptic input from either similar or differently tuned presynaptic networks. Interneuron subgroups are involved differently in sensory processing (see **1.3.3**). There is evidence that fast-spiking interneurons receive excitatory input from cells with various tuning modalities (Hofer et al., 2011). Given that sensory input can arrive to the cell at various cortical states, it is evident that different behavioral states also modulate sensory processing (e.g. Niell and Stryker, 2010; Sachidhanandam et al., 2013; Saleem et al., 2013).

1.3.3 Subtype-specific function of interneurons

Due to their role in the regulation of cortical oscillations and thereof resulting impact on sensory processing many research laboratories recently began to investigate interneuron activity in sensory cortices, mainly V1, of anesthetized and awake behaving animals.

PV-expressing interneurons Fast-spiking cells, presumably PV interneurons, are important for the generation of oscillations in the gamma range and can enhance them in cortex (Cardin et al., 2009; Sohal et al., 2009) and hippocampus (Bartos et al., 2002; 2007). While they fire APs in relation to the gamma cycles, PV neurons provide inhibition to local postsynaptic PCs, thus the spike timing of PCs can be tightly controlled (Hasenstaub et al., 2005). However, PV cells are also thought to be important for the regulation and maintenance of UP-states during slow oscillations (Kuki et al., 2015; Neske et al., 2015). In the awake animal it has been shown that PV interneurons in V1 increase their firing rates during locomotion (Polack et al., 2013; Fu et al., 2014), while fast-spiking cells in S1 have higher firing rates when the animal is quiet compared to whisking episodes (Gentet et al., 2010).

PV interneurons are generally broadly tuned and respond with an increase in firing rate to a variety of sensory stimuli in V1 (Kerlin et al., 2010; Hofer et al., 2011; Atallah et al., 2012; Polack et al., 2013) and the primary auditory cortex (A1) (Mesik et al., 2015). However, there is some controversy if PV cells in V1 serve as a gain control to decrease PC firing without affecting their tuning (Atallah et al., 2012; Wilson et al., 2012) or whether PC response to visual stimuli gets sharpened by PV activation (Lee et al., 2012). At least for A1 Seybold et al. (2015) demonstrated that whether PCs get suppressed by

PV cells in a linear fashion or not depends on a variety of factors such as firing threshold and strength of suppression.

SST-expressing interneurons The role of SST interneurons across different brain states and in sensory processing is not clearly defined, but might depend on brain regions and also behavioral tasks. In S1 the V_m of SST cells has low power in the delta and theta range and is anticorrelated to the V_m of other interneurons and PCs. Further, SST cells become hyperpolarized when the animals starts whisking and also upon whisker deflection, while firing rates are higher during quiet wakefulness (Gentet et al., 2012). Fu et al. (2014) also showed that SST spiking activity in V1 is anticorrelated to locomotion and that SST cells decrease their firing when the animal starts whisking. However, Polack et al. (2013) reported a depolarization of the V_m and thereof resulting increase in firing rate of SST cells in V1 during locomotion. Reimer et al. (2014) found two different activity patterns of SST cells during quiescence and moving. However, these two different spiking behaviors might be explained by the fact that they recorded in SST-IRES-cre mice where a subset of labeled cells are fast-spiking interneurons (Hu et al., 2013).

In V1 SST cells are broadly tuned (Kerlin et al., 2010; Polack et al., 2013) and show higher firing rates upon sensory stimulation, where they are thought to mediate surround suppression and inhibit PCs in a non-linear fashion during visual stimulation (Adesnik et al., 2012; Wilson et al., 2012). Again, Lee et al. (2012) found different results, where optogenetic activation of SST cells did not affect the tuning of PCs. However, discrepancies again might be explained by the nature of suppression patterns, which depend on a row of different factors and is also true for SST cells in A1 (Seybold et al., 2015).

VIP-expressing interneurons Since it became clear that VIP cells are a major source of inhibition onto SST interneurons and vice versa, they also have become a focus of research concerning their role and impact during ongoing network activity. Non fast-spiking cells in L2/3 of S1, presumably representing VIP interneurons to some extent, show the opposite spiking behavior compared to SST interneurons and become depolarized during whisking episodes followed by hyperpolarized epochs during quiescence (Gentet et al., 2012). Similar effects were found in V1, where VIP cells have been reported to increase their spiking activity during locomotion (Fu et al., 2014; Reimer et al., 2014). The cholinergic input from the basal forebrain targeting cortical VIP cells can cause the shift to active network states (Alitto and Dan, 2012) and therefore VIP interneurons have been suggested to serve as a gain control for cortical states (Fu et al., 2014). However, there is evidence that VIP interneurons in V1 also have high firing rates during anesthesia, immobility and visual stimulation and that their firing is correlated to the spiking of PCs rather than to locomotion only (Jackson et al., 2016).

Tuning properties of VIP neurons in V1 have been described as broadly tuned (Kerlin et al., 2010; Mesik et al., 2015), whereas in A1 they show clear intensity selectivity (Mesik et al., 2015). So far, the effect of brain states on sensory processing of VIP cells has not been investigated systematically.

Neurogliaform cells The fact that NGF mediate volume transmission of GABA, which can mediate slow $GABA_A$ and activate metabotropic $GABA_B$ receptors and form gap junctions that usually serve as low-pass filters (see **1.2**) makes them an ideal candidate to be involved in low-frequency oscillations. Indeed, slow inhibition is mainly mediated in the theta range, therefore NGF are thought to contribute to the generation of theta oscillations (Banks et al., 2000; Price et al., 2005; Capogna and Pearce, 2011). Cholinergic input to L1 modulates NGF in an activity-dependent manner: while spiking cells get inhibited, resulting in a disinhibition of L2/3 PCs, NGFs at rest get activated by acetylcholine (Brombas et al., 2014).

Not much is known so far about the role of NGF in sensory processing. Chittajallu et al. (2013), however, identified an inhibitory circuit where L4 NGF suppress PV cell mediated feedforward inhibition of thalamic input to L4 stellate cells.

1.4 Monosynaptic transmission *in vivo*

Neurons fire APs during active depolarized states, when the V_m is fluctuating around the spiking threshold. Only then synaptic transmission onto the postsynaptic cell occurs, of which the V_m also is not stable. How monosynaptic transmission is mediated in an active neuronal network remains an open question in the field. Most of the knowledge that we have today about excitatory and inhibitory synaptic transmission derives from data obtained in brain slices. The mechanical stability of a brain slice preparation and visibility of cells and recording electrodes has allowed multiple whole-cell recordings from neighboring cells. This has allowed the investigation of local connectivity rates as well as the properties of postsynaptic potentials and short-term plasticity. However, the slicing procedure has technical drawbacks. On the one hand slicing can stimulate the growth of dendritic spines and axonal boutons, and therefore the number of synapses (Kirov et al., 1999). On the other hand axonal and dendritic arborizations are truncated during slicing. Further, the synaptic release probability might be altered due to differences in spontaneous activity, extracellular calcium concentrations and tonic inhibition compared to *in vivo* (Borst, 2010). Other aspects are the different concentrations of neuromodulators and depending on the composition of the bath solution for the slice the absence of rhythmical network activity. All these limitations might influence the results on synaptic transmission received from *in vitro*

work. In order to understand how synaptic connectivity determines brain function it is therefore essential to investigate monosynaptic transmission in an active network. Only *in vivo* one can examine the impact of brain states on synaptic integration and thus the spiking of postsynaptic cells.

1.4.1 Technical approaches to study monosynaptic transmission *in vivo*

Due to the technical difficulty of obtaining simultaneous V_m recordings from multiple cells, few studies have so far measured excitatory monosynaptic transmission *in vivo*. Hence, a variety of approaches have been used to record EPSPs in the living animal. By the combination of simultaneous extracellular and intracellular recordings of unidentified cortical neurons in the precentral cortex of awake and anesthetized monkeys, Matsumura et al. (1996) identified EPSPs and IPSPs in a subset of cells. In sedated rats Bruno and Sakmann (2006) used extracellular and juxta-cellular recordings of thalamic neurons with simultaneous whole-cell recordings of cortical L4 cells in barrel cortex. They could demonstrate that the EPSP amplitude depends on brain states and short-term depression occurs at thalamo-cortical synapses *in vivo*. However, these studies used spontaneous and sensory evoked spikes of the presynaptic cell to compute spike-triggered averages of the postsynaptic cell. This is problematic because the simultaneous spiking of several presynaptic neurons could cause the postsynaptic response. Therefore it remains unclear how much of the activity of the surrounding network contributes to the recorded postsynaptic potentials. To identify unitary connections it requires the stimulation of the presynaptic neuron, independent from spontaneous activity and sensory responses, and simultaneous recording of the postsynaptic cell. Therefore Pala and Petersen (2015) used a combination of optogenetic activation of single PC and simultaneous whole-cell recordings of neighboring interneurons in barrel cortex of anesthetized mice. By triggering spikes in the presynaptic cell they showed differences in excitatory synaptic transmission onto PV and SST cells in L2/3.

These studies used extracellular recordings or optogenetic activation of the presynaptic cell to investigate postsynaptic potentials of the postsynaptic cell. Thus they were unable to measure the V_m dynamics of the presynaptic cell and correlate it with the V_m of the postsynaptic neuron. In order to investigate these correlations one needs simultaneous intracellular recordings of monosynaptically connected cells. These recordings are technically very difficult to obtain and to my knowledge only very few studies so far used this approach to systematically assess excitatory synaptic transmission *in vivo*. E.g. Crochet et al. (2005) used simultaneous sharp microelectrodes to record from synaptically connected pyramidal neurons that were blindly approached in the visual

cortex of anesthetized cats. By triggering single spikes in the presynaptic cell they also showed the modulation of postsynaptic potentials by brain states and reported high failure rates and short-term facilitation of cortico-cortical synapses in active states. A recent study from our lab (data not shown in the present study) investigated monosynaptic excitatory transmission in the DOWN-state between L2 PCs in the anesthetized mouse (Jouhanneau et al., 2015). By using two-photon-targeted whole-cell recordings of neighboring identified PCs we could show that PCs in L2 are sparsely connected with a overrepresentation of bidirectional connections. While the EPSP kinetics were comparable to or only slightly different from data derived from slice work, our data revealed higher EPSP failure rates *in vivo*. Further, we could demonstrate that across the population of recorded connections short-term plasticity was weak. However, when considering the reliability of excitatory transmission it turned out, that connections tend to show more synaptic depression the more reliable they are.

By doing paired whole-cell recordings from the somata of L1 interneurons and dendrites of L5 PCs, inhibitory monosynaptic connections have been identified *in vivo* (Jiang et al., 2013). The authors could validate functions of inhibitory circuits they had identified *in vitro*. While single-bouquet cells enhanced dendritic complex spiking via a disinhibitory circuit, elongated NGF cells directly suppressed these events.

1.5 Motivation and research goals

Although representing only a small, yet diverse population in the neocortex GABAergic interneurons play an important role for the control of inhibition. Cortical inhibitory neurons are involved in the implementation of brain states and also shape cortical activity during sensory processing. They form inhibitory connections with local excitatory and other inhibitory neurons, while synaptic integration between local cortical neurons is thought to emerge during depolarized active network states. Inhibition of postsynaptic interneurons can result in disinhibition of nearby PCs. Although first attempts have been made to examine excitatory synaptic transmission *in vivo*, it is unknown how inhibitory interneurons transmit information to their postsynaptic inhibitory cells when recorded during ongoing network activity. The aim of this study was to identify monosynaptic inhibitory connections *in vivo*, in order to answer the following questions:

- How do brain states influence inhibitory postsynaptic potentials?
- How does connectivity determine the membrane potential and spike timing of postsynaptic cells *in vivo*?

In order to address these questions we simultaneously performed two-photon targeted whole-cell recordings of two to three neighboring GABAergic interneurons in L2/3 of

the forepaw primary somatosensory cortex in anesthetized mice. Therefore we chose two different approaches: To gain insight about more general characteristics of monosynaptic inhibitory transmission between interneurons GAD67-GFP mice were used in one subset of experiments. This allowed us to target all L2/3 interneurons without respect to specific subtypes. Here we mainly recorded from non-fast spiking cells, which represent the majority among L2/3 interneurons. In a second line of experiments we were interested to investigate more specifically the interaction among SST- and VIP-expressing cells. Therefore we bred the triple transgenic mouse line GIN-VIPcre-Ai9, which allowed us to specifically target SST and VIP cells under the two-photon microscope.

2 Methods

2.1 Animals

Male and female mice (P20 to P32) of two different strains (GAD67-GFP and GIN-VIPcre-Ai9) were housed on a 12:12 light/dark cycle with food and water ad libitum.

All experimental procedures were performed according to German guidelines on animal welfare under the supervision of local ethics committee according to animal experimentation permits G0188/09 and G0204/14.

GAD67-GFP mice For experiments where interneuronal subtypes were not determined GAD67-GFP mice (n = 41) were used. From early developmental stages all GABAergic neurons are positive for the GABA synthetic enzyme glutamic acid decarboxylase (GAD). Thus, GAD is a general marker for GABAergic neurons. GAD67-GFP knock-in mice carry a green fluorescent protein (GFP) cDNA inserted between the GAD67 5' flanking region and the GAD67 codon start (Tamamaki et al., 2003). Heterozygous offspring was backcrossed to C57Bl/6 mice.

GIN-VIPcre-Ai9 mice To distinguish between somatostatin- (SST-) expressing and interneurons and interneurons that express the vasoactive intestinal peptide (VIP) the triple transgenic mouse line GIN-VIPcre-Ai9 was created, of which 25 animals were used for experiments. First VIP-IRES-cre mice were crossed with the tdTomato reporter line Ai9 (both from Jackson laboratories). In VIP-IRES-cre mice, cre recombinase expression is directed to VIP-expressing cells by the endogenous promoter elements of the vasoactive intestinal polypeptide locus (Taniguchi et al., 2011). Ai9 mice carry a targeted mutation of the *Gt(ROSA)26Sor* locus with a *loxP*-flanked STOP cassette preventing transcription of a CAG promoter-driven red fluorescent protein variant (tdTomato) (Madisen et al., 2010). In heterozygotic offspring of a cross between VIP-IRES-cre and Ai9 mice, tdTomato is expressed in VIP interneurons following cre-mediated recombination. These mice were then crossed with GIN mice (donation of Vida lab, Charité). GIN mice are homozygous for TgN(GadGFP)45704Swn and express enhanced GFP under the control of the mouse *Gad1* (GAD67) gene promoter. Transgene expression occurs in a subpopulation of SST interneurons (Oliva et al., 2000).

2.2 Immunohistochemistry

Two male GIN-VIPcre-Ai9 mice (P29) were used for control immunostaining against SST and VIP (**Fig. 3.2** and **3.3**). Animals were deeply anesthetized by intraperitoneal injection of urethane (2.5 g/kg) and then transcardially perfused with 4 % paraformaldehyde (PFA). Brains were removed, post-fixed in 4 % PFA overnight and then stored in phosphate buffer (PB). Before histological processing, brains were sliced into 50 µm-thick coronal slices containing forepaw primary somatosensory cortex (S1) using a vibratome (VT1000 S, Leica). Sections were washed with PB and treated with a blocking solution containing 5 % goat serum and 0.5 % TritonX for one hour at room temperature. Consecutive slices were processed alternately for single immunostains against SST and VIP and controls, respectively. Primary antibodies against SST (rabbit, 1:1000, Bachem T4102) and VIP (rabbit, 1:400, Abcam AB43841) were diluted in PB containing 3 % goat serum and 0.5 % TritonX. Primary antibody incubation (overnight at 4 °C) was followed by further washing steps with PB and then by incubation (two hours at room temperature) of a second anti-rabbit antibody coupled to Alexa-647 (goat, 1:400, Lifetechnologies A-21244). After further washes with PB sections were mounted in Fluoroshield (Sigma, F6182) and stored at 4 °C.

Images were obtained with a confocal microscope (Leica, DMI 6000) and a 20x oil immersion objective. GFP was excited by a single-photon Argon laser at 488 nm, tdTomato was excited by a solid state laser at 568 nm and Alexa 647 was excited by a Helium-neon laser at 633 nm. A descanned photomultiplier tube (PMT) detected GFP-, tdTomato- and Alexa 647-emission at 491 to 535 nm, 565 to 601 nm and 640 to 690 nm, respectively. Image stacks were then carefully inspected for colocalization within a window of 300 x 500 µm covering layer 2/3 (L2/3).

2.3 Surgery and intrinsic optical imaging

All steps were done under isoflurane anesthesia (1-2 % in O_2). Eye blink and paw withdrawal reflexes were absent. The mouse core body temperature was held at 37 °C with a heating pad and constantly monitored with a rectal probe. The skull was constantly covered with Ringer's solution (in mM): 135 NaCl, 5 KCl, 5 HEPES, 1.8 $CaCl_2$, 1 $MgCl_2$.

First the skin above the skull was carefully removed and a custom-made metal head-holder (aluminium, ~1 g, 1.5 cm long, 0.3 - 1 cm wide) was implanted onto the skull with glue and dental cement. Then a recording chamber was built from dental cement

above forepaw S1. Metamizol (200 mg/kg) was injected subcutaneously prior to the implantation for pain relief.

In a second step the exact position of left forepaw S1 was identified by intrinsic optical imaging (Grinvald et al., 1986) using a monochrome CCD camera (QImaging). Tactile stimuli (10 Hz, for 8 s) were delivered with a piezo stimulator to digit 3 of the right forepaw. The intrinsic stimulus response was visualized with red light illumination (630 nm) and compared to the blood vessel pattern seen under green illumination (530 nm) (**Fig. 2.1**). In some experiments stereotactic coordinates (0.5 mm posterior to bregma, 2.5 mm lateral to the midline) were used to determine S1 position. Prior to the experiment a small craniotomy (0.5 to 1 mm diameter) was drilled over forepaw S1. Then the dura was carefully removed with a 30 gauge needle.

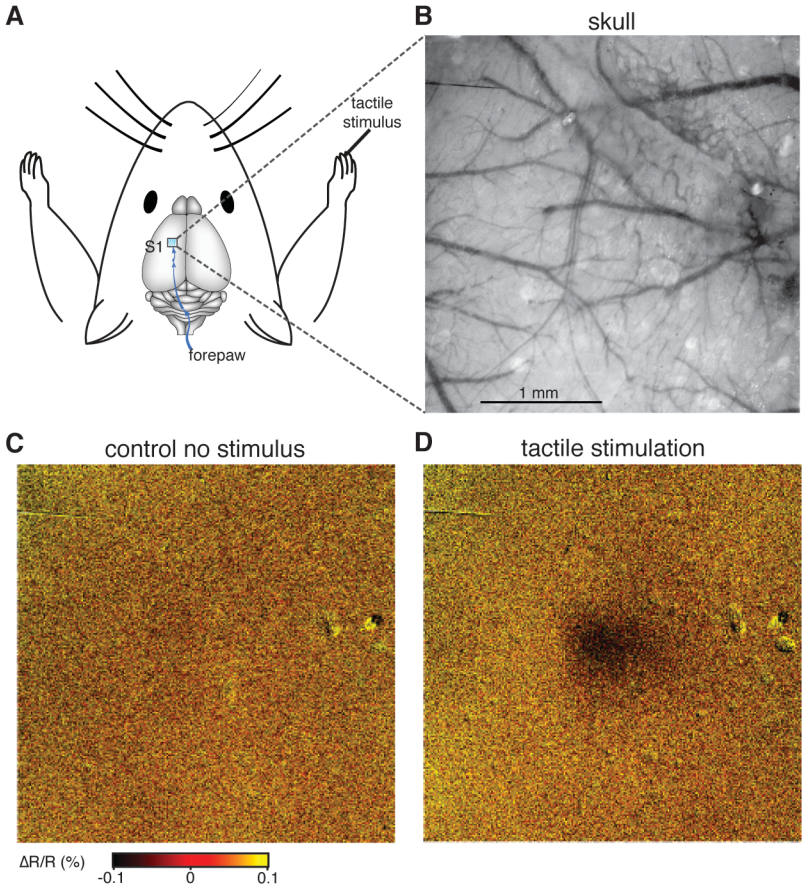

Figure 2.1: Intrinsic optical imaging to detect the position of forepaw S1. A Tactile stimuli were applied to the right forepaw, sensory information gets transmitted to forepaw S1 via the dorsal root ganglion, brainstem and thalamus. **B** Image of the skull, blood vessel pattern seen under green illumination (530 nm). **C** Control intrinsic optical imaging signal, when no tactile stimulus was applied. **D** Intrinsic optical image response to tactile stimulation of the forepaw. Both, control and stimulus responses were visualized with red illumination (630 nm).

2.4 Two-photon targeted whole cell patch clamp recordings

All recordings were done under urethane anesthesia (1.5 g/kg).

For two-photon targeted recordings (Margrie et al., 2003; Kitamura et al., 2008) mice were placed under an *in vivo* two-photon laser scanning microscope (Femto2D, Femtonics) and an Ag/AgCl ground electrode was placed in the recording chamber.

Whole-cell patch clamp recordings were made with 2 mm external diameter borosilicate glass pipettes (Hilgenberg), with a resistance of 5-7 MΩ. Two or three pipettes were filled with intracellular solution (in mM): 135 K-gluconate, 4 KCl, 10 HEPES, 10 Na_2phosphocreatine, 4 MgATP, 0.3 Na_3GTP (adjusted to pH 7.3 with KOH), 2 mg/ml biocytin and 30 μM Alexa-594 (Invitrogen). Using motorized micromanipulators (Luigs & Neumann) the pipettes were inserted into the brain under visual control at an angle of 30 ° from vertical applying positive pressure of 130 mbar. While lowering pipettes into the tissue until about 120 μm depth pressure was gradually reduced to 50 to 80 mbar. Then a region of interest was scanned with a mode-locked Ti:sapphire laser beam (Coherent) using a 40 x 0.8 NA water immersion objective (Olympus). Imaging was controlled with MES software (Femtonics) running in MATLAB (MathWorks). Two high-sensitivity PMT were used to detect red for shadow-targeting and tdTomato-expressing, and green for GFP-expressing GABAergic neurons. Cells were imaged with the laser tuned to 820 or 950 nm.

Two to three cells within a range of 100 μm were approached one after the other while positive air pressure was reduced to 25 to 30 mbar. In GAD67-GFP mice up to three GFP-expressing cells (GAD) were targeted, while in GIN-VIPcre-Ai9 animals pipettes were targeted towards one GFP- (SST) and two tdTomato-expressing (VIP) cells. In both preparations dark 'shadows' were avoided, as they represented negative images of unlabeled cells and blood vessels, visualized by fluorescent dye in the intracellular solution, which was perfused in the extracellular space (**Fig. 2.2**). Contact between the patch pipette and cell membrane was monitored by live two-photon images and by deflections of the current injection pulses that were visually identified on an oscilloscope (TDS2014C, Tektronix). A gigaseal was formed by applying negative pressure and passing hyperpolarizing current. Once a gigaseal was established on all cells whole-cell configuration was achieved in voltage clamp mode by rupturing each cell membrane with negative pressure. Current clamp recordings were then made using an Axon Multiclamp 700B amplifier (Molecular Devices), digitized at 20 kHz by an analog to digital converter (ITC-18, Heka) and low-pass filtered at 10 kHz. Data was collected in 30 s to 120 s sweeps using custom written scripts in IgorPro (Wavemetrics). Recordings were not compensated for the liquid junction potential.

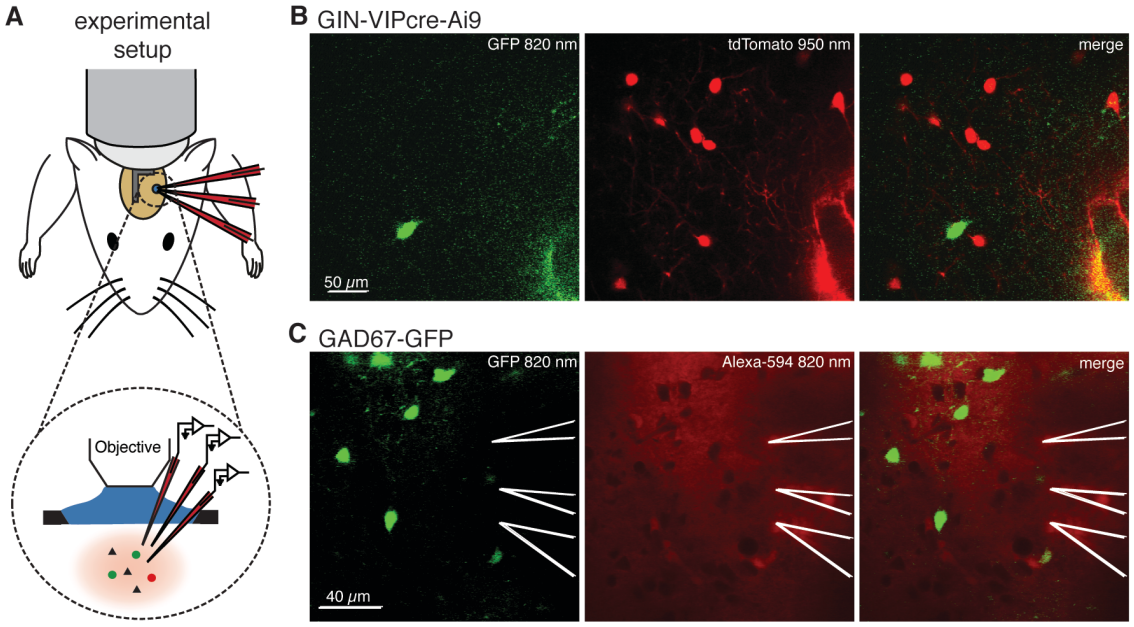

Figure 2.2: Triple whole-cell recordings of labeled neurons *in vivo*. **A** Schematic overview: three pipettes are targeted under visual control of a two-photon microscope towards interneurons expressing fluorescent dye. **B** Visualization of GFP-expressing SST cells and tdTomato-expressing VIP cells in GIN-VIPcre-Ai9 animals before inserting pipettes into the brain; laser was tuned to 820 nm and 950 nm to image SST and VIP interneurons, respectively. **C** Visualization of GFP-expressing GAD cells in GAD67-GFP mice while Alexa-594 was perfused into the extracellular space by three patch pipettes to distinguish them from pyramidal cells appearing as dark shadows; laser was tuned to 820 nm.

Initially after break-in firing patterns were recorded with current injection (500 ms, -200 to 300 pA in 50 to 100 pA steps). To test for synaptic connectivity each recorded cell was manually tested for the current threshold needed to trigger a single spike. Short current pulses (5 to 20 ms, 40 to 350 pA) were then injected into each cell at 0.5 to 1 Hz. Single action potentials (APs) were alternated between recorded cells. Further, sweeps of spontaneous activity were collected. Both, initial longer current pulses to record firing patterns and short current pulses to detect synaptic connectivity were used to visually inspect for electrical connectivity between simultaneously recorded neighboring cells.

2.5 Data analysis and statistics

Data analysis was carried out in IgorPro (Wavemetrics) using custom written scripts. Only traces with an average membrane potential (V_m) below -45 mV were included for further analysis. Population data are represented as mean ± standard deviation (SD). To compare two groups of unpaired and paired data statistical significance was assessed by non-parametric Wilcoxon rank-sum test and Wilcoxon signed-rank test, respectively. All tests were two-tailed, significance level was $p < 0.05$. Further, the

StatsLinearCorrelation test was used to analyze the correlation between the amplitude of the inhibitory postsynaptic potential (IPSP) and the V_m.

Electrophysiological properties For quantification of electrophysiological properties (**Fig. 3.4**) data from single (n = 27 single recordings), double (n = 30 double recordings) and triple recordings (n = 10 triple recordings) (GAD, n = 76 cells; SST, n = 10 cells; VIP, n = 31 cells) were included into the analysis.

The V_m was computed from all sweeps excluding current steps, and spontaneous firing rate of APs was determined across UP- and DOWN-states.

The V_m value corresponding to the time of the peak of the third derivative of the AP waveform was taken as AP threshold. The afterhyperpolarization (AHP) relative to the AP threshold was measured 20 ms after the peak of the AP.

Current injections (-100 pA, ≥ 200 ms) at the beginning of whole-cell recordings were used to measure input resistance (IR) and membrane time constant (tau). Only current steps injected during DOWN-states were considered for analysis. IR was determined offline by fitting a double exponential on average V_m responses to current steps from +0.4 ms to +50 ms in order to subtract the early fast component of the response, which occurs due to the series resistance (Crochet and Petersen, 2006; Pala and Petersen, 2015). The difference of V_m prior (-40 to -10 ms) and during (+70 to 100 ms) the current pulse was corrected for the series resistance (GAD cells, 21.8 ± 10.8 MΩ, n = 74; SST cells, 34.7 ± 25.0 MΩ, n = 9; VIP cells, 24.2 ± 11.1 MΩ, n = 25) and divided by the amount of current injection to obtain the IR. Tau was determined by fitting a single exponential to average V_m from 1 ms to 60 ms after onset of current injection (Pala and Petersen, 2015).

Fast Fourier Transforms (FFTs) were derived from 5 s segments of spontaneous V_m dynamics during spontaneous activity across UP- and DOWN-states using a multidimensional prime factor decomposition algorithm computed in IgorPro. Low frequency power was calculated by taking the integral of the FFT between 1 and 5 Hz.

Splitting of DOWN- and UP-states Under urethane anesthesia cortical neurons oscillate between periods of depolarized (UP-states) and hyperpolarized (DOWN-states) activity. To determine UP- and DOWN-states, first spontaneous and triggered APs were cut from a given trace by applying binomial smoothing (20 smoothing operations). Then a histogram of the V_m distribution was generated, which in most cases showed a bimodal distribution of V_m values. For these cases, DOWN-state thresholds were determined by taking the maximum of the peak representing hyperpolarized V_m values and adding 2 mV to that value; UP-state thresholds were determined by subtracting the trough V_m value of the maximum of the peak representing depolarized V_m values and dividing it by the factor of 2 (**Fig. 2.3**). For histograms of V_m traces with no bimodal distribution thresholds to define DOWN- and UP-state were determined

visually. For GAD cells average DOWN- and UP-state thresholds were 2.4 ± 1.2 mV and 6.3 ± 2.8 mV, respectively, above the most hyperpolarized sweep. Average DOWN- and UP-state thresholds for SST cells were 2.0 ± 0.5 mV and 2.7 ± 0.8 mV, and for VIP cells average DOWN- and UP-state thresholds were 2.6 ± 1.5 mV and 5.3 ± 2.7 mV.

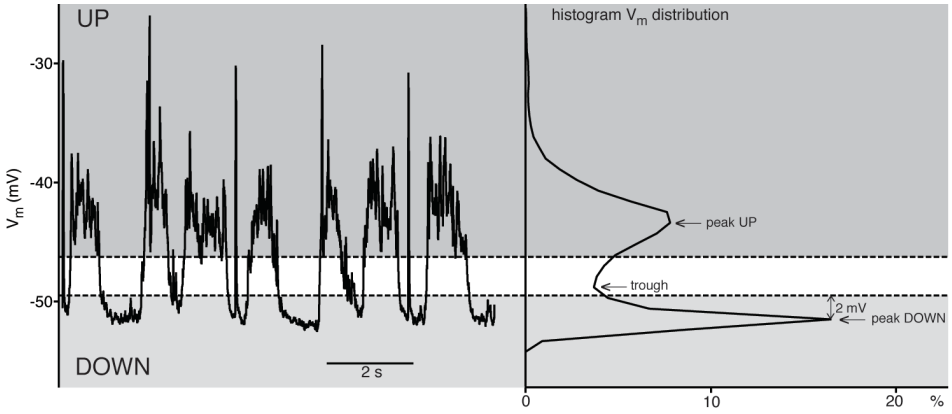

Figure 2.3: Splitting of DOWN- and UP-states. Left panel: example trace of an interneuron recorded in an urethane anesthetized GAD67-GFP animal, which shows typical DOWN- and UP-state modulation. Spontaneous and triggered spikes were cut. Right panel: Histogram of the V_m distribution from the example cell pictured on the left shows a bimodal distribution of V_m values. Dashed lines indicate thresholds for DOWN- and UP-state, respectively.

Average V_m values of single sweeps were determined in separate time windows ranging from 20 to 5 ms preceding and 40 to 60 ms after the triggered AP in the neighboring recorded cell. To be considered as a DOWN-state, V_m values of sweeps of a given recorded cell had to be smaller than the previously determined DOWN-state threshold for both time windows. To be considered as an UP-state, V_m values had to be larger than the previously determined UP-state threshold for both time windows.

SST cells, and some of the VIP and GAD cells, did not show a clear bimodal distribution of V_m values (**Fig. 3.4B**). However, paired recordings of cells with and without clear bimodal V_m distributions showed that DOWN-state episodes occurred simultaneously with episodes of hyperpolarized V_m in cells without clear DOWN-states. Similar findings were observed for UP-states and depolarized V_m episodes for paired recordings (**Fig. 3.16B**). Therefore the terms DOWN- and UP-states are used for all cell types.

Detection of inhibitory connections and analysis of IPSPs To detect IPSPs evoked by single current evoked APs in a simultaneously recorded neighboring cell trial-by-trial response amplitudes were measured in a time window from 2 ms to 6 - 30 ms after the triggered spike. In addition, two distinct shuffled amplitude measurements of the same time interval were computed prior the response for each sweep, one shuffled between 65 to 25ms, the other one between 32 to 18 ms prior to the triggered spike. These two shuffled amplitude measurements were compared with the connection amplitude after

the triggered spike (to examine for connectivity) as well as between themselves (to serve as an internal control). An unpaired Wilcoxon rank-sum test was used to assess statistical significance of postsynaptic responses. This analysis was done on traces where spikes had been clipped as described above (**Fig. 3.5**).

This analysis was done for several conditions. First trial-by-trial response amplitudes were calculated across all sweeps aligned to a single current evoked AP in the putative presynaptic cell (225.2 ± 154.2 sweeps per cell). In a second step these sweeps were divided into DOWN- and UP-state data and separately tested again for inhibitory responses. To be taken into account for IPSP detection, DOWN-state responses needed to consist of at least 10 sweeps (100.0 ± 65.0 sweeps per cell), and UP-state responses of at least 20 sweeps (91.0 ± 74.76 sweeps per cell), due to higher noise during UP-states because of higher levels of synaptic activity. Further UP-state responses to the first of a doublet of triggered spikes were also analyzed for inhibitory responses. Finally, average response traces for all conditions mentioned above were generated and visually inspected to confirm connectivity analysis.

Among simultaneously recorded GAD cells, 81 connections were tested, but only 38 could clearly be distinguished as either connected or unconnected and be used for further analysis. 41 tested connections had to be discarded due to too low repetition rates of sweeps during DOWN- and/ or UP-states. Another pair of cells (two tested connections) was excluded from further analysis, as this pair turned out to be electrically coupled by visual inspection and did not classify as synaptically connected or unconnected. From SST to VIP cells 16 connections were tested, whereof one was excluded, three out of 13 tested connections from VIP to SST cells and three out of 15 tested connections from VIP to VIP cells had to be excluded for the same reasons as mentioned above for the GAD cells. Connections from SST to SST interneurons were not tested, due to the low density of these cells in GIN mice. The very low abundance of only one or two SST cells within a field of view and the high difficulty of establishing targeted whole-cell recordings *in vivo* did not allow for regular double whole-cell recordings of these cells.

For comparison of IPSPs across brain states the average response of each postsynaptic cell to single current evoked APs was analyzed for response in UP- and DOWN-states to single current evoked APs (**Fig. 3.8** and **3.9**). Amplitudes were defined as the difference in V_m in a time window from 2 ms after the presynaptic spike to the peak time. The peak was determined as the time point where V_m reached its minimum within a time window of 2 to 40 ms after the presynaptic spike, and was visually controlled. Amplitudes were then plotted against the average V_m measured 20 to 5 ms before the presynaptic spike and a linear regression was performed. Only UP-state responses averaged from at least 10 sweeps were taken into account. For the connection from VIP to SST cells, the

threshold for splitting DOWN- and UP-state was determined across the whole time for the recording of the SST cell, rather than considering every trace separately.

Spike-triggered averages The spike times of spontaneous APs of one neuron (cell 1) of simultaneously recorded cells were determined. Only cells with at least ten spontaneous APs were included in the analysis (124 ± 140 APs per cell). Then APs were filtered from corresponding sweeps of the neighboring cell and segments of V_m dynamics aligned to previously determined spike times were averaged (cell 2). If enough spontaneous APs were detected in both cells, analysis was performed in both directions. For each cell, both cell 1 and cell 2, a linear fit (IgorPro) was fitted to the average V_m trajectory from -20 ms to -1 ms prior the peak of the spike. The gradient of the fitted line served for comparison of the synaptic input to both cells. For each spike-triggered average (STA) of cell 2 the slope for rise and decay relative to spike time of the presynaptic or unconnected neighboring cell was calculated in a 20 ms time window. Further the peak time of each STA was determined, as where the V_m reached its maximum relative to the spike time of the neighboring cell (**Fig. 3.10, 3.11, 3.12, 3.13** and **3.14**).

Peristimulus time histograms Peristimulus time histograms (PSTHs) were computed relative to the time of spontaneous or triggered spikes of a cell, and calculated either for the cell itself or for its simultaneously recorded neighboring cell (**Fig. 3.10, 3.11, 3.13, 3.14** and **3.15**). Bin width was 20 ms and spike counts per bin were displayed as firing rates in Hz.

Cross-correlations Within one pair of simultaneously recorded cells, the mean V_m cross-correlation during spontaneous activity was averaged from several 2 s segments. The average V_m value was subtracted from each trace and traces were normalized by their standard deviation prior to generating cross-correlograms in IgorPro (**Fig. 3.16** and **3.17).** Further STAs of cell 1 and 2 were used to compute cross-correlations for short time segments of 20 ms each before and after the spike of cell 1 (**Fig. 3.18**).

3 Results

3.1 Histological characterization of GIN-VIPcre-Ai9 mice

GABAergic interneurons are a heterogeneous population of neurons. In order to visualize them for *in vivo* recordings we examined mice lines where interneurons were labeled with fluorescent markers. In a subset of experiments GAD67-GFP mice were used. In these mice nearly all GABAergic interneurons are labeled with GFP (Tamamaki et al., 2003), including all major subgroups. Therefore it is impossible to visually distinguish different subpopulations of interneurons in this mouse line. In order to specifically target interneurons expressing somatostatin (SST) and the vasoactive intestinal peptide (VIP), which are thought to be highly interconnected (Caputi et al., 2009; Lee et al., 2013; Pfeffer et al., 2013; Pi et al., 2013), we created a triple transgenic mouse line. First VIP-IRES-cre mice (Taniguchi et al., 2011) were crossed with the tdTomato reporter line Ai9 (Madisen et al., 2010), to get VIP cells labeled with red fluorescence. Subsequently the offspring was crossed with GIN mice (Oliva et al., 2000), where a subpopulation of SST interneurons is labeled with GFP, to generate mice with both SST and VIP neurons fluorescently labeled with GFP and tdTomato, respectively.

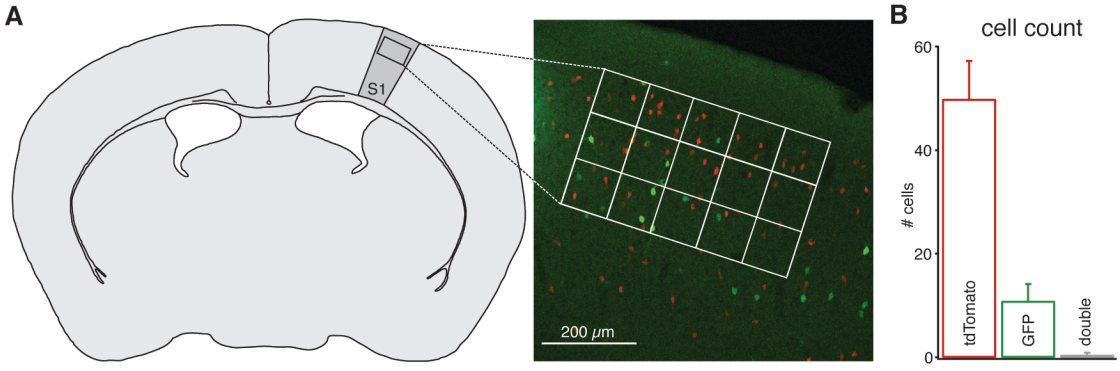

Figure 3.1: Quantification of GFP- and tdTomato-labeled neurons in GIN-VIPcre-Ai9 mice. A Left: coronal slice, dark grey area represents forepaw S1 (adapted from Paxinos et al., 2013); right: confocal image of GFP- and tdTomato-labeled cells in L2/3 of mouse forepaw S1 of the left hemisphere, grid shows area of 500 x 300 µm used for cell count. **B** Quantification of labeled cells across 50 µm-thick slices within grid shown in A. Data are represented as mean ± SD.

Confocal images of 50 µm-thick coronal slices (n = 12 slices, 2 animals) containing forepaw primary somatosensory cortex (S1) revealed that the offspring showed one group of cells labeled with tdTomato and one group of cells labeled with GFP. Both tdTomato- and GFP-labeled cells were more apparent in cortical layers 2 and 3 (L2/3). Thereby tdTomato-labeled cells were found predominantly in a band ~100 to 250 µm below the pial surface, corresponding to L2. In layers 4-6 appearance of tdTomato-labeled cells was more sparse. The distribution of GFP-labeled cells was evenly sparse across superficial layers 2 and 3, and an even smaller fraction could be observed in deeper layers. To quantify fluorescence labeling in L2/3, for each slice cells were counted in a 500 x 300 µm window covering L2/3 (**Fig. 3.1A**). While 10.8 ± 3.5 GFP-labeled cells were counted per slice, the number of tdTomato-labeled cells was 5-fold higher (49.8 ± 7.7 cells per slice). Double-labeling was rare (0.4 ± 0.8 cells per slice) (**Fig. 3.1B**).

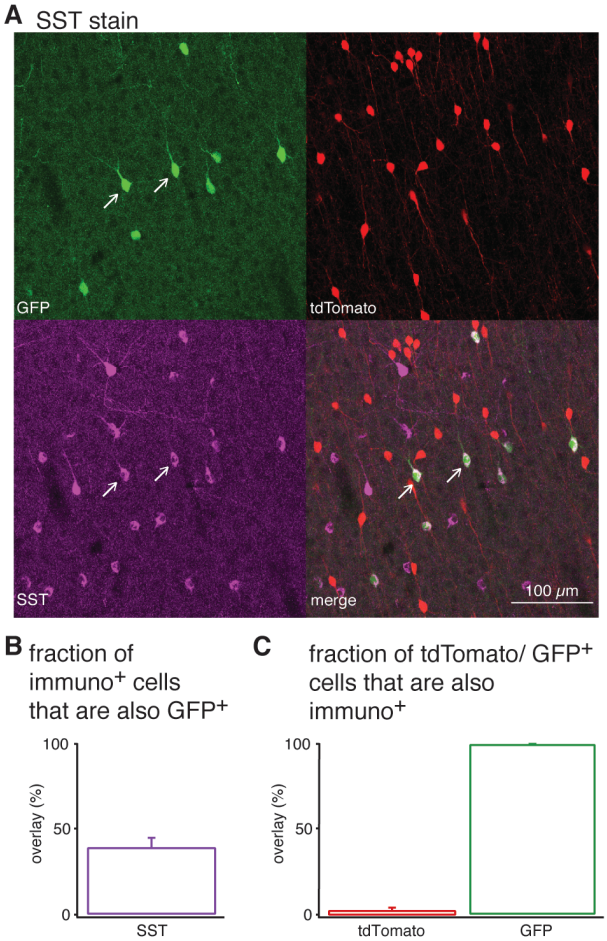

Figure 3.2: GFP-labeled neurons in L2/3 forepaw S1 of GIN-VIPcre-Ai9 mice express SST. A Immunohistochemistry indicated that only GFP-, but not tdTomato-labeled cells express SST. **B** Quantification of SST-expressing neurons that are also labeled for GFP. **C** Quantification of GFP- and tdTomato-labeled cells that express SST. Data are represented as mean ± SD.

In order to verify that GFP-labeled cells were SST-expressing interneurons immunohistochemistry was performed (**Fig. 3.2A**), by incubating coronal slices (2 slices per animal, n = 2 mice) with primary antibodies against SST and then with a secondary antibody coupled to Alexa-647. Confocal imaging revealed that only 39.5 ± 5.5 % of SST interneurons were labeled with GFP (**Fig. 3.2B**), however all GFP-labeled (100 ± 0 %) and only 2.1 ± 1.9 % of tdTomato-labeled cells expressed SST (**Fig. 3.2C**). These results indicate that only a subset of SST-expressing cells are labeled with GFP in the GIN-VIPcre-Ai9 mice, as already shown for GIN-mice (Oliva et al., 2000).

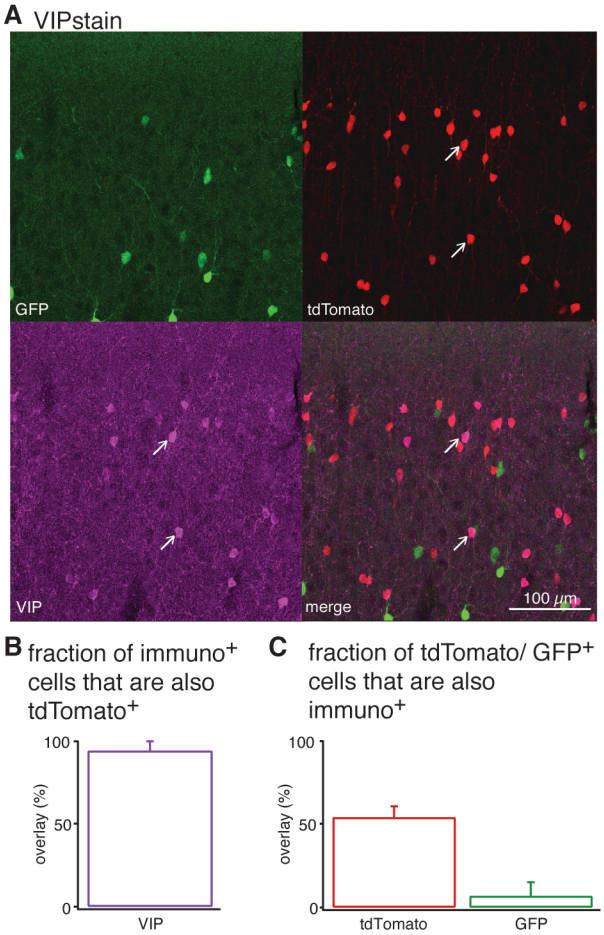

Figure 3.3: tdTomato-labeled neurons in L2/3 forepaw S1 of GIN-VIPcre-Ai9 mice partially express VIP. A Immunohistochemistry indicated that only tdTomato-, but not GFP-labeled cells express VIP. **B** Quantification of VIP-expressing neurons that are also labeled for tdTomato. **C** Quantification of tdTomato- and GFP-labeled cells that express VIP. Data are represented as mean ± SD.

In separate, consecutive, slices immunohistochemistry with antibodies staining against VIP (2 slices per animal, n = 2 mice) (**Fig. 3.3A**) uncovered that although 94.4 ± 5.6 % of VIP-expressing cells were labeled for tdTomato (**Fig. 3.3B**), only 54.4 ± 6.4 % of all tdTomato-labeled cells were expressing VIP. Further 7.0 ± 8.1 % of GFP-labeled cells expressed VIP (**Fig. 3.3C**). However, it is possible that VIP antibody staining might be

unreliable (as reported in Pfeffer et al., (2013)), so it is unclear if unstained tdTomato-labeled cells possibly could also express VIP. Nevertheless, the distribution of tdTomato-labeled cells across layers matched well with the reported distribution of VIP cells in neocortex (Rudy et al., 2011). Overall, we generated a mouse to label SST and VIP neurons within the same mouse line, that we were able to visualize *in vivo* (**Fig. 2.2**). We went on to make *in vivo* whole-cell recordings from GABAergic neurons in the GAD67-GFP mouse and from SST and VIP neurons in the GIN-VIPcre-Ai9 mouse line.

3.2 Electrophysiological properties of L2/3 GABAergic interneurons

Two-photon targeted whole cell recordings were obtained in L2/3 of forepaw S1 of urethane anesthetized mice. In GAD67-GFP mice L2/3 was identified when pipettes were ~120 µm below the pial surface and pyramidal cells (PCs) appeared as 'shadows', visualized by fluorescent dye that was perfused in the extracellular space. Then GABAergic GFP-expressing cells (GAD) were targeted for whole-cell recordings. In GIN-VIPcre-Ai9 mice L2/3 was recognized when red fluorescent VIP cells started to appear while lowering the pipettes into the brain (see **2.4**).

To describe electrophysiological properties (**Fig. 3.4, Table 3.1**) among these cell types and also to test if SST and VIP interneurons are potentially represented in the data set of the recorded GAD population we quantified the following parameters: Both GAD (0.6 ± 1.1 Hz, n = 76) and VIP interneurons (0.9 ± 1.1 Hz, n = 31) had significantly higher spontaneous action potential (AP) firing rates compared to SST cells (0.1 ± 0.1 Hz, n = 10) (**Fig. 3.4E**). We wondered whether the low firing rates of SST cells was due to a low membrane potential (V_m), but found that both the V_m of SST (-49.8 ± 3.6 mV, n = 10) and VIP cells (-50.9 ± 3.8, n = 31) were significantly more depolarized than the V_m of GAD interneurons (-54.2 ± 4.3 mV, n = 76) (**Fig. 3.4D**). Differences in firing rates could also be explained by different thresholds to generate APs or different afterhyperpolarizations (AHP). However, the threshold for spontaneous APs (**Fig. 3.4F**) did not differ among the three measured populations of GAD, SST and VIP cells (-38.9 ± 4.7 mV, n = 69; -35.4 ± 2.5 mV, n = 5 and -37.2 ± 3.6 mV, n = 24). GAD interneurons showed bigger AHPs (**Fig. 3.4G**) after spontaneous APs (8.1 ± 3.7 mV, n = 69) compared to VIP interneurons (4.1 ± 2.6 mV, n = 24), indicating that the V_m of VIP cells could more easily reach threshold again. The AHP of SST cells (4.1 ± 2.0 mV, n = 5) was comparable to those of VIP cells. Membrane time constant (tau) and input resistance (IR) were measured in response to hyperpolarizing current steps during DOWN-states. While tau (**Fig. 3.4H**) was

significantly different among GAD, SST and VIP cells (6.1 ± 2.2 ms, n = 74; 22.2 ± 4.7 ms, n = 9 and 7.8 ± 1.7 ms, n = 25), IR (**Fig. 3.4I**) of SST (280.6 ± 61.1 MΩ, n = 9) and VIP interneurons (272.2 ± 66.0 MΩ, n = 25) were similar. GAD cells showed significantly lower IR (171.0 ± 49.5 MΩ, n = 74), which would suggest lower excitability, but was not the case for GAD cells. Taken together the higher firing rates of GAD and VIP cells could not easily be explained by a difference in the V_m or IR.

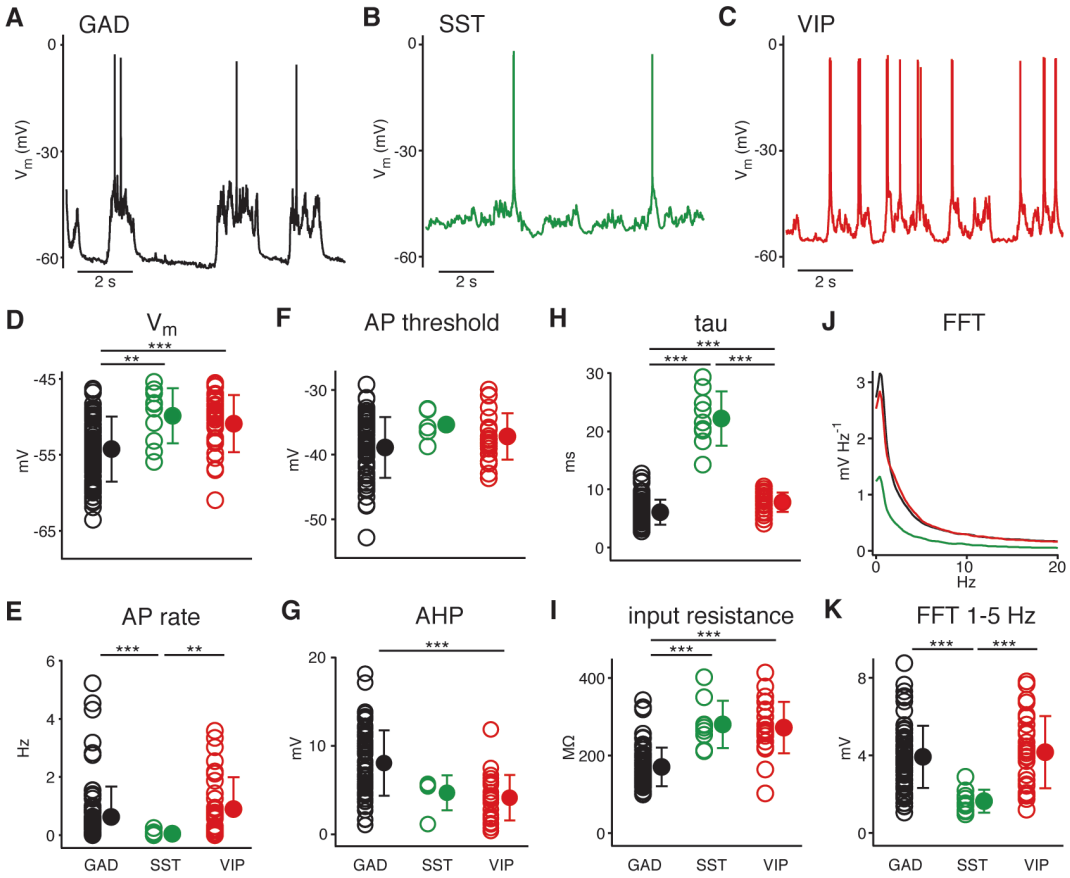

Figure 3.4: Electrophysiological properties of GABAergic cells in L2/3 of mouse forepaw S1. A-C Example whole-cell recordings of membrane potentials during spontaneous activity in urethane anesthetized mice of GABAergic cells in GAD67-GFP mice (GAD, black), SST-expressing (green) and VIP-expressing cells (red) in GIN-VIPcre-Ai9 mice, respectively. **D-I** Population analysis of spontaneous V_m (D), spontaneous AP firing rate (E), threshold of spontaneous APs (F), AHP (G), tau (H) and IR (I) for all three cell types. **J** FFT of the V_m dynamics was computed for GAD, SST and VIP cells. **K** The FFT of the V_m integrated over 1-5 Hz for all three cell types. Data are represented as mean ± SD. Wilcoxon rank-sum test assessed statistical significance, indicated by ** for $p < 0.01$ and *** for $p < 0.001$.

During slow wave sleep and under urethane anesthesia, cortical neurons generate rhythmic fluctuations of V_m activity termed UP- and DOWN-states (Steriade et al., 1993; Wilson and Kawaguchi, 1996). Fast Fourier Transforms (FFTs) (**Fig. 3.4J**) were computed from 5 s segments of spontaneous activity to quantify the fluctuations in the V_m of all neuronal subtypes. The amplitudes of V_m fluctuations in the 1-5 Hz frequency range (**Fig. 3.4K**) were significantly smaller for SST interneurons

(1.6 ± 0.6 mV, n = 10) compared to GAD and VIP cells (3.9 ± 1.6 mV, n = 74 and 4.2 ± 1.9 mV, n = 30). Small amplitudes indicate the absence of distinct UP- and DOWN-states in SST cells.

Table 3.1: P-values to assess statistical significance of electrophysiological properties between different interneuronal cell types, related to **Fig. 3.4**. Non-parametric Wilcoxon rank-sum test was used.

	GAD – GAD	GAD – VIP	SST – VIP
V_m	0.003	< 0.001	0.337
AP rate	0.001	0.411	0.006
AP threshold	0.071	0.127	0.233
AHP	0.077	< 0.001	0.465
tau	< 0.001	< 0.001	< 0.001
IR	< 0.001	< 0.001	0.909
FFT 1-5 Hz	< 0.001	0.518	< 0.001

In the GAD67-GFP mouse it was likely that we recorded from non-fast spiking (NFS) L2/3 GABAergic interneurons, rather than fast spiking (FS) parvalbumin (PV) interneurons. Visual inspection of spikes elicited during long current injections at the beginning of each recording indicated that the majority of recorded GAD cells had broad APs and thus were likely to be NFS interneurons (Gentet et al., 2010; Mateo et al., 2011; Avermann et al., 2012). Further evidence that we mainly recorded from NFS interneurons was the fact that values of our measured spontaneous firing rate for GAD cells were even lower than reported previously for NFS L2/3 interneurons in urethane anesthetized mice (Mateo et al., 2011). Additionally, our measured value for IR for GAD cells was in the range of IR determined by other studies for NFS interneurons in the awake animal (Gentet et al., 2010) and brain slices (Avermann et al., 2012), both demonstrating that IR for NFS interneurons is about 2fold higher than for FS interneurons. Taken together these observations suggest that our population of recorded GAD cells mainly if not exclusively consists of NFS interneurons, since no cells were excluded from the analysis.

Although some of the measured parameters were significantly different between recorded populations of GAD, SST and VIP cells their distributions overlap for all electrophysiological parameters extensively, beside tau, being about three times higher for SST interneurons and showing no overlap of distributions. Therefore it is likely that among the recorded GAD cells in GAD67-GFP animals also VIP interneurons were represented. However, it also indicates that SST cells recorded in GIN-VIPcre-Ai9 mice might represent a different subpopulation of GABAergic interneurons, than covered by the GAD data. To describe connectivity among L2/3 GABAergic interneurons

(see **3.3 ff.**) we therefore decided to separately analyze the data sets derived from GAD67-GFP and GIN-VIPcre-Ai9.

3.3 Detection of inhibitory connections

In order to identify inhibitory monosynaptic connections between L2/3 GABAergic interneurons we performed double and triple *in vivo* whole-cell recordings within a distance of 100 µm (examples shown in **Fig. 3.5**). Short depolarizing current steps of 5 to 20 ms were injected into each cell to trigger single APs at 0.5 to 1 Hz (**Fig. 3.5B** and **E**). This approach allowed us to test for 2 possible connections in a double recording and for 6 possible connections in a triple recording. In GAD67-GFP animals 81 connections were tested, while in GIN-VIPcre-Ai9 mice 16 connections from SST to

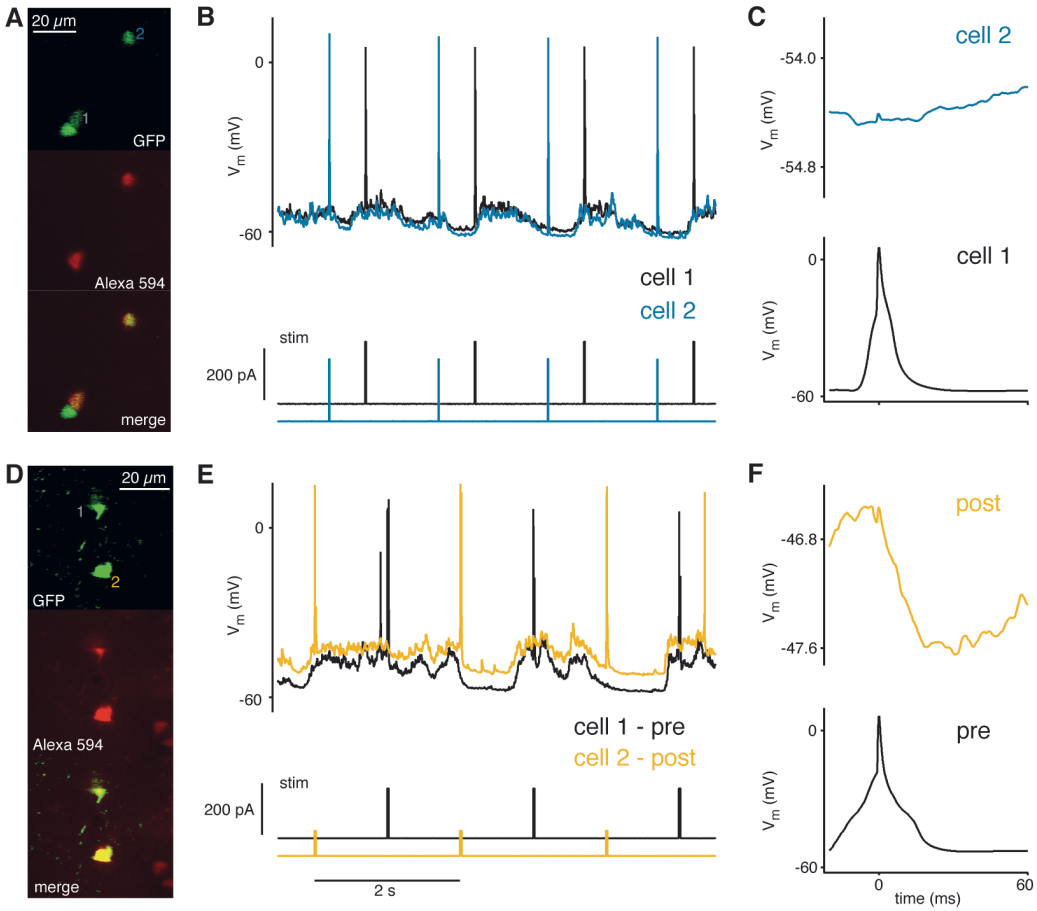

Figure 3.5: Detection of IPSPs in GAD67-GFP animals. A *In vivo* 2-photon image after a simultaneous whole-cell recording of L2/3 GFP-expressing cells filled with Alexa 594. **B** Recording of cells pictured in A showing V_m traces (top) and corresponding current traces with the stimulation paradigm used to test for synaptic connectivity (bottom). **C** Averaged response (blue, n = 260 trials) to single APs triggered in neighboring cell (black) reveals no synaptic connection. **D-F** same as for A-C but for connected cell pair, orange trace shows postsynaptic cell (n = 39 trials).

VIP cells, 13 from VIP to SST cells and 15 from VIP to VIP cells were tested. The response of one cell to single triggered APs in the neighboring cell was first analyzed across all trials (**Fig. 3.5C** and **F**).

Although exact ion concentrations of the extracellular space cannot be determined *in vivo*, we estimated the GABA reversal potential to be ~ -70 mV using our intracellular solution, thus responses in DOWN-states near the reversal potential should be small in amplitude and it may be difficult to detect a connection. Thus in a next step hyperpolarized DOWN- and depolarized UP-state responses were considered separately. Due to higher levels of synaptic activity levels in UP-states and the challenge of detecting inhibitory postsynaptic potentials (IPSPs) during DOWN-states (see **3.4**) it remained difficult to clearly distinguish between connected versus unconnected cells. After careful statistical comparison of tested connections with shuffled trials we restricted our further analysis to clear cases only, and excluded all tested connections that could not explicitly be identified as connected or unconnected (see **2.5**).

Overall, we were able to identify 11 monosynaptic inhibitory connections, and 27 unconnected neighboring cells in GAD67-GFP animals, giving a connectivity probability of 29 % among GAD cells (**Fig. 3.6A**). 4 of those 11 identified connections were part of a bidirectionally-connected cell pair (**Fig. 3.6B**). The connectivity probability among GAD cells was slightly lower than among NFS interneurons measured in a cortical slice study (Avermann et al., 2012), which was 38 %.

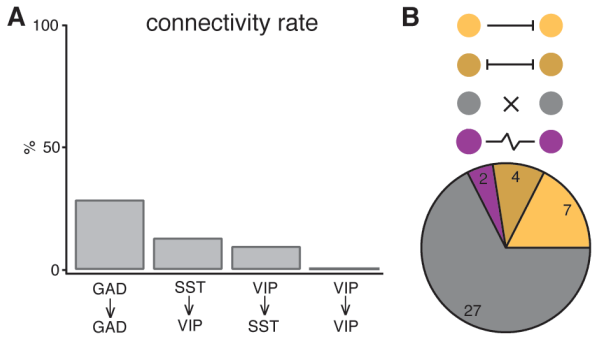

Figure 3.6: Overview of connectivity rates in the entire data set. A Histogram shows connectivity rates tested between interneurons in GAD67-GFP animals (GAD to GAD) and from SST to VIP, from VIP to SST and VIP to VIP interneurons, tested in GIN-VIPcre-Ai9 mice. **B** Pie chart shows the proportion of unconnected (grey), unidirectionally connected (orange), bidirectional connected (dark orange) and electrically coupled (purple) GAD cell pairs, tested in GAD67-GFP animals.

In GIN-VIPcre-Ai9 mice we found 2 monosynaptic connections from SST to VIP interneurons, while 13 VIP cells were not connected to the tested SST cell, resulting in a connectivity rate of 13.3 % from SST to VIP cells (2 out of 16 tested connections, whereof 1 was discarded). From VIP to SST cells we found 1 monosynaptic connection, and 9 unconnected SST cells, resulting in a probability for connectivity of 10 % for VIP to SST cells (1 out of 13 tested connections, whereof 3 were discarded). When testing for

connections from VIP to VIP cells we did not find any connection, therefore 12 unconnected cells, hence, connectivity rate was 0 % from VIP to VIP cells (0 out of 15 tested connections, whereof 3 were discarded). Previous findings in cortical slices of visual cortex report much higher connectivity rates for VIP to SST interneurons (63 %), when connectivity was verified by paired recordings (Pfeffer et al., 2013). Indirect assessment of interneuron connectivity by a combination of photostimulation of distinct cell classes and recording of inhibitory synaptic currents in specified interneurons suggest a high connectivity rate for SST to VIP cells, but low connectivity rate among VIP cells (Pfeffer et al., 2013). However, reported connectivity rates between SST and VIP vary (Jiang et al., 2015; Karnani et al., 2016b), and further research is needed to validate connectivity across cortices, layers and interneuron subtypes.

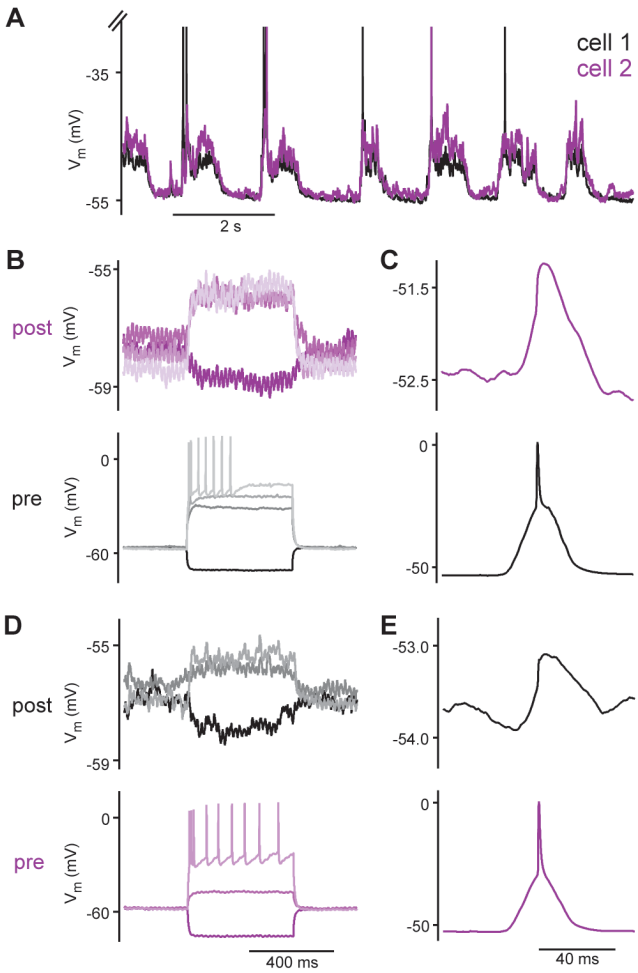

Figure 3.7: Electrically coupled pair of GABAergic interneurons measured in GAD67-GFP animal. **A** V_m recording during spontaneous activity of electrically coupled L2/3 interneurons. **B** Single V_m traces of one cell (purple) responding to long current injections to neighboring cell (black). Light purple traces correspond to light grey traces. **C** Averaged response (purple, n = 149 trials) to single APs triggered in neighboring cell (black). **D and E** Same as for A and B but tested in reversed direction (E average of n = 146 trials).

Electrical connectivity was examined by visual inspection of responses in the V_m to hyper- and depolarizing current injections in the neighboring cell. One cell pair recorded in GAD67-GFP mice (**Fig. 3.7A**) we identified as electrically coupled and excluded it from further analysis regarding the connectivity of L2/3 GABAergic interneurons. During long hyper- or depolarizing current injections of 500 ms in one cell, the V_m in the neighboring cell also de- or increased, respectively (**Fig. 3.7B** and **D**). The coupling coefficient for this cell pair was determined to be 0.1 by comparing the voltage changes before and during the current stimulus in a 300 ms time window and building the ratio between the non-injected and injected cell. Eliciting single APs via short current injections of 20 ms in one cell resulted in a depolarization of 1.2 mV (**Fig. 3.7C**) or 0.8 mV (**Fig. 3.7E**) in the V_m of the neighboring cell, respectively.

3.4 Modulation of inhibitory synaptic transmission across brain states

Under urethane anesthesia the majority of cortical neurons follow a slow rhythm (< 1 Hz) of sequences of hyperpolarized DOWN-states followed by depolarized synaptically active UP-states (Steriade et al., 1993; Wilson and Kawaguchi, 1996). So far only few attempts have been made to describe how monosynaptic transmission between excitatory neurons is modulated by an active network (Crochet et al., 2005; Bruno and Sakmann, 2006), both demonstrating that the amplitude of excitatory postsynaptic potentials (EPSPs) decreases during depolarized states. However, Pala and Petersen (2015) report no difference in the amplitude of EPSPs onto PV and SST interneurons across brain states. We therefore asked whether and how different brain states affect inhibitory synaptic transmission between L2/3 GABAergic interneurons. Once we had identified an inhibitory connection between two interneurons, the amplitude of the IPSP of the postsynaptic cell was quantified separately for UP- and DOWN-states. Only IPSP responses to single triggered APs of the presynaptic cell were analyzed.

3.4.1 IPSPs measured in GAD67-GFP mice during network activity

In GAD67-GFP mice we identified 11 monosynaptic inhibitory connections among L2/3 GABAergic interneurons. However, one of these connections showed an IPSP response only to doublets of triggered spikes in the presynaptic cell and therefore was excluded from this part of the analysis. Further, only UP-state responses of postsynaptic cells where more than 10 sweeps (51.0 ± 35.3 UP-state sweeps per recording) could be collected were included into this analysis. First, the average peak time of the IPSPs was determined as 18.0 ± 4.4 ms (**Fig. 3.8C**). Then average amplitude size of IPSPs was

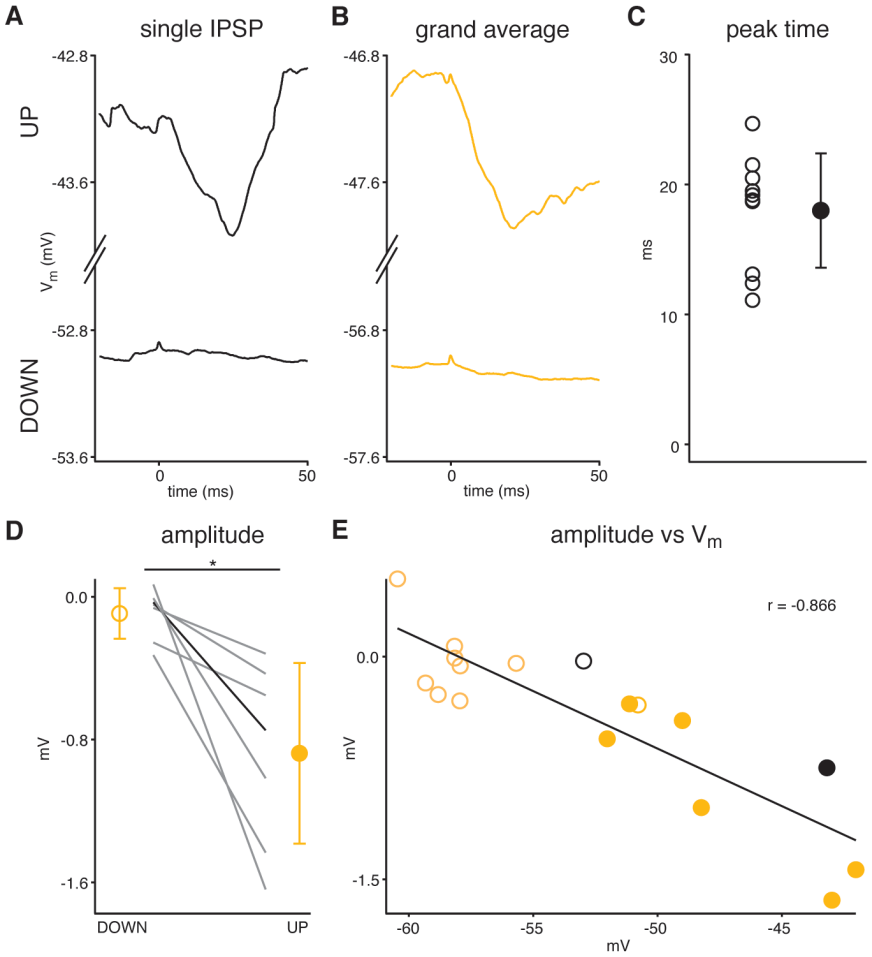

Figure 3.8: IPSP amplitude depends on brain states in GAD67-GFP animals. A Example of an average response of a postsynaptic cell during UP- (n = 42 sweeps) and DOWN-state (n = 114 sweeps) to single current evoked APs in the presynaptic cell. **B** Grand averages of IPSPs during UP- (n = 7 cells) and DOWN-states (n = 10 cells). **C** Distribution of IPSP peak times. **D** IPSP amplitudes are larger during UP- than DOWN-states. Each line represents one postsynaptic cell (n = 7), black line shows example pictured in A. **E** Linear correlation between IPSP amplitude and V_m. Open circles show IPSP amplitudes measured during DOWN-states, filled circles during UP-states, respectively. Black circles show example pictured in A. Data are represented as mean ± SD. Wilcoxon signed-rank test assessed statistical significance, indicated by * for $p < 0.05$.

analyzed separately for DOWN- and UP-state responses, revealing -0.1 ± 0.3 mV (n = 10 connections) and -0.9 ± 0.5 mV (n = 7 connections), respectively (**Fig. 3.8B**). Thus across all cells, where both, enough DOWN- and UP-state responses could be collected, IPSP amplitude was 0.8 ± 0.5 mV larger during the UP- than during the DOWN-state (p = 0.016, n = 7 connections) (**Fig. 3.8D**). Plotting IPSP amplitudes for both DOWN- and UP-states against the V_m prior to the response revealed a strong negative correlation (r = -0.866, $p < 0.001$) (**Fig. 3.8E**) and a calculated reversal potential of -58.3 mV. This suggests that *in vivo* the electrochemical driving force for Cl^- is bigger the more depolarized the V_m of a postsynaptic cell is, leading to a bigger influx of Cl^- through $GABA_A$ receptors into the cell. The same is true for $GABA_B$-mediated K^+ efflux. Given that the exact ion concentration of the extracellular space cannot be determined

in our *in vivo* recording situation and that we did not compensate for the liquid junction potential, calculated to be 7 mV (Lee et al., 2009), our calculated reversal potential was different from the estimated equilibrium potential of -96.0 mV for Cl^- or -88.8 mV for K^+. Therefore, the ion concentrations of intracellular and Ringer's solution were regarded using the Nernst equation. The kinetics of IPSPs were difficult to assess due to the difficulty in detecting IPSPs during DOWN-states and to low signal-to-noise levels, especially during UP-states, often resulting in not clearly visible decay phases of the IPSPs. Overall, during depolarized network activity inhibitory interneurons appeared to have stronger inhibition compared to hyperpolarized silent network periods.

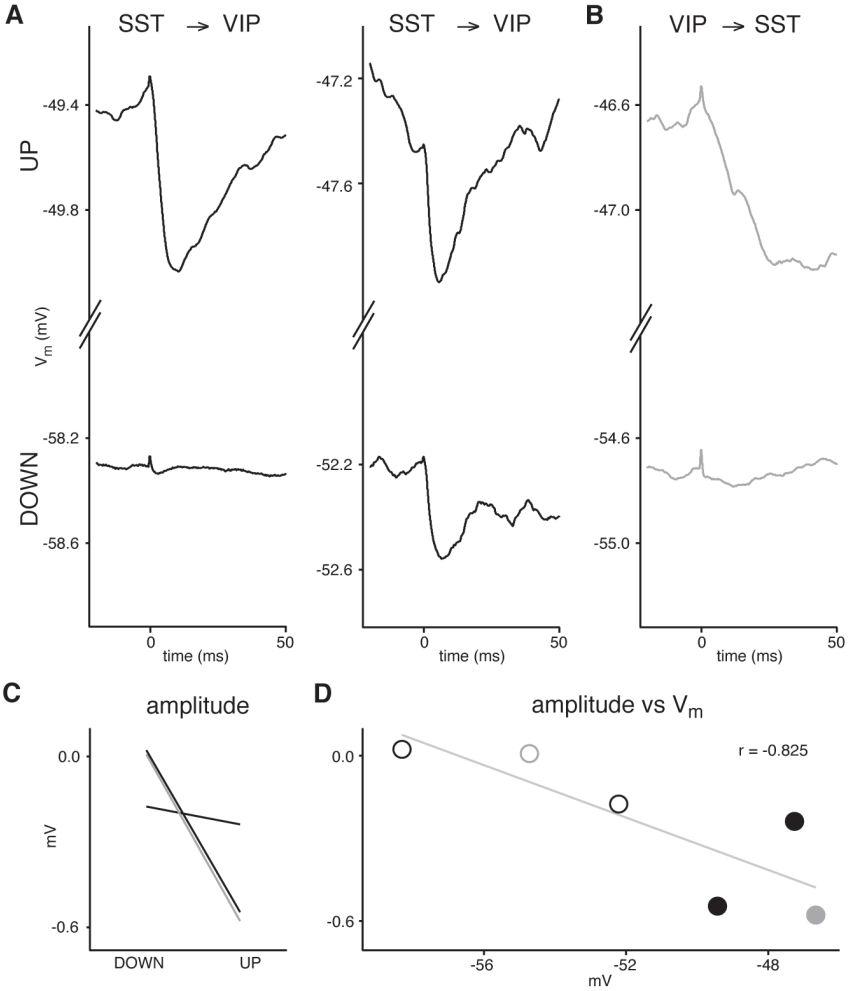

Figure 3.9: Brain states affect IPSP amplitude in GIN-VIPcre-Ai9 mice. A Average response of two postsynaptic VIP-interneurons during UP- and DOWN-states to single current evoked APs in presynaptic SST cells. **B** Average response of a postsynaptic SST interneuron during UP- and DOWN-states to single current evoked APs in the presynaptic VIP cell. **C** IPSP amplitudes are larger during UP- than DOWN-states. Black lines represent VIP cells shown in A, grey line represents SST cell shown in B. **D** Linear correlation between IPSP amplitude and V_m. Open circles show IPSP amplitudes measured during DOWN-states, filled circles during UP-states, respectively. Black symbols represent VIP cells shown in A, grey symbols represent SST cell shown in B.

3.4.2 IPSPs measured in GIN-VIPcre-Ai9 mice

In GIN-VIPcre-Ai9 mice we identified 2 monosynaptic inhibitory connections from SST to VIP cells (**Fig. 3.9A**) and one from a VIP to a SST interneuron (**Fig. 3.9B**). All 3 connections showed 0.4 ± 0.3 mV larger IPSP amplitudes for UP- than for DOWN-states, though for one SST to VIP connection the difference was only very small.

Plotting the IPSP amplitudes for both DOWN- and UP-states for connections between VIP and SST cells against the V_m prior to the response also revealed a correlation ($r = -0.825$, $p = 0.043$) (**Fig. 3.9D**) and a calculated reversal potential of -56.8 mV. Visual inspection indicated that IPSPs measured in VIP cells postsynaptic to SST cells seem to have faster kinetics than postsynaptic SST cells or other GAD cells. This aspect was not further quantified due to low sample size, but it suggests that IPSPs from SST projections onto VIP cells might be mediated solely via ionotropic $GABA_A$ receptors. In contrast, metabotropic $GABA_B$ receptors might also be involved in the generation of IPSPs in the other inhibitory cell types measured in this study, causing slower rise and decay times of IPSPs.

3.5 Comparison of V_m dynamics and spike timing during spontaneous activity

During spontaneous activity APs in cortical neurons only appear during depolarized UP- but never during hyperpolarized DOWN-states. We next examined the subthreshold events triggering spontaneous APs during an UP-state and the effect of spontaneous APs on neighboring cells. Therefore we performed spike-triggered averages (STA) of spontaneous spikes and measured the subthreshold events triggering a spike and the change in V_m before and after a spontaneous spike in a neighboring cell. STAs were made for both cells of a neighboring cell pair, based on the spike timing of one of these cells (cell 1). If both cells were spontaneously spiking, STAs were generated in both directions. We further computed peristimulus time histograms (PSTH) of cell 2 to calculate the impact of a spontaneous spike on the firing rates of neighboring cells.

From recordings obtained in GAD67-GFP animals we made n = 54 STAs and PSTHs. We observed a depolarizing peak in the average V_m of cell 2 around the time of the spike from cell 1 (**Fig. 3.10A**). However, the subthreshold synaptic input from 20 to 1 ms prior to the AP was significantly smaller for cell 2 (0.1 ± 0.1 mV/ms) than for cell 1 (0.2 ± 0.1 mV/ms, $p < 0.001$) (**Fig. 3.10C**). Nevertheless, PSTH of cell 2 in GAD-GAD cell pairs showed that APs were also generated in cell 2 around the spike times of cell 1 with firing rates ranging from 2.9 to 3.8 Hz in a 40 ms time window around the spike of

cell 1 (**Fig. 3.10B**). Further away from the spike in cell 1 the firing rates of cell 2 were around 1 to 2 Hz. In contrast, STAs and PSTHs from VIP-VIP cell pairs (n = 11) showed a broader depolarizing peak of the V_m of cell 2 (**Fig. 3.10J**) and also firing rates above 3.7 Hz in a broader time window of 80 ms around the spike time of cell 1 (**Fig. 3.10K**). Still, subthreshold input of cell 1 (0.2 ± 0.1 mV/ms) was bigger than of cell 2 (0.0 ± 0.0 mV/ms, p = 0.001) (**Fig. 3.10L**). Interestingly, when we made STAs and PSTHs for pairs of SST and VIP cells (n = 3 for SST vs VIP, n = 7 for VIP vs SST) we did not observe a depolarizing peak of the V_m of cell 2 during the spike of cell 1 (**Fig. 3.10D** and **G**). This was also reflected in the low spike rates of almost 0 Hz of cell 2 (**Fig. 3.10 E** and **H**). These observations applied for both cases, STAs and PSTHs based on the spontaneous APs of SST cells (cell1) and VIP interneurons as neighboring cells (cell 2) and vice versa. Considering VIP-SST cell pairs synaptic input prior the spike of VIP interneuron was again lower for the SST cell (0.0 ± 0.0 mV/ms) compared to the

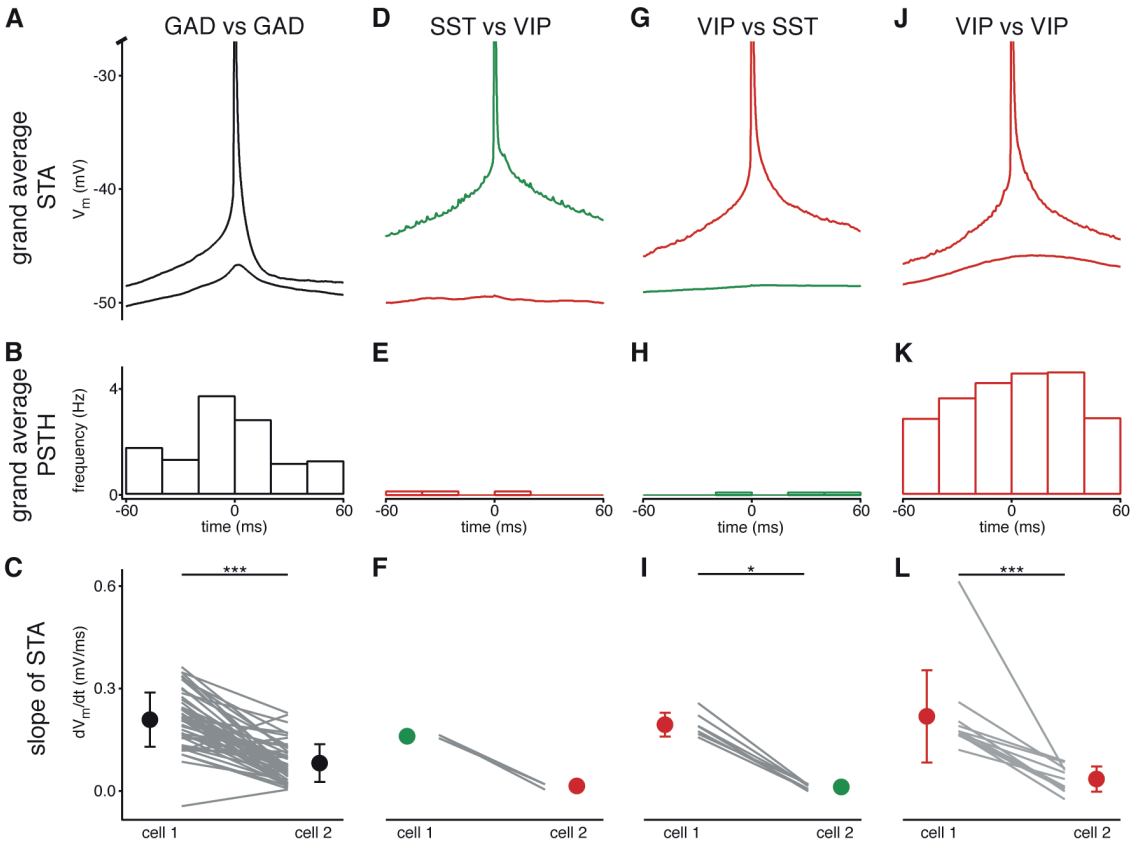

Figure 3.10: Subthreshold events and spontaneous spiking of simultaneously recorded neighboring cells. A Grand average of STAs of GAD cell pairs (n = 54, black): Upper trace shows STA of spontaneous spikes (cell 1) and lower trace shows STAs of cell 2, which are aligned to spike times of cell 1. **B** Grand averages for PSTHs, displayed as AP frequency binned in 20 ms bins, relative to spontaneous spikes of neighboring cell. **C** Comparison of the slopes of STAs prior the spike for cell 1 and cell 2, representing the subthreshold input, slopes were determined 20 to 1 ms prior the AP. **D-F** Same as for A-C, but for pairs of SST (green) and VIP cells (red), with STAs based on spontaneous spiking of SST cells (n = 3). **G-H** Same as for A-C, but for pairs of VIP and SST cells, with STAs based on spontaneous spiking of VIP cells (n = 7). **J-L** Same as for A-C, but for VIP cell pairs (n = 11). Data are represented as mean ± SD. Wilcoxon signed-rank test assessed statistical significance, indicated by * for $p < 0.05$ and *** for $p < 0.001$.

VIP cell (0.2 ± 0.0 mV/ms, p = 0.016) (**Fig. 3.10I**). Due to the overall low spike rates of SST interneurons we could make only 3 STAs and PSTHs based on the spontaneous spiking of SST cells. Therefore we found no statistical difference in the synaptic input for SST (0.2 ± 0.0 mV/ms) and VIP cells (0.0 ± 0.0 mV/ms, p = 0.250) when regarding SST-VIP cell pairs (**Fig. 3.10F**).

3.5.1 Connectivity determines spike timing during spontaneous activity in GAD67-GFP animals

Previous studies of *in vivo* connectivity typically used spike triggered averaging of spontaneous spikes to confirm connectivity (Matsumura et al., 1996; Bruno and Sakmann, 2006; Constantinople and Bruno, 2013; Yu and Ferster, 2013). We wondered whether we could correlate the connectivity that we had determined from our triggered spike analysis (see **3.3**) with the subthreshold events and spiking data we had derived from our STA and PSTH analysis. From recordings obtained in GAD67-GFP animals we made n = 27 STAs and PSTHs, that from our spike triggered analysis we had clearly determined as either monosynaptically connected (n = 8) or unconnected (n = 19) cells.

We observed that the STA of both connected and unconnected cells had a depolarizing peak around the spontaneous spike of the neighboring cell, reflecting simultaneous excitatory input from the surrounding network to both cells (**Fig. 3.11E**). The average mean V_m for STAs in a time window of 100 ms before and after the spontaneous AP in the neighboring cell did not differ for connected (-46.9 ± 4.0 mV) and unconnected neighboring cells (-49.6 ± 2.8 mV, p = 0.101). However, the peak of the V_m relative to the time of the AP in the spiking neighboring cell was more delayed for unconnected cells (3.6 ± 4.1 ms) than for connected cells (-0.3 ± 2.0 ms, p < 0.001) (**Fig. 3.11G**). We next examined the fine tuning of the synaptic input in 20 ms windows before and after the spontaneous spike and therefore determined the slope gradients during rise and decay phase (**Fig. 3.11F**). We found no difference for the rising phase of the peak between connected (0.1 ± 0.1 mV/ms) and unconnected neighboring cells (0.1 ± 0.0 mV/ms, p = 0.603). In contrast, slopes of the peak decay phase were steeper for connected (-0.1 ± 0.1 mV/ms) than for unconnected neighboring cells (-0.1 ± 0.0 mV, p < 0.001). Hence, STAs of the V_m of postsynaptic cells hyperpolarized faster than the ones of unconnected cells, presumably as a direct consequence of the IPSP caused by the presynaptic spike. We wondered what impact the rapid decrease during the peak decay phase in the V_m had on the spontaneous spike rate of postsynaptic cells (**Fig. 3.11H**). Spike rates of unconnected cells did not differ between the 20 ms time windows before (t_{bef}, 2.6 ± 3.1 Hz) and after (t_{aft}, 3.0 ± 3.4 Hz) the spontaneous AP in the neighboring cell (p = 0.415). Though not reaching significance level (p = 0.063) we observed a trend that connected cells reduced their firing rates after

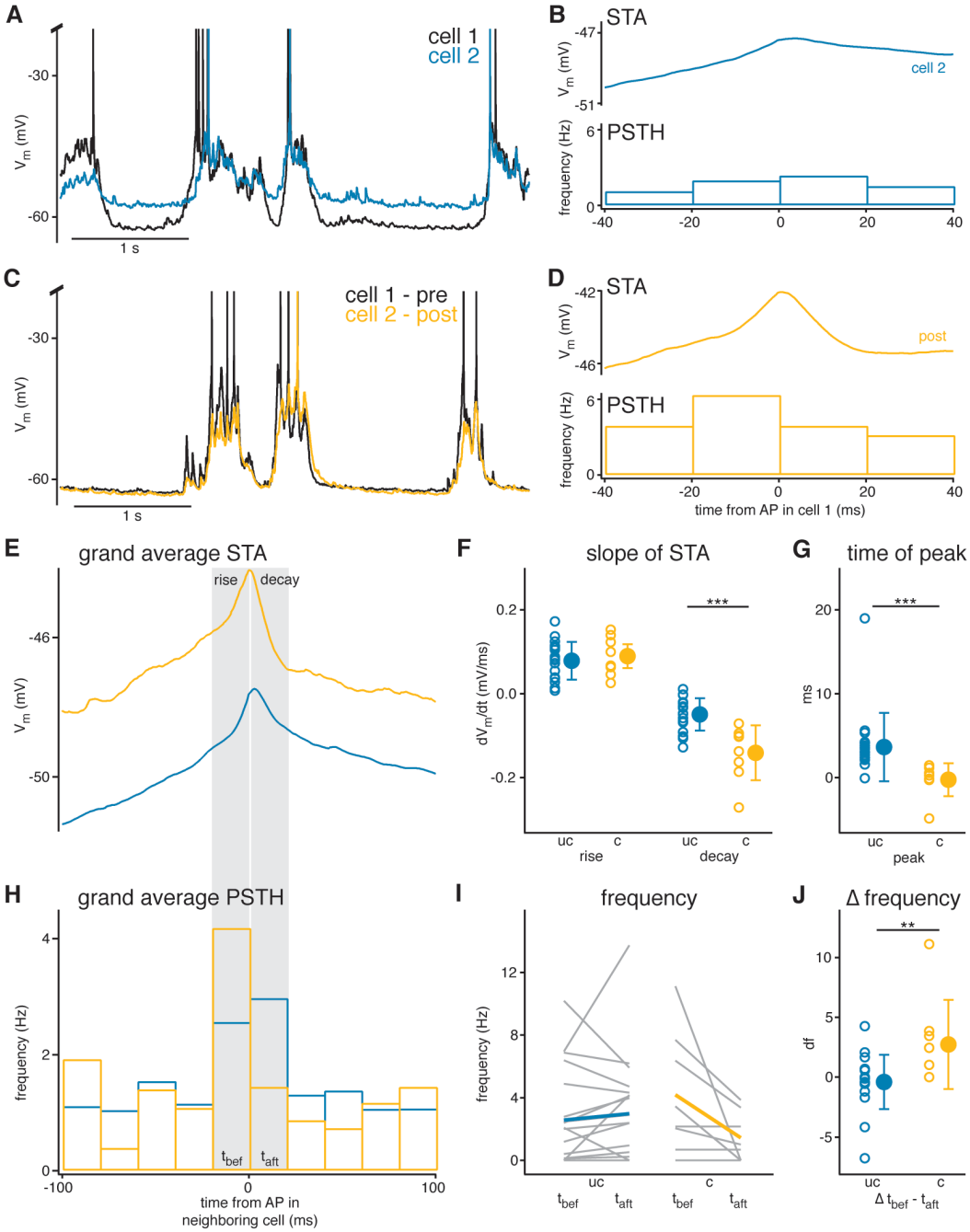

Figure 3.11: V_m and spike timing relative to spontaneous APs of neighboring cells in GAD67-GFP mice. **A** Example trace of simultaneously recorded pair of unconnected cells. **B** Upper panel: STA of cell 2 (blue trace) aligned to spike times of cell 1 (black trace) in A; lower panel: PSTH derived from cell 2 relative to spike timing of cell 1. **C and D** same as for A and B, respectively, but for pair of connected cells; black trace: presynaptic cell, orange trace: postsynaptic cell. **E** Grand averages of STAs for unconnected (n = 19, blue) and postsynaptic cells (n = 8, orange); aligned to spontaneous spikes of neighboring cell. **F** Slopes of STAs differ for unconnected (uc) and connected postsynaptic (c) cells for decay, but not for rise times. **G** Peak time of STA is more delayed for unconnected compared to postsynaptic cells. **H** Grand averages for PSTHs, displayed as AP frequency binned in 20 ms bins, for unconnected (blue) and postsynaptic cells (orange), relative to spontaneous spikes of neighboring cell. **I** Comparison of AP frequencies in 20 ms bins before (t_{bef}) and after (t_{aft}) spontaneous spikes of neighboring cells reveals no statistical difference for unconnected and postsynaptic cells. **J** Difference in AP frequency before and after spontaneous spikes of neighboring cell is higher for postsynaptic than for unconnected cells. Data are represented as mean ± SD. Wilcoxon rank-sum test assessed statistical significance, indicated by ** for $p < 0.01$ and *** for $p < 0.001$.

(t_{aft}, 1.5 ± 1.7 Hz) compared to before (t_{bef}, 4.2 ± 3.9 Hz) the occurrence of the presynaptic AP (**Fig. 3.11I**). Nonetheless, when comparing the differences in firing rates by subtracting the firing rate after from the firing rate before the spontaneous spike in the neighboring cell (**Fig. 3.11J**), we found that Δ frequency was bigger for connected (2.7 ± 3.7 Hz) than for unconnected cells (-0.4 ± 2.3 Hz, p = 0.007). This indicates, that IPSPs caused by presynaptic spikes not only affected the V_m of the postsynaptic cell, but also the firing rate. Taken together, by sharpening the slope of the V_m during the peak decay time, accompanied by a reduction in firing of spontaneous APs, the IPSP led to a shorter time window where the V_m could reach spike threshold resulting in more precise spike timing relative to the presynaptic spike. In contrast, peak decay phases were unaffected in unconnected cells, meaning that firing rates were not altered and therefore APs not so tightly time-locked to the spike in the neighboring cell.

Regarding the differences in subthreshold input and firing rates of postsynaptic connected cells compared to unconnected cells, we finally asked whether the spontaneous spikes of presynaptic cells of a connected cell pair also differed from spikes of unconnected cells (**Fig. 3.12**). Interestingly we found that spontaneous spikes of presynaptic cells of a connected cell pair showed bigger subthreshold synaptic input prior the spike (0.1 ± 0.1 mV/ms) than spikes of unconnected cells (0.1 ± 0.0 mV/ms, p = 0.374) (**Fig. 3.12B**). Further we found spikes of connected presynaptic cells to have bigger AHPs (10.6 ± 2.7 mV) than of unconnected cells (5.7 ± 2.6 mV, p < 0.001) (**Fig. 3.12C**). The different AHP values suggest that the connected GAD cell pairs might represent different cell types than the unconnected pairs. Notably, we also measured low values of AHPs of spontaneous spikes of VIP and SST, which showed low connectivity rates (see **3.2** and **3.3**).

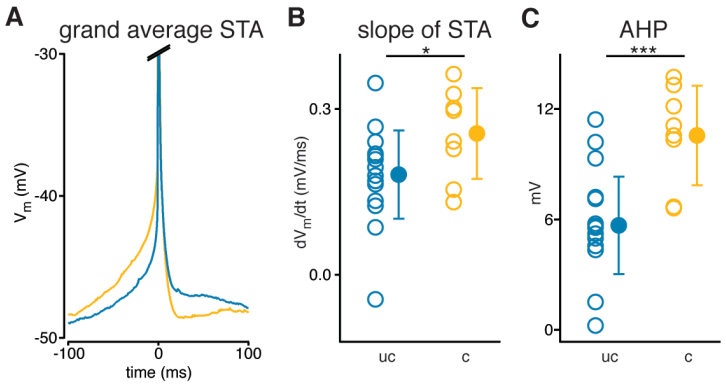

Figure 3.12: Spontaneous APs of connected presynaptic and unconnected neighboring cells in GAD67-GFP mice. A Grand average of spontaneous APs of connected presynaptic (n = 8, orange) and unconnected cells (n = 19, blue). **B** Subthreshold input triggering the spontaneous spike is bigger for connected than for unconnected cells. **C** Comparison of the AHP shows bigger AHPs for connected presynaptic cells than for unconnected cells. Data are represented as mean ± SD. Wilcoxon rank-sum test assessed statistical significance, indicated by ** for p < 0.01 and *** for p < 0.001.

3.5.2 V_m dynamics and spike timing during spontaneous activity of neighboring interneurons in GIN-VIPcre-Ai9 animals

We went on to also analyze the V_m dynamics and spike timing of connected and unconnected VIP and SST interneurons from recordings we obtained in GIN-VIPcre-Ai9 animals.

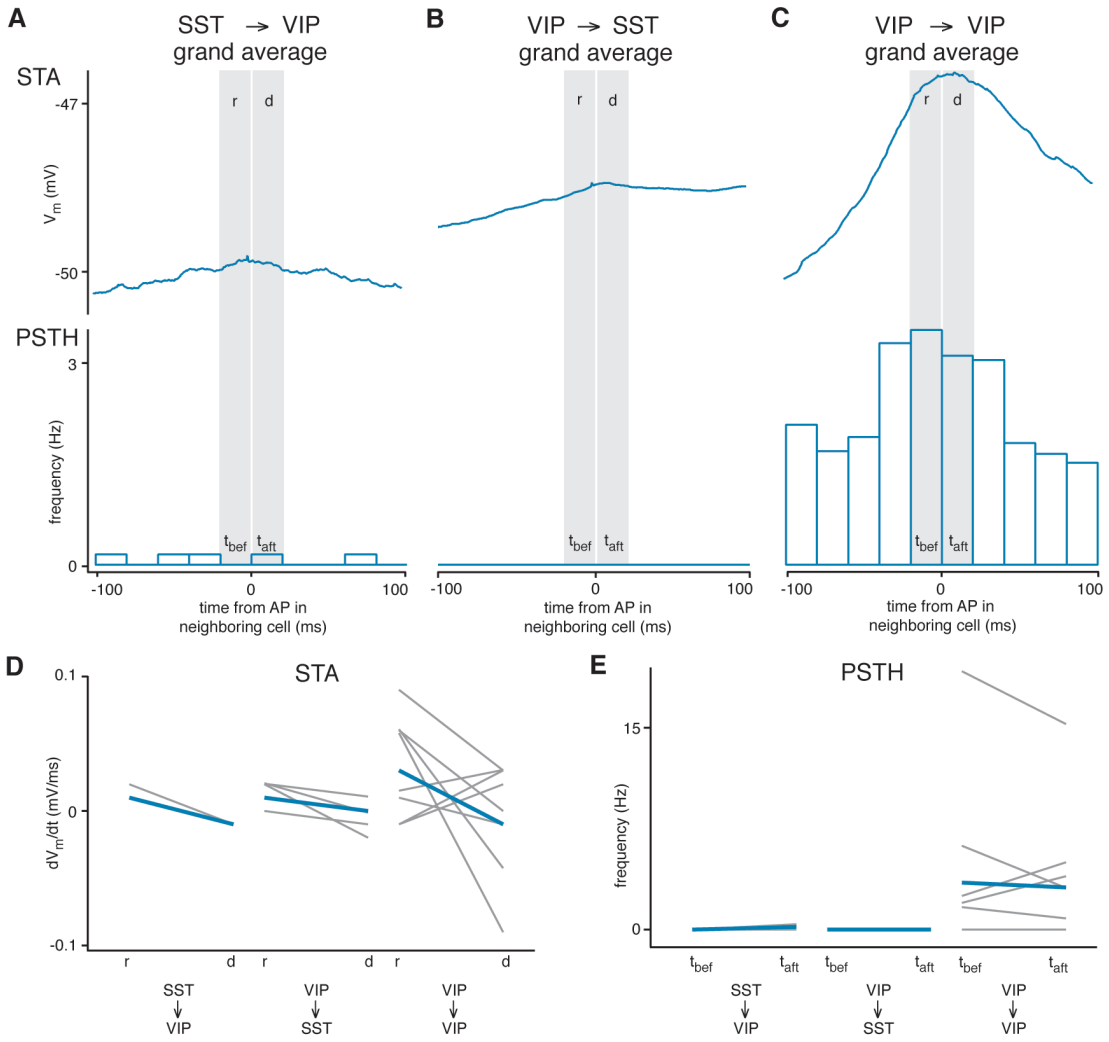

Figure 3.13: V_m dynamics and spike timing relative to spontaneous APs to unconnected neighboring cell in GIN-VIPcre-Ai9 mice. A Upper panel: Grand averages of STAs for unconnected VIP cells (n = 2) aligned to spontaneous spikes of neighboring SST cells; lower panel: Grand averages for PSTHs, displayed as AP frequency binned in 20 ms bins, for unconnected VIP cells relative to spontaneous spiking of neighboring SST cells. **B** same as for A, but for STA and PSTH of unconnected SST cells (n = 6) aligned to spontaneous spiking of VIP cells. **C** same as for A and B, but for STA and PSTH of unconnected VIP cells (n = 9) aligned to spontaneous spiking of neighboring VIP cells. **D** Slopes of STA for rise and decay times. **E** Comparison of AP frequencies in 20 ms bins before (t_{bef}) and after (t_{aft}) spontaneous spikes of unconnected neighboring cells. Grey lines represent single examples, blue lines show averages.

From the unconnected dataset we made STAs and PSTHs from n = 2 spiking SST with neighboring VIP cells (**Fig. 3.13A**). We observed that slopes for STA peak rise (0.0 ± 0.0 mV/ms) and decay times (0.0 ± 0.0 mV/ms) were more flat compared to STAs data derived from GAD67-GFP animals, without showing a distinct depolarizing peak (**Fig 3.13D**). This suggests that only little common excitatory input from the surrounding network occurred in VIP cells during spontaneous APs of SST cells. This suggestion was supported by the low levels of spike synchrony and overall spontaneous firing rates of VIP cells, quantified for 20 ms time windows before (t_{bef}, 0.0 ± 0.0 Hz) and after (t_{aft}, 0.2 ± 0.3 Hz) the APs in SST cells (**Fig. 3.13E**). We made the same observations, when comparing in reversed direction, by deriving STAs and PSTHs from unconnected SST cells aligned to spontaneous spikes of unconnected neighboring VIP cells (n = 6) (**Fig. 3.13 B**). Slopes for STA peak rise (0.1 ± 0.0 mV/ms) and decay times (0.0 ± 0.0 mV/ms) were also flat (**Fig. 3.13D**), while SST cells did not show any spontaneous firing before (t_{bef}, 0.0 ± 0.0 Hz) or after (t_{aft}, 0.0 ± 0.0 Hz) the spontaneous spike in the VIP interneuron (**Fig. 3.13E**). In contrast STAs derived from unconnected neighboring VIP cells (n = 9) (**Fig. 3.13C**) showed a depolarizing peak around the spike of the neighboring cell. Slopes were 0.0 ± 0.0 mV/ms for peak rise and 0.0 ± 0.0 mV/ms for peak decay times. Firing rates determined in 20 ms windows before and after the spontaneous AP of the neighboring rates were 3.5 ± 6.2 Hz and 3.1 ± 5.0 Hz, respectively.

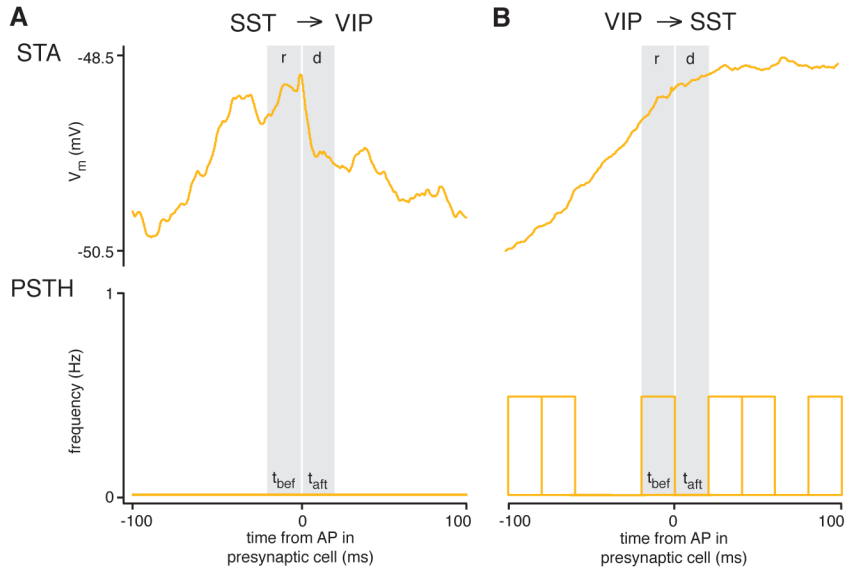

Figure 3.14: Two examples for V_m and spike timing relative to spontaneous APs of presynaptic cell in GIN-VIPcre-Ai9 mice. A Upper panel: STA of postsynaptic VIP cell aligned to spike times of presynaptic SST cell (n = 51 spikes); lower panel: PSTH derived from VIP cell relative to spike timing of the SST cell. **B** same as for A, but for presynaptic VIP and postsynaptic SST cell (n = 99 spikes).

From the connected dataset we had enough spikes only from two pairs of recordings of known connected cells to generate STAs and PSTHs. One yielded from a spiking SST

cell with a neighboring postsynaptic VIP cell (**Fig. 3.14A**). While it also showed a deflection in the V_m it did not fire any spontaneous APs before or after the presynaptic spike of the SST interneuron. The other STA was from a spiking VIP cell with a neighboring postsynaptic SST interneuron (**Fig. 3.14B**). Interestingly we did not observe any deflection in the V_m, despite being part of a known connection. However, it reached a plateau after the presynaptic AP in the VIP cell, while spike rates were low around that time window.

3.6 Comparison of V_m dynamics and spike timing relative to triggered spikes

In recordings from GAD67-GFP animals we found that V_m dynamics and spontaneous firing rates of postsynaptic, but not of unconnected neighboring cells, were altered in a 20 ms time window after the spontaneous presynaptic spike (see **3.5.1**). Due to common synaptic input driving an AP in neighboring GABAergic cells (**Fig. 3.11**), it is likely that some local cells may fire synchronously with the recorded spiking cell. We wondered whether the effect of the spontaneous AP on the postsynaptic cell was solely due to the spiking of the recorded presynaptic neuron or if there was an impact of unrecorded local GABAergic cells. Therefore we repeated the same analysis and derived STAs and PSTHs from postsynaptic (n = 7) and unconnected neighboring cells (n = 21), but this time aligned them to triggered instead of spontaneous spikes. During urethane anesthesia spontaneous spikes only occur during depolarized UP-states, hence, we only considered traces, aligned to triggered spikes, which occurred during UP-states. For triggered STAs derived in postsynaptic and unconnected cells there was no distinct depolarizing peak around the triggered spike of the neighboring cell (**Fig. 3.15A**). This indicates that the peak we observed in 3.5.1 (**Fig. 3.11E**) is mainly derived from the ongoing network activity. The average V_m for STAs in a time window of 100 ms before and after the triggered AP in the neighboring cell did not differ for postsynaptic (-47.7 ± 3.9 mV) and unconnected cells (-49.9 ± 3.8 mV, p = 0.260). This allowed us to compare the V_m dynamics around the triggered spike. We found no difference for the rising phase in a 20 ms time window before the triggered spike for postsynaptic (0.0 ± 0.0 mV/ms) and unconnected neighboring cells (0.0 ± 0.0 mV/ms, p = 0.659), indicating that synaptic input to cells was the same before the triggered spike. However, when comparing the 20 ms after the triggered spike we found that V_m dynamics were steeper for postsynaptic (-0.1 ± 0.0 mV/ms) than for unconnected cells (0.0 ± 0.0 mV/ms, p = 0.002), displaying the IPSP measured during UP-states (**Fig. 3.15B**). To test whether the descending slope of postsynaptic STAs aligned

to spontaneous presynaptic spikes only reflects the IPSP coming from the presynaptic

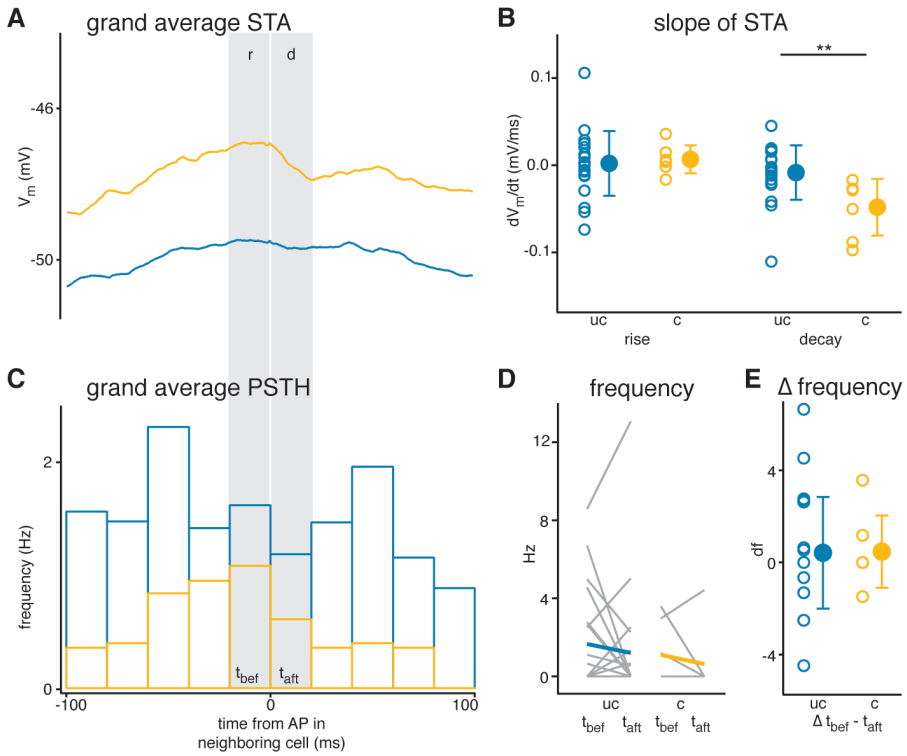

Figure 3.15: V_m dynamics and spike timing relative to triggered APs of neighboring cells in GAD67-GFP mice. A Grand averages of STAs for unconnected (n = 21, blue) and postsynaptic cells (n = 7, orange); aligned to triggered spike of neighboring cell. **B** Slopes of STAs differ for unconnected (uc) and postsynaptic (c) cells for decay, but not for rise times. **C** Grand averages for PSTHs, displayed as AP frequency binned in 20 ms bins, for unconnected (blue) and postsynaptic cells (orange), relative to triggered spike of neighboring cell. **D** Comparison of AP frequencies in 20 ms bins before (t_{bef}) and after (t_{aft}) triggered spikes of neighboring cells reveals no statistical difference for unconnected and postsynaptic cells. **E** Difference in AP frequency is not different for postsynaptic and unconnected cells before and after triggered spike of neighboring cell. Data are represented as mean ± SD. Wilcoxon rank-sum test assessed statistical significance, indicated by ** for $p < 0.01$.

cell we compared it to the slope of postsynaptic STAs aligned to triggered presynaptic spikes. We found the first case to be steeper than the latter (-0.1 ± 0.0 vs -0.1 ± 0.0 mV/ms, p = 0.004), indicating that not only the excitatory input causing the peak but also inhibitory input causing the following hyperpolarization presumably derives from the ongoing activity from the network surrounding the connected cell pair. Further, we found no change in firing rate of postsynaptic cells when comparing 20 ms bins before (t_{bef}, 1.1 ± 1.6 Hz) and after (t_{aft}, 0.6 ± 1.7 Hz, p = 0.750) the triggered presynaptic spike. Also firing rates of unconnected cells were not altered after (t_{aft}, 1.2 ± 3.0 Hz) compared to the time window before (t_{bef}, 1.6 ± 2.5 Hz, p = 0.478) the triggered spike (**Fig. 3.15D**). Therefore also the differences in firing rates before and after the triggered spike in the neighboring cell were similar for postsynaptic (0.5 ± 1.6 Hz) and unconnected cells (0.4 ± 2.4 Hz, p = 0.897) (**Fig. 3.15E**). Taken together this means, that spontaneous spikes of presynaptic GAD interneurons

and their impact on the postsynaptic GAD interneuron cannot be regarded without taking the ongoing network activity into account. Thus the effect on the spiking of a neighboring neuron from the spontaneous spike of a single GAD-positive cell is likely because of the synchronous firing of unrecorded GABAergic interneurons. Moreover a single AP in one GABAergic cell is not sufficient to alter the ongoing firing rate of a neighboring neuron even if it were synaptically connected.

3.7 Correlated activity during urethane anesthesia

Recent work has shown that connectivity in cortex is correlated to the function of the neurons. Excitatory cells in L2/3 of primary visual cortex (V1) show more connectivity if they are tuned to similar sensory stimuli (Hofer et al., 2011; Ko et al., 2011; Wertz et al., 2015). It is unknown, however, whether function is also related to connectivity between GABAergic interneurons. The slope of the rising phase of STAs aligned to spontaneous spikes of a neighboring interneuron already gives a good measurement of the nature of potential common input in nearby cells. We went on to examine whether V_m fluctuations of simultaneous recorded cell pairs under urethane anesthesia show specificity in correlated activity.

3.7.1 Characterization of correlated activity during urethane anesthesia across different cell types

We computed cross correlations of time segments of 2 s for GAD-GAD cell pairs (n = 40) recorded in GAD67-GFP animals and for VIP-SST (n = 12) as well as VIP-VIP cell pairs (n = 7) recorded in GIN-VIPcre-Ai9 animals (**Fig. 3.16, Table 2**). Cross-correlograms (**Fig. 3.16D**) showed that GAD-GAD cell pairs were highly correlated with a zero-time cross correlation coefficient of 0.8 ± 0.1, while VIP-VIP cell pairs were significantly less correlated with zero-time cross correlation coefficients of 0.6 ± 0.1. V_m dynamics of VIP-SST cell pairs showed even less synchrony with a significantly lower zero-time cross correlation coefficient of 0.5 ± 0.2 (**Fig. 3.16E**). Peak latencies (**Fig. 3.16G**) indicate the fine timing of the correlation between cell pairs. Between GAD-GAD cell pairs we observed a peak time of 0.8 ± 5.0 ms and for VIP-VIP cell pairs of 2.4 ± 5.9 ms. VIP cells were followed by SST cells by 17.0 ± 39.4 ms, with a median peak latency of 7.9 ms. As a consequence of the small peak latencies the values for the cross correlation peaks (**Fig. 3.16F**) were very similar to time-zero coefficients, namely 0.8 ± 0.1, 0.6 ± 0.1 and 0.5 ± 0.2 for pairs of GAD-GAD, VIP-VIP and VIP-SST cell pairs, respectively. Another parameter to measure the synchrony of V_m fluctuations is the halfwidth of the cross-correlogram. We determined the halfwidth at the half

amplitude measured between the zero correlation value to the peak value (**Fig. 3.16H**). A narrow halfwidth indicated that simultaneous recorded cell pairs were synchronous only in shorter time windows compared to broader halfwidth. Values for halfwidth from zero to peak for pairs of VIP and SST cells were significantly broader (374.4 ± 98.5 ms) than for GAD-GAD cell pairs (269.1 ± 53.0 ms). VIP-VIP cell pairs had significantly sharper halfwidth than the other measured cell pairs (229.1 ± 76.0 ms).

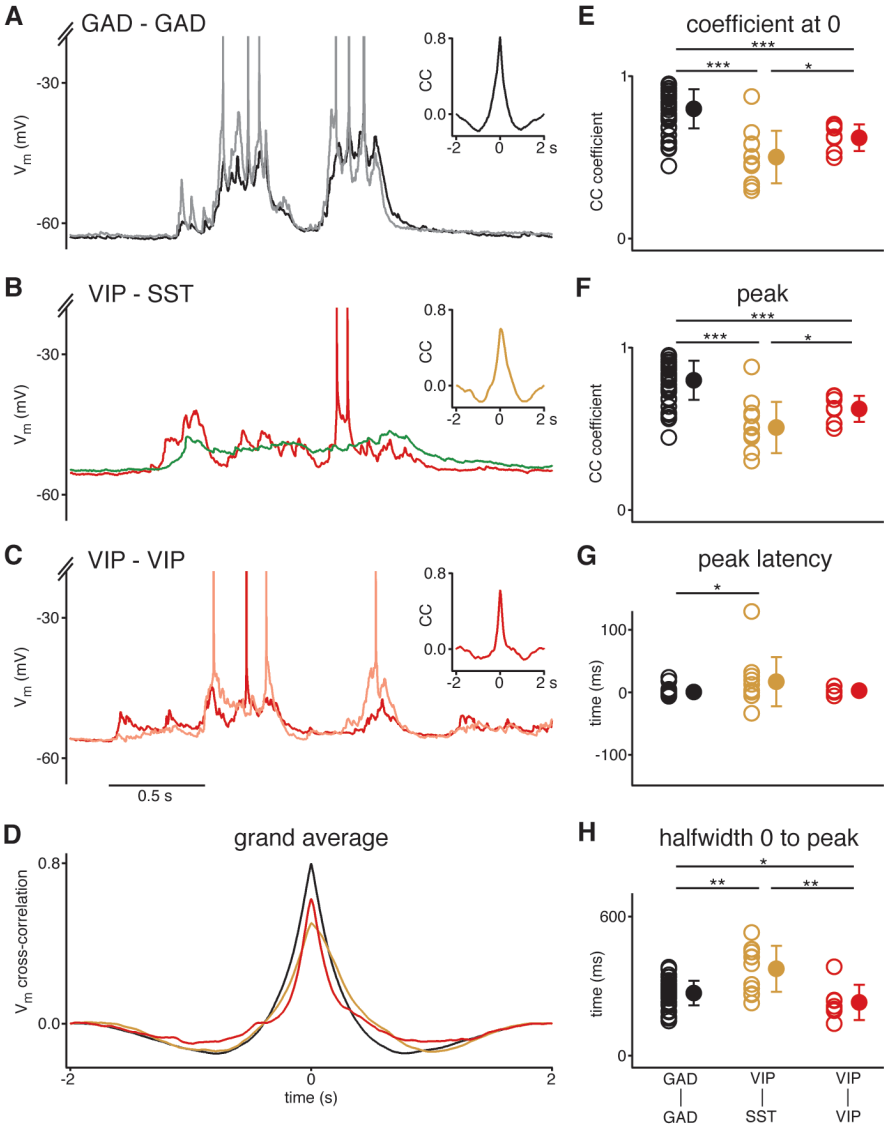

Figure 3.16: Correlated activity of different interneuron classes during urethane anesthesia. A Simultaneous dual whole-cell recording of two interneurons (GAD-GAD) shows highly synchronous activity, quantified in a cross-correlogram (inset). **B** Simultaneous recording of one VIP (red) and one SST (green) interneuron, cross-correlation shown in inset. **C** same as for A and B but for simultaneous recording of two VIP cells. **D** Grand averages of cross-correlograms for recordings of cell pairs: GAD-GAD (n = 40, black), VIP-SST (n = 12, brown), VIP-VIP (n = 7, red). **E-H** Population analysis of cross-correlograms for GAD-GAD, VIP-SST and VIP-VIP cell pairs, the following parameters were analyzed: correlation coefficient (E), peak (F), peak latency (G) and halfwidth from 0 to peak (H). Data are represented as mean ± SD. Wilcoxon rank-sum test assessed statistical significance, indicated by * for $p < 0.05$, ** for $p < 0.01$ and *** for $p < 0.001$.

Taken together all interneurons followed slow membrane oscillations during urethane anesthesia and their V_m fluctuations were highly correlated, although SST cell showed less synchrony than GAD and VIP interneurons. This appears to be in contrast to recordings yielded in awake animals, where SST interneurons were shown to be anticorrelated to excitatory cells (Gentet et al., 2012), while NFS interneurons were highly synchronous to excitatory cells (Gentet et al., 2010). Thus indicating that in the awake condition SST cells must also be anticorrelated to other interneuron types, though this has not been directly measured. VIP neurons, however, appear to have sharper temporal dynamics.

Table 3.2: P-values to assess statistical significance of cross-correlations between different interneuronal cell types, related to **Fig. 3.16**. Non-parametric Wilcoxon rank-sum test was used.

	GAD-GAD I VIP-SST	VIP-SST I VIP-VIP	GAD-GAD I VIP-VIP
coefficient at 0	< 0.001	0.032	< 0.001
peak	< 0.001	0.032	< 0.001
peak latency	0.030	0.319	0.146
halfwidth 0 to peak	0.010	0.009	0.037

3.7.2 Comparison of correlated activity between connected and unconnected GABAergic cell pairs

In a next step we compared correlated activity in connected and unconnected cell pairs. For GAD-GAD cell pairs (**Fig. 3.17A** and **C**) we found no difference ($p = 0.363$) for zero-time cross-correlation coefficients between connected (0.8 ± 0.1, $n = 9$) and unconnected pairs (0.8 ± 0.1, $n = 9$). Unexpectedly, by separating connected from unconnected cell pairs of simultaneous recordings of VIP and SST cells (**Fig. 3.17B** and **D**), we found that connected pairs were significantly less correlated ($p = 0.048$) than unconnected pairs. Zero-time cross-correlation coefficients were 0.4 ± 0.2 ($n = 3$) for connected VIP-SST cell pairs and 0.6 ± 0.2 ($n = 9$) for unconnected pairs. Since we did not find connections among VIP cells, these could not be considered for this comparison.

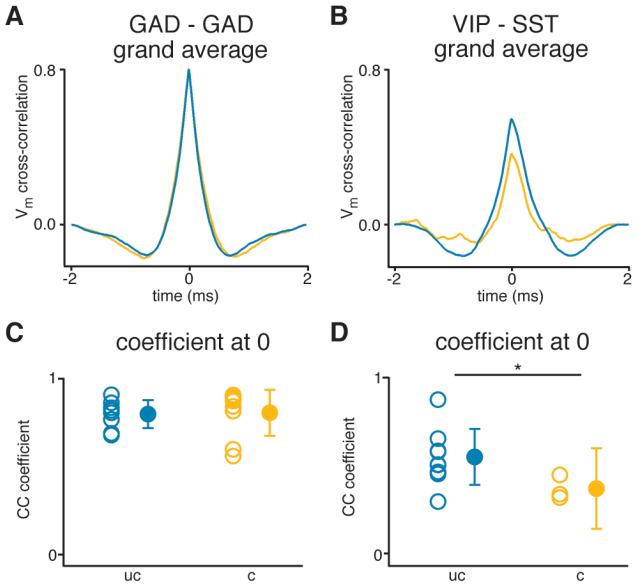

Figure 3.17: Correlated activity between connected and unconnected cell pairs. A Grand averages of cross-correlograms of connected (orange, n = 9) and unconnected (blue, n = 9) GAD-GAD cell pairs. **B** same as for A but for VIP-SST cell pairs (connected: n = 3, unconnected: n = 9). **C** Population analysis of correlation coefficient shows no difference for connected and unconnected GAD cell pairs. **D** Correlation coefficients of unconnected are higher than of connected VIP-SST cell pairs. Data are represented as mean ± SD. Wilcoxon rank-sum test assessed statistical significance, indicated by * for $p < 0.05$.

We wondered whether the strong correlations we observed for connected and unconnected GAD-GAD cell pairs were due to the synchronized activity during phases of DOWN- and UP-states, which both were covered in the time segments of 2 s that we had used for the cross-correlation analysis so far. Therefore we went on to compute cross-correlations of the STAs of cell 1 and cell 2 (see also **3.5**). To exclude any DOWN-state activity we restricted the analysis to short time segments of 40 ms, 20 ms each before and after the spontaneous spike of cell 1. This allowed us to examine the correlated activity of neighboring cells in a short time window around spontaneous spikes (**Fig. 3.18A** and **B**), and the discrimination between connected (n = 8) and unconnected (n = 19) cell pairs. We found that the cross-correlation coefficient determined at the peak was higher for connected (0.7 ± 0.1) than for unconnected cell pairs (0.6 ± 0.1, p = 0.012) (**Fig. 3.18C**). Further we could show that peak latencies were shorter for connected (0.3 ± 0.8) than for unconnected cells (1.4 ± 1.6, p = 0.032) (**Fig. 3.18D**). Overall this shows that in short time windows around spontaneous spikes connected cell pairs receive more similar synaptic input from the surrounding network than unconnected cells, as already suggested by the results from the STA analysis (see **3.5.1**).

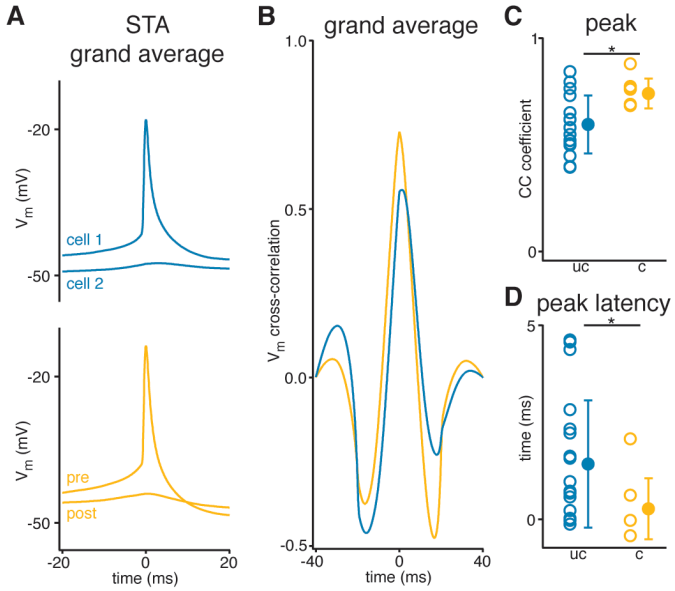

Figure 3.18: Cross-correlations of STAs of connected and unconnected cell pairs in GAD67-GFP mice. **A** Grand averages of STAs showing the V_m of the spontaneously spiking cell and the corresponding V_m of the neighboring cell, upper panel: unconnected cells, lower panel: connected cells. **B** Grand averages of cross-correlograms of STAs of connected (orange, n = 8) and unconnected (blue, n = 19) cell pairs. **C** Correlation coefficients at the peak are higher for connected than for unconnected cell pairs. **D** Peak times of unconnected cell pairs are more delayed compared to connected pairs. Data are represented as mean ± SD. Wilcoxon rank-sum test assessed statistical significance, indicated by * for $p < 0.05$.

4 Discussion

The aim of this study was to identify monosynaptic inhibitory connections between cortical interneurons *in vivo* in order to investigate (i) how brain states influence inhibitory postsynaptic potentials (IPSPs) and (ii) how connectivity determines the activity of neighboring interneurons. Therefore *in vivo* targeted whole-cell recordings were made simultaneously from layer 2/3 (L2/3) interneurons in the primary somatosensory cortex (S1) of anesthetized mice. Monosynaptic connections could be identified between interneurons recorded in GAD67-GFP animals, where interneurons are labeled without regard to specific subtypes. Although to a lesser extent, monosynaptic connections could also be identified between inhibitory cells expressing somatostatin (SST) and the vasoactive intestinal peptide (VIP) in the triple transgenic mouse line GIN-VIPcre-Ai9, which had been created in order to specifically target these interneurons. Further, recordings in both experimental settings also allowed to correlate subthreshold, but also spontaneous activity of neighboring interneurons and compare activity between connected and unconnected cell pairs.

In the following I will first discuss more general and technical aspects of the experimental approach as a basis for the results concerning the questions mentioned above. Then I will focus on characteristics of monosynaptic inhibitory transmission *in vivo* and finally relate these subjects to the ongoing cortical network activity.

4.1 Investigation of L2/3 interneurons in anesthetized mice

4.1.1 Two-photon targeted whole-cell recordings - technical aspects

Two-photon microscopy allows to image with high resolution up to several hundreds of µm deep in a tissue (Helmchen and Denk, 2005). First developed by Denk et al. (1990), it takes advantage of the two-photon effect (Göppert-Mayer, 1931), in order to emit fluorescence by using a pulsed infrared laser beam and avoid light scattering in the tissue. Today it is widely used in neuroscience for *in vitro* and *in vivo* approaches, where e.g. fine neuronal structures like spines or calcium transients indicating spiking activity need to be imaged (Svoboda and Yasuda, 2006).

Whole-cell patch clamp recordings are a standard method in neuroscience to record either ion currents across the cell membrane ('voltage clamp') or changes of the membrane potential ('current clamp') of neuronal cells in cell cultures and brain slices (Sakmann and Neher, 1984). Applied *in vivo* whole-cell current clamp recordings are a powerful tool to record sub- and suprathreshold events simultaneously in a single cell. First, these experiments have been performed as a blind patching approach (Margrie et al., 2002), where the experimenter can identify the subtype of the cell only according to the electrophysiological properties and post-hoc histological staining. Due to their relatively big soma size and numerous appearance compared to interneurons it is therefore most likely to record from pyramidal cells (PCs) using a blind approach.

By combining two-photon imaging with *in vivo* whole-cell recordings Margrie et al. (2003) first described guided patching of fluorescent genetically labeled cells in deep tissue. This technique finally allows to systematically record from sparsely occurring interneurons in the living brain and even differentiate between certain subtypes by using transgenic animals. As in our previous study (Jouhanneau et al., 2015) we extended this technique and performed whole-cell recordings simultaneously of two to three cells in anesthetized animals. It allowed to not only record from identified cells, but also to have a tight control of recording depths and distances. This approach is technically very demanding and needed several precautions: first, in order to bring three pipettes within a certain angle into the field of view one needs to carefully place and insert the pipettes into the brain and avoid too much damage of the tissue. Further by fluorescent dye which is applied to the tissue from the 3 recording pipettes with positive pressure the tissue gets saturated much faster than by using only one electrode. This together with bleaching, which occurs during imaging, yielded bad image qualities after several attempts of inserting pipettes into the brain in order to establish simultaneous whole-cell-recordings. Therefore we limited our experiment to maximum 4 trials per animal. In our previous study, we had recorded from PCs, which were filled with Alexa-594 during the recording, thus dendritic morphology could be identified. While recording from interneurons in GAD67-GFP animals we were hoping to do so again, in order to determine the interneuron subtype post-hoc by relating the anatomy with the electrophysiological properties. Unfortunately, we were not able to fill dendrites of the cells systematically, probably due to the thinner structure of interneuron dendrites.

In vivo whole-cell recordings often lack stability (Margrie et al., 2002), compared to slice recordings. Especially when recording from several cells simultaneously, where the risk of losing one of the recordings is quite high, one is very limited in the number of stimulus repeats during an experiment. To test if our two or three recorded cells were monosynaptically connected, we therefore decided to elicit spikes in neighboring neurons in an alternate fashion to be able to test in several directions the same time (see **3.3**). Further, we chose to use current clamp over voltage clamp recordings,

although during voltage clamp recordings excitatory and inhibitory conductances of the cell can easily be recorded and distinguished by clamping the cell soma to different holding potentials. However, this approach has its disadvantages: it is thought that the voltage can only be controlled at the soma, but not on the dendrites, where the majority of synaptic integration occurs; therefore measurements taken at the soma do not reflect the true nature of synaptic events (Williams and Mitchell, 2008). Additionally, current clamp recordings allowed us to record spontaneous membrane potential (V_m) and spike activity, in order to relate synaptic input to spiking output.

4.1.2 Effects of urethane anesthesia

All experiments in this study have been conducted under urethane anesthesia. In oocytes transfected with several neurotransmitters urethane has been shown to potentiate the function of $GABA_A$, glycine and nicotinic acetylcholine receptors, while inhibiting AMPA and NMDA receptors (Hara and Harris, 2002). However, as shown in visual cortical and brainstem neurons, inhibitory synaptic transmission remains unaltered upon urethane anesthesia regarding the amplitudes and time courses of GABA-mediated inhibitory events (Sceniak and Maciver, 2006; Accorsi-Mendonça et al., 2007). This makes urethane an ideal anesthetic to study inhibitory synaptic transmission *in vivo* and eventually even allows comparison with the awake condition.

Urethane anesthesia is thought to resemble natural sleep closer than other anesthetics (Clement et al., 2008), where natural sleep cycles between activated and deactivated states alternate every few minutes. However, in our recordings mainly large-amplitude oscillations, as characteristic for deactivated states have been observed, although more activated epochs also occurred rarely, but have not been examined closer. Interneurons recorded in GAD67-GFP animals and VIP cells in GIN-VIPcre-Ai9 animals typically showed slow oscillations around 1-2 Hz with alternating hyperpolarized DOWN- and depolarized UP-states as described previously (Steriade et al., 1993; Wilson and Kawaguchi, 1996). In SST interneurons UP- and DOWN-states were more difficult to distinguish, as the V_m did not show a clear bimodal distribution. Nevertheless, simultaneous recordings with VIP cells revealed that epochs of more hyper- or depolarized V_m were correlated with DOWN- or UP-states of the VIP cell, respectively.

During DOWN-states GAD and VIP cells never fired spontaneous action potentials (APs) and overall firing rates were relatively low (see **3.2**). Reduced spike rates during urethane anesthesia can be explained by the urethane mediated activation of K^+ conductances that decreases the membrane resistance (Sceniak and Maciver, 2006), while other passive membrane properties remain unaltered (Accorsi-Mendonça et al., 2007). Further, also the sparse spontaneous spiking of SST cells only occurred during UP-states, while in the awake animal the V_m of SST cells as well as their spiking behavior

tend to be anticorrelated to other cell types (Gentet et al., 2012; Fu et al., 2014). This suggests that the effect of urethane overruled other mechanisms that control brain states and interneuron activity in the awake animal. Although, various activity patterns of hippocampal interneurons during anesthesia and slow wave sleep have been reported (Isomura et al., 2006; Katona et al., 2014), it still needs to be determined to what extent neocortical interneuron activity during slow wave sleep is reflected under anesthesia.

4.1.3 Interneurons in GAD67-GFP mice

We recorded from GFP-labeled cells in L2/3 in GAD67-GFP mice, where nearly all GABAergic cells are labeled including all interneuron subgroups (Tamamaki et al., 2003). Previous studies, where recordings from L2/3 interneurons in these animals had been performed, distinguished between fast (FS) and non-fast spiking (NFS) cells, where the distinction has been made based on the AP waveform (Gentet et al., 2010; Mateo et al., 2011; Avermann et al., 2012). FS cells had thin narrow APs and were associated with higher firing rates and lower input resistances (IRs) than NFS cells, which had broader APs and were more abundant in L2/3. Avermann et al. (2012) further showed that FS but not NFS did express parvalbumin (PV). However, considering electrophysiological parameters like spontaneous AP firing rates and IR taken together with the observed broad AP waveforms, we conclude that we mainly recorded from NFS cells. This might be explained by the fact that targeting cells for whole-cell recordings was started as soon as pipettes were lowered into L2/3 indicated by the appearance of 'shadows', which reveal PCs. Thus most of the recordings were established in L2 rather than in deeper sections of L2/3, where PV interneurons get more abundant and density of NFS cells decreases (Rudy et al., 2011).

The majority of L2/3 interneuron recorded in GAD67-GFP animals showed clear UP- and DOWN-state activity with a bimodal distribution of the V_m, which was also reflected in the values derived from the Fast Fourier Transform (FFT) analysis for low frequency power. However, identified SST interneurons recorded under urethane anesthesia typically showed V_m dynamics which were distinct from the features described above. Further, we observed longer membrane time constants in SST compared to GAD cells (see **3.2**). These facts suggest that our recorded NFS interneurons also hardly included any SST cells. This might be due to two reasons: on the one hand, like PV cells, SST interneurons also get more abundant towards deeper layers (Lee et al., 2010; Rudy et al., 2011). On the other hand it has been shown that in GAD67-GFP mice the expression level of GFP in SST cells of the piriform cortex is lower compared to other interneurons (Suzuki and Bekkers, 2010). Thus the probability of SST cells to be overlooked could be relatively high if imaging conditions are not ideal. Further, during the targeting procedure one is biased to aim towards cells with bright fluorescence.

Taken together we assume that in our dataset the majority of recorded interneurons in GAD67-GFP animals belong to the group of interneurons, which express the ionotropic serotonin receptor 5HT3a. Among other, not yet fully characterized subgroups, 5HT3aR cells include VIP-expressing interneurons and neurogliaform cells (NGF) (Rudy et al., 2011). Both cell types typically have rather low firing rates and also other electrophysiological features (Jiang et al., 2015) as well their rich abundance in superficial cortical layers (Rudy et al., 2011) makes it likely that these cells match the GAD interneurons we have recorded.

4.1.4 SST and VIP interneurons in GIN-VIPcre-Ai9 mice

In order to be able to specifically target SST and VIP simultaneously we created a new mouse line. Therefore we bred triple transgenic animals (GIN-VIPcre-Ai9), by first crossing VIP-IRES-cre mice with the tdTomato reporter line Ai9. The offspring was subsequently crossed with GIN mice. Thus all VIP cells were labeled with tdTomato and a subset of SST interneurons with GFP (see **2.1** and **3.1**).

SST interneurons GFP-labeled cells were sparse, but were more apparent in L2/3 than in deeper layers (see **3.1**). However, also in L2/3 not all SST-expressing cells were labeled with GFP, but only about 40 %, which has already been shown previously (Oliva et al., 2000; Ma et al., 2006). Although we did not reconstruct dendritic and axonal projections, we could assume that all our recorded SST interneurons were Martinotti cells, as previously reported by Ma et al. (2006), who showed that GFP-expressing cells in GIN mice were Martinotti cells. Our recordings of SST interneurons in anesthetized mice revealed higher V_m and IR compared to GAD cells. Together with small low frequency power values in the FFT these results are comparable to recordings derived from SST cells in awake GIN mice (Gentet et al., 2012). However, the spontaneous firing rate seemed to be remarkably reduced in the anesthetized compared to firing rates reported for the awake state: in our condition SST interneurons hardly fired any spontaneous APs and had lower firing rates than GAD interneurons, while Gentet et al. (2012) observed the opposite. Electrophysiological parameters derived from SST interneurons recorded in anesthetized SST-cre mice were comparable to our results (Pala and Petersen, 2015).

VIP interneurons Cells expressing tdTomato were more abundant in superficial cortical layers and their appearance became sparse towards deeper layers. This observation was in line with reports from the literature (Rudy et al., 2011; Pfeffer et al., 2013). VIP interneurons have been shown to be either bitufted or bipolar cells, where both cell types are associated with irregular firing patterns (Jiang et al., 2015). There are only very few studies which performed *in vivo* electrophysiological recordings of

VIP cells, which to my knowledge do not report basic electrophysiological properties, rather than low spontaneous firing rates in the primary visual (V1) and auditory (A1) cortex (Mesik et al., 2015). However, the fact that for any electrophysiological parameter we measured the distribution of single data points did not exceed the distribution we received for GAD cell recordings, supports the idea, that VIP interneurons were also represented in the GAD population.

4.2 Measuring monosynaptic inhibitory transmission *in vivo*

4.2.1 Detection of IPSPs

The detection of monosynaptic inhibitory synaptic transmission *in vivo* is not trivial, and holds several pitfalls, regarding the stimulus paradigm, but also the post-hoc analysis. Several considerations have to be made in order to identify IPSPs and thus determine the connection probability of certain subclasses in a data set. Due to the reasons discussed below monosynaptic inhibitory connections between two cells can easily be missed and thus result in an underestimation of the connectivity rate.

A standard approach to assess connectivity in brain slices is the triggering of spike trains in the presynaptic cell with intracellular current injection (e.g. Markram et al., 1997; Jiang et al., 2015; Karnani et al., 2016b). In our approach single spikes were triggered by injecting short depolarizing current steps in two or three cells in an alternating manner in order to detect IPSPs (see **3.3**). While in brain slices triggered APs during a current pulse can be precisely timed, current injection *in vivo* results in a high jitter at a time scale of several ms during double spikes or even spike trains, thus making it difficult to relate the postsynaptic response to the presynaptic spike. Hence, single spikes were chosen on the one hand in order to be able to analyze the kinetics of IPSPs. However, this turned out to be possible only in a limited way (see **3.4** and **4.2.2**). On the other hand we aimed to avoid short-term plasticity: it is assumed that the vast majority of inhibitory synapses between L2/3 is depressing (Markram et al., 2015). However, during UP-states it often was not avoidable to trigger double rather than single spikes. Thus we found one facilitating inhibitory monosynaptic connection, which would not haven been detectable upon single spike stimulation.

During post-hoc analysis detection of IPSPs was difficult for two reasons. First, during DOWN-states the V_m of the postsynaptic cell was closer to the reversal potential for Cl^- than during UP-states, and therefore IPSPs could not always be differentiated from the resting V_m. Second, during UP-states the fluctuation of the V_m is very high due to the ongoing synaptic input from the surrounding network. Even high repetition rates of triggered spikes often did not allow for reliable detection upon averaging single trials.

Further, high failure rates of synaptic transmission might affect the detection of IPSPs, e.g. regarding excitatory synaptic transmission SST cells show higher failure rates than PV interneurons (Pala and Petersen, 2015).

Connectivity in GAD67-GFP mice We found a connectivity rate of 29 % between GAD cells in L2/3. In brain slices of GAD67-GFP animals the connection probability between NFS cells was 38 % and therefore slightly higher than in our conditions (Avermann et al., 2012). Since all interneurons in L2/3 receive dense inhibitory input from local NGF (up to 65 %) it is very likely that in our recordings NGF are represented among the presynaptic neurons; however, the likelihood of NGF belonging to the population of postsynaptic interneurons is lower, as in L2/3 they only are postsynaptic targets of either NGF or Martinotti cells (Jiang et al., 2015).

Connectivity in GIN-VIPcre-Ai9 mice In GIN-VIPcre-Ai9 mice we found only very low connectivity rates from SST to VIP cells and vice versa. Although the functional connectivity from VIP to SST cells has clearly been demonstrated (e.g. Lee et al., 2013; Pi et al., 2013; Zhang et al., 2014), reported numbers of actual monosynaptic connectivity rates still vary. Pfeffer et al. (2013) have shown high connectivity rates of more than 60 % from local VIP to SST interneurons but did not report actual rates for testing in the reverse direction from SST to VIP cells. Karnani et al. (2016b) found a connection probability of almost 30 % from VIP to SST and about 35 % from SST to VIP cells. Further they report that for both connection types the connectivity rate was higher in S1 compared to V1. However, Jiang et al. (2015) described a more differentiated scenario, as they distinguished between SST-expressing Martinotti cells, VIP-expressing bipolar cells and bitufted cells, which can express either SST or VIP: Martinotti cells have considerably high connectivity probabilities both to bitufted (48 %) and bipolar cells (44 %). In return, Martinotti cells in L2/3 receive inhibitory input only from bitufted cells (26 %), while bipolar cells exclusively target Martinotti cells in L5 (31 %). However, in all these studies mentioned above as well as for our data set the sample size for testing connectivity between SST and VIP interneurons was rather low, therefore it is difficult to give a valid estimate.

From VIP to VIP cell we did not find any monosynaptic connections. This result is according to the recent literature, which reports very low connectivity rates between VIP interneurons (Jiang et al., 2015; Karnani et al., 2016b). Sparse monosynaptic connectivity between VIP cells only exists between cells of the same morphological type, namely bitufted cells or from presynaptic bitufted to postsynaptic bipolar cells; however, one has to keep in mind that some bitufted cells can express SST rather than VIP (Jiang et al., 2015).

4.2.2 Appearance of IPSPs

In order to describe IPSPs usually several parameters are analyzed, such as amplitude, latency, half-width and decay time. However, it emerged that these parameters were very difficult to assess from *in vivo* IPSPs. Due to the synaptic input from the surrounding network often only the rising phase could be detected while especially the very start and the decay phase were not distinguishable from the background noise. We therefore limited our analysis to amplitudes and peak times of the IPSPs (see **3.4**).

$GABA_A$ versus $GABA_B$ mediated synaptic inhibition Although we were not able to systematically determine decay times of our recorded IPSPs, we recognized broad shapes of IPSPs in several of our recordings. These could be either tonic $GABA_A$ or $GABA_B$ or a combination of $GABA_A$ and $GABA_B$ mediated synaptic inhibition (Farrant and Nusser, 2005; Ulrich and Bettler, 2007). To distinguish between $GABA_A$ and $GABA_B$ mediated inhibition in our data set is difficult for two reasons. First, in our recordings derived from GAD67-GFP animals we recorded from several different interneuron subtypes. Although it is known, that e.g. NGF cells also mediate $GABA_B$ inhibition (Tamás et al., 2003; Oláh et al., 2009), there is still a lack of knowledge of IPSP kinetics for specific connections between cortical interneurons. This fact makes a further specification even more difficult for our situation. Second, due to the relatively short recording times *in vivo* it is not possible to apply pharmacological blockers for $GABA_A$ and $GABA_B$ receptors in order to differentiate between these two types of inhibition. However, we could observe fast IPSPs in postsynaptic VIP cells recorded in GIN-VIPcre-Ai9 animals. This suggests that VIP cells might only express $GABA_A$ receptors.

Amplitude differences of IPSPs across brain states *In vivo* synaptic transmission mainly occurs during depolarized network activity, where the V_m is rapidly fluctuating. Therefore it is important to distinguish and compare postsynaptic events across different network states. For excitatory postsynaptic potentials (EPSPs) mediated onto cortical PCs *in vivo* it has been shown that the EPSP amplitude depends on the brain state, with higher amplitudes in hyperpolarized states (Crochet et al., 2005; Bruno and Sakmann, 2006). However, recent unpublished data from our lab (JS Jouhanneau) showed no change of the EPSP amplitude across brain states. Further, when postsynaptic cells are either PV or SST interneurons the EPSP amplitude is on average the same for DOWN- and UP-states (Pala and Petersen, 2015). In our experiments we observed a clear increase in IPSP amplitudes from hyperpolarized DOWN-states to depolarized UP-states. Regardless if IPSPs are mediated by $GABA_A$ or $GABA_B$ receptors, this increase can be explained by the increase of electrical driving force for Cl^- or K^+ ions, respectively. However, the reversal potential for GABA in our experiments did not match our calculated reversal potentials for Cl^- or K^+, which were more negative.

This can be explained by the fact that GABA reversal potentials depend on the postsynaptic cell type (Martina et al., 2001; Chavas and Marty, 2003), and thus are regulated by interneuron specific chloride homeostatic mechanisms (Martina et al., 2001). This shunting effect has been demonstrated for inhibition in interneurons throughout development (Banke and McBain, 2006) and is thought to confer robustness of gamma oscillations (Vida et al., 2006).

IPSP amplitudes can also depend on the subtype of the postsynaptic cell. In our data set the IPSP amplitudes depended on the V_m in a linear fashion without showing any outlier data points. This argues that the postsynaptic cells recorded in GAD67-GFP animals might belong to a more homogeneous group than expected.

Other factors, such as the IR of the postsynaptic cell, might also play a role to influence the IPSP amplitude. IR measurements across brain states reveal different results: in excitatory cortical cells Mateo et al. (2011) did not find any changes, while Waters and Helmchen (2006) reported an increase during UP-states, which also has been observed in neostriatal spiny cells (Wilson and Kawaguchi, 1996). Based on findings *in vitro* and theoretical approaches other research groups assume a decrease in IR during UP-states (Destexhe et al., 2003). Not having been tested in cortical interneurons *in vivo* so far, these experiments will have to be repeated in the future for these cells.

Further, neurotransmitter release of the presynaptic cell can be influenced by the brain state (Shu et al., 2006). Another factor which is likely to influence the amplitudes of both EPSPs and IPSPs *in vivo* are the fluctuations of ion composition in the extracellular space which recently has been shown to induce changes of brain states (Ding et al., 2016).

4.2.3 Electrical coupling

We visually inspected V_m traces for responses to negative and positive current injections in the neighboring cell, which were applied in the beginning of our recordings. In doing so, we found one electrically coupled pair of GAD cells (see **3.3**). Gap junctions mainly are built between interneurons belonging to the same subgroup (Galarreta and Hestrin, 2001a), suggesting that in GAD67-GFP animals we rarely recorded from two interneurons of the same subtype simultaneously. However, Simon et al. (2005) demonstrated that NGF show gap-junctional coupling also with other interneuron subgroups. They further showed that the connectivity rate of electrical coupling was 20 % between NGF and regular-spiking non-pyramidal cells, which probably at least partly resemble our 5HT3aR-population. Therefore we might underestimate the electrical connectivity rate in our data set, if we assume that the recordings of GAD cells represent 5HT3aR-expressing interneurons and thereof some NGF cells.

In GIN-VIPcre-Ai9 we did not observe electrical coupling between SST and VIP interneurons. This again is supported by the idea that gap junctions are only built among interneurons of the same subtype. However, we were also not able to detect coupling when we recorded from two VIP cells simultaneously. This might be explained by the recently reported low electrical connection probability between VIP interneurons (Karnani et al., 2016b). Due to our low sample size it is therefore likely that we might have missed coupling between VIP cells.

Other factors can further influence the strength of electrical coupling, and thus the likelihood of detecting gap junctions *in vivo*: the number of gap junctions between coupled cells and their distance to the soma, further, the IR of the recorded cells, and also the occurrence of active conductances on soma or dendrite, which especially in our *in vivo* recording situation can not be reduced (Galarreta and Hestrin, 2001a). Finally, electrical and chemical synapses can coexist, leading to a mixed response of electrically mediated depolarization, followed by a GABA-mediated hyperpolarization (Galarreta and Hestrin, 2001a). Taking into account the ongoing network activity in our recordings it is likely that this activity masked such complex responses and that therefore we missed electrical but maybe even chemical monosynaptic connections.

4.3 Inhibitory transmission during ongoing network activity

The big advantage to assess monosynaptic connectivity *in vivo* by whole-cell recordings is the possibility to directly relate connectivity to the function of cortical neurons. E.g. investigating the activity of synaptically connected neurons allows correlations of their tuning properties upon processing sensory information. One approach to answer these questions has been accomplished by Hofer et al. (2011) and Ko et al. (2011) who determined sensory responses of ensembles of cortical neurons in V1 by calcium-imaging and post-hoc determined their synaptic connectivity by *in vitro* electrophysiological recordings. Although technically very demanding, the drawback of these experiments is the lack of information on *in vivo* subthreshold activity and thus brain-state related changes in the V_m that might differ between synaptically connected and unconnected neurons. In line with these assumptions it has been suggested that e.g. oscillatory activity in the gamma range is cell-type specific and especially affects inhibition in cortical microcircuits (Otte et al., 2010; Hasenstaub et al., 2016).

Although we did not specifically investigate sensory processing in this study we collected periods of spontaneous activity in simultaneously recorded interneurons. This allowed us to directly relate the subthreshold and spiking activity of these cell pairs with their synaptic connectivity. Using this data we were able to perform two distinct analysis. Regarding longer time segments we calculated cross-correlograms of the

V_m fluctuations. This allowed us to determine the specificity of correlated activity under urethane anesthesia. In order to examine the synaptic input but also the spiking output of a cell in relation to the spike of the neighboring cell we performed spike-triggered averages (STAs) of the V_m and peristimulus time histograms (PSTHs).

4.3.1 Correlated activity of cortical interneurons regardless of synaptic connectivity

In a first step we analyzed the impact of network activity in simultaneously recorded cortical interneurons regardless of their synaptic connectivity. This allowed us to draw conclusions on correlated activity during urethane anesthesia of interneuron subgroups in our different experimental conditions.

Cross-correlations Cross-correlation analysis was done on 2 s time segments, which generally comprised 2-4 DOWN- and UP-states periods (see **3.7.1**). It revealed high correlations in the V_m recorded during spontaneous activity almost regardless of the interneuron subtype, indicating highly synchronized cortical states under urethane anesthesia. Different mechanisms have been discussed to control cortical states. There is evidence that thalamus plays a major role in inducing desynchronized cortical states in the awake animal (Poulet et al., 2012). Further, neuromodulators also play a key role in the control of network activity, where 5HT3aR-expressing cells receive major input from serotonergic and cholinergic systems (Wester and McBain, 2014; Zagha and McCormick, 2014). However, the fluctuations of the V_m during synchronized activity might have intracortical recurrent excitatory mechanisms as theirs source (Harris and Thiele, 2011), where especially L5 PCs have been suggested to entrain cortical UP-states (Beltramo et al., 2013). Nevertheless, it is also evident that cortical interneuron activity contributes to the persistence and partially the termination of UP-states as well (Neske et al., 2015). Especially interneurons recorded simultaneously in GAD67-GFP animals showed high correlations in the V_m and distinct UP- and DOWN-state epochs. Assuming that we mainly recorded from 5HT3aR-expressing cells it suggests that this subtype plays a major role in the synchronization of the local network activity. This is supported by the fact that these cells are involved in disinhibitory circuits to entrain PC firing (Wester and McBain, 2014). However, also simultaneous V_m recordings of SST and VIP cells were correlated, although to a lesser extent. This result is in stark contrast to data from experiments, which have been carried out in awake animals where during behavior such as locomotion or whisking the activity of SST cells has been shown to be anticorrelated to the activity of other cells in the network (Gentet et al., 2012; Fu et al., 2014; Reimer et al., 2014). This suggests that urethane anesthesia has a major impact on the synchronization of the activity of cortical cells.

Another factor that helps to explain the high correlations in the V_m of GAD but also VIP cells is the fact that these cells are part of electrically coupled subnetworks, which are thought to entrain synchrony (Galarreta and Hestrin, 2001a; Overstreet-Wadiche and McBain, 2015; Karnani et al., 2016b; van Welie et al., 2016). However, experimental work in the cerebellum (Vervaeke et al., 2010) and also theoretical work (Ostojic et al., 2009a; Pfeuty et al., 2003; 2007) proposed that electrical coupling can promote asynchronous states in certain conditions.

Spike-triggered averages and peristimulus time histograms Our cross-correlation analysis of longer time segments including both DOWN- and UP-state episodes picture the synchronized network activity in the anesthetized state. However, it has been suggested that UP-state periods during anesthesia and slow-wave sleep resemble desynchronized states of the awake animal (Destexhe et al., 2007). We therefore went on to focus our analysis to time segments around spontaneous APs, which only occur during UP-states. STA and PSTH analysis allowed us to investigate the subthreshold synaptic input and spiking output, respectively, to one cell during the time of a spike in the neighboring cell and thus to draw conclusions about the synchrony of synaptic input of certain cells in the local network (see **3.5**). We found that local and temporal synchrony depended on the cell type and was reflected on the level of the V_m and even spiking. Similar to excitatory cells recorded in the awake animal (Poulet and Petersen, 2008; Gentet et al., 2010), SST and VIP cells did not show shared common excitatory or inhibitory input. In contrast, neighboring VIP interneurons were both driven by excitatory input, which, however, was temporally not strictly confined. This result was comparable to previous findings, where NFS cells showed large and broad depolarizations around the spike-timing of a fast-spiking cell in the awake animal (Gentet et al., 2010). However, when we recorded from neighboring GAD cells we observed common synaptic input to both cells in a narrow time window around the AP of cell 1 on top of a broad depolarization, which was also reflected in the spiking output, suggesting that GAD cells are also highly synchronous during UP-states. Since we assume that also VIP cells were recorded in GAD67-GFP animals there is a discrepancy in the temporal precision of synaptic input in the two data sets. This might be explained by the fact that probably we only rarely recorded from two VIP cells simultaneously in GAD67-GFP mice rather than from VIP and other interneurons. If this assumption is true, it argues that correlated activity of different interneuron subclasses, but not SST cells, is crucial for the fine-tuning of spiking output of L2/3 interneurons in a timely precise manner, supported by the view that specific interneuron types are differently engaged during certain network states (Klausberger and Somogyi, 2008). However, *in vitro* interneurons of several subclasses did not show correlated firing during network activity (Sippy and Yuste, 2013). This might argue that GAD cells in our recording

situation receive synchronized excitatory input from other brain regions, which cannot be measured *in vitro*.

4.3.2 Impact of the presynaptic spike to the postsynaptic V_m during network activity

Connectivity between cortical cells and thus the impact on spiking of the postsynaptic cells previously has only been measured indirectly *in vivo* (Snider et al., 1998; Barthó et al., 2004; Fujisawa et al., 2008). By cross-correlating the firing rates of extracellularly recorded cells the authors of these studies concluded that certain cell pairs were synaptically connected. Therefore we wondered whether the correlations we had observed between different cell types not only were subtype specific but also if monosynaptic connectivity among cells had an impact on the firing of the postsynaptic cell. Furthermore, our simultaneous whole-cell recordings not only allowed us to directly assess monosynaptic connectivity but also to relate presynaptic firing to subthreshold responses of the postsynaptic cell. Therefore we finally split our data set with regard to the connectivity we had measured beforehand.

Cross-correlations We found no difference in the cross-correlations for longer time segments comprising DOWN- and UP-states when we distinguished between connected and unconnected GAD cell pairs (see **3.7.2**). This certainly was due to the highly synchronized network activity during urethane anesthesia (see **4.3.1**), where subtle changes and short-term changes in the V_m are masked by the brain-state dependent fluctuations. We therefore went on to perform cross-correlation analysis for shorter segments only around the time of the presynaptic spike. To this end we found connected GAD cell pairs to be more correlated than unconnected pairs, suggesting that monosynaptically connected interneuron cell pairs share common synaptic input shortly before and after the presynaptic spike. Here, we assessed the correlated activity of synaptically connected cortical interneurons, which to my knowledge has not been reported in the literature so far. However, computational (Ostojic et al., 2009b) and experimental (Binder and Powers, 2001) studies regarding the connectivity either among excitatory or between excitatory and inhibitory cells also reported that the shared input to connected cells can determine the correlated activity of synaptically connected cells.

In contrast, simultaneously recorded VIP and SST cells turned out to be less correlated when they where monosynaptically connected compared to unconnected pairs. This was true for cross-correlation analysis using longer time segments comprising fluctuations of DOWN- and UP-states. Due to the low sample size in this condition these results have to be interpreted carefully. However, one can speculate whether this reflects the anticorrelated spiking of VIP and SST cells during behavior, resulting in

disinhibition of PCs, which has been reported in the awake animal (Lee et al., 2013; Fu et al., 2014). Since recordings under urethane anesthesia still reveal strong fluctuations in the V_m during DOWN- and UP-states we might not be able to observe anticorrelated activity but rather a reduction in the correlated activity of monosynaptically connected VIP and SST cells. Nevertheless, whether the reduced correlated activity in the anesthetized and the anticorrelated activity in the awake animal is solely due to monosynaptic connectivity between these cells, and to what extent further input from the local and distal network contributes to this effect, still has to be determined.

Spike-triggered averages and peristimulus time histograms By comparing the subthreshold input of cells recorded in GAD67 animals we observed a depolarizing peak in the V_m for both postsynaptic and unconnected cells around the spontaneous AP of the presynaptic cell. However, for connected cells the time of the peak was more locked to the time of the presynaptic AP and the decay in the V_m was steeper and more prominent than in unconnected cells (see **3.5.1**). These observations lead to the question whether the steep slope of the decay in the V_m and also the reduced firing of postsynaptic cells in response to the spontaneous AP was solely due to the firing of the presynaptic cell or if synchronous firing of the local network caused these effects. For excitatory cortical neurons it has been shown that artificially adding additional APs (London et al., 2010) and even EPSPs (London et al., 2002) to the network activity can cause changes in firing of the local cortical network. In our situation triggering single APs in L2/3 interneuron was not sufficient to observe similar effects, but differed from the results we had obtained while recording spontaneous activity (see **3.6**), suggesting that synchronized activity of synaptically connected interneurons in the network is necessary to cause a profound hyperpolarization and thus an alteration in the firing of the postsynaptic interneuron. This argues that different strategies might play a role in the shaping of spiking output of cortical excitatory and inhibitory cells. It has been suggested that the firing of one excitatory neuron can result in the simultaneous activation of several postsynaptic interneurons (Houweling and Brecht, 2008; London et al., 2010; Doron et al., 2014). Densely interconnected interneurons thus can fire synchronously and provide shared input to postsynaptic cells. Indeed, it has been shown that at least for fast-spiking interneurons IPSPs are more synchronized than EPSPs during recurrent network activity (Hasenstaub et al., 2005).

For cell pairs of SST and VIP cells recorded in GIN-VIPcre-Ai9 animals it was not possible to make a quantitative comparison between connected and unconnected cells, due to the low sample size (see **3.5.2**). Nevertheless for the one postsynaptic VIP cell we also observed a strong decay upon the spontaneous AP of the presynaptic SST cells, like we had seen in postsynaptic GAD cells. Interestingly, SST cells only recently have been shown to modulate excitatory synaptic transmission via presynaptic $GABA_B$ receptors during network activity (Urban-Ciecko et al., 2015). To what extent this modulation

also might play a role for inhibitory synaptic transmission onto postsynaptic VIP cells remains an open question. In the postsynaptic SST cell we could not detect such a decay in the V_m upon the presynaptic AP of the VIP cell. This might argue that spontaneous activity of VIP cells only, which in our experimental situation did not fire APs in a timely precise and correlated manner during UP-states, is not sufficient to evoke common synaptic input to SST cells. Recently it has been shown that synaptic transmission not only is modulated by network states but further by the strength of sensory stimulation (Reig et al., 2015). Therefore one could speculate if stimulus dependent activation of VIP cells from distant cortical or thalamic networks is necessary in order to effectively inhibit SST interneurons and modulate inhibitory input to these cells.

Due to the relatively low firing rates under urethane anesthesia we pooled all data regardless if presynaptic cells preferentially fired single or bursts of spontaneous APs. However, one has to keep in mind that not only the spontaneous activity of the surrounding network, but also short-term plasticity can affect and shape the appearance of IPSPs in postsynaptic cells (Markram et al., 2015; Pala and Petersen, 2015).

4.4 Future directions to investigate inhibitory monosynaptic connectivity *in vivo*

Methodical aspects and open questions By using GAD67GFP animals we were able to specify interneurons subtypes only post-hoc by analyzing the electrophysiological properties of the cells. However, this analysis does not allow to specify for genetic markers, which have been proven to help classifying cortical interneurons. For the future it therefore will be important to characterize *in vivo* IPSPs more detailed and cell type specific. Hence, it will be necessary to record from transgenic animals, where only cell types of interest are labeled. This will allow to investigate cell type specific interactions in great detail. The ongoing development of cre- and reporter lines (e.g. Madisen et al., 2010; Taniguchi et al., 2011) is of great help to specifically label and target neuronal subclasses. In a first approach we were able to record simultaneously from SST- and VIP-expressing cells by breeding the triple transgenic line GIN-VIPcre-Ai9. However, it will also be interesting to record inhibition to and from PV interneurons, but also NGF cells.

By simultaneously recording from two to three neighboring cells we could correlate their V_m dynamics and therefore also draw conclusions about the activity of the surrounding network. However, the combination of calcium imaging (Svoboda and Yasuda, 2006) with two-photon targeted recordings of synaptically connected cells would allow more detailed information of the activity of neuronal ensembles in relation

to their synaptic connectivity. This information can then be used in order to correlate the processing of sensory information in different ensembles. One aspect of particular interest will then be to investigate how sensory responses in the circuit possibly can be altered by the activation of unitary IPSPs between synaptically connected interneurons.

Our recordings were all done under urethane anesthesia, which strongly reduces neuronal firing rates and therefore has a big impact on the network activity. The ultimate goal would be to eventually even record from awake animals in order to relate monosynaptic transmission to cortical network activity during behavior and sensory processing. However, this approach would be even more demanding and difficult to achieve than recordings in anesthetized animals. Therefore it would be helpful to visualize connected cells already beforehand to specifically target synaptically connected cells. The use of retrograde transsynaptic tracing techniques with the rabies virus might be a helpful approach (Wickersham et al., 2007a; 2007b).

Conclusions Despite the limitations described above this work is the first approach to examine monosynaptic inhibitory synaptic transmission *in vivo* and investigate it during ongoing network activity. Monosynaptic inhibitory connections have been identified *in vivo* between L2/3 interneurons by using simultaneous two-photon targeted whole-cell recordings in anesthetized mice. It could be shown that the synaptic transmission was modulated by the state of the cortex with larger IPSP amplitudes during depolarized active network states. While this was true independent of interneuronal subclasses, correlated activity of neighboring cells turned out to be subtype-specific. GAD cells recorded in GAD67-GFP animal were highly correlated and also showed synchronous spiking. This effect was even pronounced when neighboring interneurons were monosynaptically connected, and also reflected in the subthreshold activity. Although still showing correlated V_m dynamics under urethane anesthesia, firing and subthreshold synaptic input were less correlated among VIP cell pairs and synchrony during UP-states was absent between SST and VIP interneurons recorded in GIN-VIPcre-Ai9 animals. Taken together this shows that correlated inhibitory network activity depends on cell-type specific subnetworks. For some of these networks firing synchrony among neighboring interneurons could be enhanced by direct monosynaptic connectivity, suggesting different functions of cortical inhibitory networks for maintaining ongoing activity and sensory processing.

Abbreviations

A1	primary auditory cortex
AHP	afterhyperpolarization
AP	action potential
EPSP	excitatory postsynaptic potential
FFT	Fast Fourier Transform
FS	fast spiking
GABA	γ -aminobutyric acid
GAD	glutamic acid decarboxylase
GFP	green fluorescent protein
IPSP	inhibitory postsynaptic potential
IR	input resistance
L	layer
MGE	medial ganglionic eminence
NFS	non-fast spiking
NGF	neurogliaform
PB	phosphate buffer
PC	pyramidal cell
PFA	paraformaldehyde
PMT	photomultiplier tube
PSTH	peristimulus time histogram
PV	parvalbumin
S1	primary somatosensory cortex
SD	standard deviation
SST	somatostatin
STA	spike-triggered average
tau	membrane time constant

V1	primary visual cortex
VIP	vasoactive intestinal peptide
V_m	membrane potential
5HT3aR	ionotropic serotonin receptor

References

Accorsi-Mendonça D, Leão RM, Aguiar JF, Varanda WA, Machado BH (2007) Urethane inhibits the GABAergic neurotransmission in the nucleus of the solitary tract of rat brain stem slices. *Am J Physiol Regul Integr Comp Physiol* 292:R396–R402.

Adesnik H, Bruns W, Taniguchi H, Huang ZJ, Scanziani M (2012) A neural circuit for spatial summation in visual cortex. *Nature* 490:226–231.

Alger BE, Nicoll RA (1979) GABA-mediated biphasic inhibitory responses in hippocampus. *Nature* 281:315–317.

Alitto HJ, Dan Y (2012) Cell-type-specific modulation of neocortical activity by basal forebrain input. *Front Syst Neurosci* 6:79.

Andersen P, Dingledine R, Gjerstad L, Langmoen IA, Laursen AM (1980) Two different responses of hippocampal pyramidal cells to application of gamma-amino butyric acid. *J Physiol* 305:279–296.

Ascoli GA, Alonso-Nanclares L, Anderson SA, Barrionuevo G, Benavides-Piccione R, Burkhalter A, Buzsáki G, Cauli B, DeFelipe J, Fairén A, Feldmeyer D, Fishell G, Fregnac Y, Freund TF, Gardner D, Gardner EP, Goldberg JH, Helmstaedter M, Hestrin S, Karube F, Kisvárday ZF, Lambolez B, Lewis DA, Marin O, Markram H, Muñoz A, Packer A, Petersen CCH, Rockland KS, Rossier J, Rudy B, Somogyi P, Staiger JF, Tamas G, Thomson AM, Toledo-Rodriguez M, Wang Y, West DC, Yuste R (2008) Petilla terminology: nomenclature of features of GABAergic interneurons of the cerebral cortex. *Nat Rev Neurosci* 9:557–568.

Atallah BV, Bruns W, Carandini M, Scanziani M (2012) Parvalbumin-expressing interneurons linearly transform cortical responses to visual stimuli. *Neuron* 73:159–170.

Avermann M, Tomm C, Mateo C, Gerstner W, Petersen CCH (2012) Microcircuits of excitatory and inhibitory neurons in layer 2/3 of mouse barrel cortex. *J Neurophysiol* 107:3116 –3134.

Banke TG, McBain CJ (2006) GABAergic input onto CA3 hippocampal interneurons remains shunting throughout development. *J Neurosci* 26:11720–11725.

Banks MI, White JA, Pearce RA (2000) Interactions between distinct GABA(A) circuits in hippocampus. *Neuron* 25:449–457.

Barthó P, Hirase H, Monconduit L, Zugaro M, Harris KD, Buzsáki G (2004) Characterization of neocortical principal cells and interneurons by network interactions and extracellular features. *J Neurophysiol* 92:600–608.

Bartos M, Vida I, Frotscher M, Meyer A, Monyer H, Geiger JRP, Jonas P (2002) Fast synaptic inhibition promotes synchronized gamma oscillations in hippocampal interneuron networks. *Proc Natl Acad Sci USA* 99:13222–13227.

Bartos M, Vida I, Jonas P (2007) Synaptic mechanisms of synchronized gamma oscillations in inhibitory interneuron networks. *Nat Rev Neurosci* 8:45–56.

Bayraktar T, Staiger JF, Acsady L, Cozzari C, Freund TF, Zilles K (1997) Co-localization of vasoactive intestinal polypeptide, gamma-aminobutyric acid and choline acetyltransferase in neocortical interneurons of the adult rat. *Brain Res* 757:209–217.

Bayraktar T, Welker E, Freund TF, Zilles K, Staiger JF (2000) Neurons immunoreactive for vasoactive intestinal polypeptide in the rat primary somatosensory cortex: morphology and spatial relationship to barrel-related columns. *J Comp Neurol* 420:291–304.

Beaulieu C (1993) Numerical data on neocortical neurons in adult rat, with special reference to the GABA population. *Brain Res* 609:284–292.

Beltramo R, D'Urso G, Dal Maschio M, Farisello P, Bovetti S, Clovis Y, Lassi G, Tucci V, De Pietri Tonelli D, Fellin T (2013) Layer-specific excitatory circuits differentially control recurrent network dynamics in the neocortex. *Nat Neurosci* 16:227–234.

Ben-Ari Y (2002) Excitatory actions of gaba during development: the nature of the nurture. *Nat Rev Neurosci* 3:728–739.

Bennett MVL, Zukin RS (2004) Electrical coupling and neuronal synchronization in the Mammalian brain. *Neuron* 41:495–511.

Berger TK, Perin R, Silberberg G, Markram H (2009) Frequency-dependent disynaptic inhibition in the pyramidal network: a ubiquitous pathway in the developing rat neocortex. *J Physiol* 587:5411–5425.

Binder MD, Powers RK (2001) Relationship between simulated common synaptic input and discharge synchrony in cat spinal motoneurons. *J Neurophysiol* 86:2266–2275.

Borst JGG (2010) The low synaptic release probability in vivo. *Trends Neurosci* 33:259–266.

Brombas A, Fletcher LN, Williams SR (2014) Activity-dependent modulation of layer 1 inhibitory neocortical circuits by acetylcholine. *J Neurosci* 34:1932–1941.

Bruno RM, Sakmann B (2006) Cortex is driven by weak but synchronously active thalamocortical synapses. *Science* 312:1622–1627.

Butt SJB, Fuccillo M, Nery S, Noctor S, Kriegstein A, Corbin JG, Fishell G (2005) The temporal and spatial origins of cortical interneurons predict their physiological subtype. *Neuron* 48:591–604.

Buzsáki G, Chrobak JJ (1995) Temporal structure in spatially organized neuronal ensembles: a role for interneuronal networks. *Curr Opin Neurobiol* 5:504–510.

Buzsáki G, Draguhn A (2004) Neuronal oscillations in cortical networks. *Science* 304:1926–1929.

Capogna M, Pearce RA (2011) GABA A,slow: causes and consequences. *Trends Neurosci* 34:101–112.

Caputi A, Rozov A, Blatow M, Monyer H (2009) Two calretinin-positive GABAergic cell types in layer 2/3 of the mouse neocortex provide different forms of inhibition. *Cereb Cortex* 19:1345–1359.

Cardin JA, Carlén M, Meletis K, Knoblich U, Zhang F, Deisseroth K, Tsai L-H, Moore CI (2009) Driving fast-spiking cells induces gamma rhythm and controls sensory responses. *Nature* 459:663–667.

Cauli B, Audinat E, Lambolez B, Angulo MC, Ropert N, Tsuzuki K, Hestrin S, Rossier J (1997) Molecular and physiological diversity of cortical nonpyramidal cells. *J Neurosci* 17:3894–3906.

Cauli B, Porter JT, Tsuzuki K, Lambolez B, Rossier J, Quenet B, Audinat E (2000) Classification of fusiform neocortical interneurons based on unsupervised clustering. *Proc Natl Acad Sci USA* 97:6144–6149.

Chalifoux JR, Carter AG (2011) GABAB receptor modulation of synaptic function. *Curr Opin Neurobiol* 21:339–344.

Chavas J, Marty A (2003) Coexistence of excitatory and inhibitory GABA synapses in the cerebellar interneuron network. *J Neurosci* 23:2019–2031.

Chen JL, Carta S, Soldado-Magraner J, Schneider BL, Helmchen F (2013) Behaviour-dependent recruitment of long-range projection neurons in somatosensory cortex. *Nature* 499:336–340.

Chittajallu R, Pelkey KA, McBain CJ (2013) Neurogliaform cells dynamically regulate somatosensory integration via synapse-specific modulation. *Nat Neurosci* 16:13–15.

Clement EA, Richard A, Thwaites M, Ailon J, Peters S, Dickson CT (2008) Cyclic and sleep-like spontaneous alternations of brain state under urethane anaesthesia. *PLoS One* 3:e2004.

Connors BW, Long MA (2004) Electrical Synapses in the Mammalian Brain. *Annu Rev Neurosci* 27:393–418.

Constantinople CM, Bruno RM (2013) Deep cortical layers are activated directly by thalamus. *Science* 340:1591–1594.

Crochet S, Chauvette S, Boucetta S, Timofeev I (2005) Modulation of synaptic transmission in neocortex by network activities. *Eur J Neurosci* 21:1030–1044.

Crochet S, Petersen CCH (2006) Correlating whisker behavior with membrane potential in barrel cortex of awake mice. *Nat Neurosci* 9:608–610.

Cruikshank SJ, Ahmed OJ, Stevens TR, Patrick SL, Gonzalez AN, Elmaleh M, Connors BW (2012) Thalamic control of layer 1 circuits in prefrontal cortex. *J Neurosci* 32:17813–17823.

Cruikshank SJ, Lewis TJ, Connors BW (2007) Synaptic basis for intense thalamocortical activation of feedforward inhibitory cells in neocortex. *Nat Neurosci* 10:462–468.

DeFelipe J, López-Cruz PL, Benavides-Piccione R, Bielza C, Larrañaga P, Anderson S, Burkhalter A, Cauli B, Fairén A, Feldmeyer D, Fishell G, Fitzpatrick D, Freund TF, González-Burgos G, Hestrin S, Hill S, Hof PR, Huang J, Jones EG, Kawaguchi Y, Kisvárday Z, Kubota Y, Lewis DA, Marín O, Markram H, McBain CJ, Meyer HS, Monyer H, Nelson SB, Rockland K, Rossier J, Rubenstein JLR, Rudy B, Scanziani M, Shepherd G, Sherwood CC, Staiger JF, Tamás G, Thomson A, Wang Y, Yuste R, Ascoli GA (2013) New insights into the classification and nomenclature of cortical GABAergic interneurons. *Nat Rev Neurosci* 14:202–216.

DeNardo LA, Berns DS, DeLoach K, Luo L (2015) Connectivity of mouse somatosensory and prefrontal cortex examined with trans-synaptic tracing. *Nat Neurosci* 18:1687–1697.

Denk W, Strickler JH, Webb WW (1990) Two-photon laser scanning fluorescence microscopy. *Science* 248:73–76.

Destexhe A, Hughes SW, Rudolph M, Crunelli V (2007) Are corticothalamic "up" states fragments of wakefulness? *Trends Neurosci* 30:334–342.

Destexhe A, Rudolph M, Paré D (2003) The high-conductance state of neocortical neurons in vivo. *Nat Rev Neurosci* 4:739–751.

Ding F, O'Donnell J, Xu Q, Kang N, Goldman N, Nedergaard M (2016) Changes in the composition of brain interstitial ions control the sleep-wake cycle. *Science* 352:550–555.

Doron G, von Heimendahl M, Schlattmann P, Houweling AR, Brecht M (2014) Spiking Irregularity and Frequency Modulate the Behavioral Report of Single-Neuron Stimulation. *Neuron* 81:653–663.

Dutar P, Nicoll RA (1988) A physiological role for GABAB receptors in the central nervous system. *Nature* 332:156–158.

Evans WH, Martin PEM (2002) Gap junctions: structure and function (Review). *Mol Membr Biol* 19:121–136.

Farrant M, Nusser Z (2005) Variations on an inhibitory theme: phasic and tonic activation of GABA(A) receptors. *Nat Rev Neurosci* 6:215–229.

Férézou I, Cauli B, Hill EL, Rossier J, Hamel E, Lambolez B (2002) 5-HT3 receptors mediate serotonergic fast synaptic excitation of neocortical vasoactive intestinal peptide/cholecystokinin interneurons. *J Neurosci* 22:7389–7397.

Fino E, Yuste R (2011) Dense inhibitory connectivity in neocortex. *Neuron* 69:1188–1203.

Fogarty M, Grist M, Gelman D, Marin O, Pachnis V, Kessaris N (2007) Spatial genetic patterning of the embryonic neuroepithelium generates GABAergic interneuron diversity in the adult cortex. *J Neurosci* 27:10935–10946.

Fu Y, Tucciarone JM, Espinosa JS, Sheng N, Darcy DP, Nicoll RA, Huang ZJ, Stryker MP (2014) A cortical circuit for gain control by behavioral state. *Cell* 156:1139–1152.

Fujisawa S, Amarasingham A, Harrison MT, Buzsáki G (2008) Behavior-dependent short-term assembly dynamics in the medial prefrontal cortex. *Nat Neurosci* 11:823–833.

Gabernet L, Jadhav SP, Feldman DE, Carandini M, Scanziani M (2005) Somatosensory integration controlled by dynamic thalamocortical feed-forward inhibition. *Neuron* 48:315–327.

Galarreta M, Hestrin S (1999) A network of fast-spiking cells in the neocortex connected by electrical synapses. *Nature* 402:72–75.

Galarreta M, Hestrin S (2001a) Electrical synapses between GABA-releasing interneurons. *Nat Rev Neurosci* 2:425–433.

Galarreta M, Hestrin S (2001b) Spike transmission and synchrony detection in networks of GABAergic interneurons. *Science* 292:2295–2299.

Gentet LJ, Avermann M, Matyas F, Staiger JF, Petersen CCH (2010) Membrane potential dynamics of GABAergic neurons in the barrel cortex of behaving mice. *Neuron* 65:422–435.

Gentet LJ, Kremer Y, Taniguchi H, Huang ZJ, Staiger JF, Petersen CCH (2012) Unique functional properties of somatostatin-expressing GABAergic neurons in mouse barrel cortex. *Nat Neurosci* 15:607–612.

Gibson JR, Beierlein M, Connors BW (1999) Two networks of electrically coupled inhibitory neurons in neocortex. *Nature* 402:75–79.

Glickfeld LL, Roberts JD, Somogyi P, Scanziani M (2009) Interneurons hyperpolarize pyramidal cells along their entire somatodendritic axis. *Nat Neurosci* 12:21–23.

Göppert-Mayer M (1931) Über Elementarakte mit zwei Quantensprüngen. *Ann Phys* 401:273–294.

Grinvald A, Lieke E, Frostig RD, Gilbert CD, Wiesel TN (1986) Functional architecture of cortex revealed by optical imaging of intrinsic signals. *Nature* 324:361–364.

Gulledge AT, Stuart GJ (2003) Excitatory actions of GABA in the cortex. *Neuron* 37:299–309.

Haider B, Häusser M, Carandini M (2013) Inhibition dominates sensory responses in the awake cortex. *Nature* 493:97–100.

Hao J, Wang XD, Dan Y, Poo MM, Zhang XH (2009) An arithmetic rule for spatial summation of excitatory and inhibitory inputs in pyramidal neurons. *Proc Natl Acad Sci USA* 106:21906–21911.

Hara K, Harris RA (2002) The anesthetic mechanism of urethane: the effects on neurotransmitter-gated ion channels. *Anesth Analg* 94:313–318.

Harris KD, Shepherd GMG (2015) The neocortical circuit: themes and variations. *Nat Neurosci* 18:170–181.

Harris KD, Thiele A (2011) Cortical state and attention. *Nat Rev Neurosci* 12:509–523.

Hasenstaub A, Otte S, Callaway E (2016) Cell Type-Specific Control of Spike Timing by Gamma-Band Oscillatory Inhibition. *Cereb Cortex* 26:797–806.

Hasenstaub A, Shu Y, Haider B, Kraushaar U, Duque A, McCormick DA (2005) Inhibitory postsynaptic potentials carry synchronized frequency information in active cortical networks. *Neuron* 47:423–435.

Helmchen F, Denk W (2005) Deep tissue two-photon microscopy. *Nat Methods* 2:932–940.

Hofer SB, Ko H, Pichler B, Vogelstein J, Ros H, Zeng H, Lein E, Lesica NA, Mrsic-Flogel TD (2011) Differential connectivity and response dynamics of excitatory and inhibitory neurons in visual cortex. *Nat Neurosci* 14:1045–1052.

Holmgren C, Harkany T, Svennenfors B, Zilberter Y (2003) Pyramidal cell communication within local networks in layer 2/3 of rat neocortex. *J Physiol* 551:139–153.

Hooks BM, Hires SA, Zhang Y-X, Huber D, Petreanu L, Svoboda K, Shepherd GMG (2011) Laminar analysis of excitatory local circuits in vibrissal motor and sensory cortical areas. *PLoS Biol* 9:e1000572.

Houweling AR, Brecht M (2008) Behavioural report of single neuron stimulation in somatosensory cortex. *Nature* 451:65–68.

Hu H, Cavendish JZ, Agmon A (2013) Not all that glitters is gold: off-target recombination in the somatostatin-IRES-Cre mouse line labels a subset of fast-spiking interneurons. *Front Neural Circuits* 7:195.

Isaacson JS, Scanziani M (2011) How inhibition shapes cortical activity. *Neuron* 72:231–243.

Isomura Y, Sirota A, Ozen S, Montgomery S, Mizuseki K, Henze DA, Buzsáki G (2006) Integration and segregation of activity in entorhinal-hippocampal subregions by neocortical slow oscillations. *Neuron* 52:871–882.

Jackson J, Ayzenshtat I, Karnani MM, Yuste R (2016) VIP+ interneurons control neocortical activity across brain states. *J Neurophysiol* 115:3008–3017.

Jessell TM, Kandel ER (1993) Synaptic transmission: a bidirectional and self-modifiable form of cell-cell communication. *Cell* 72 Suppl:1–30.

Jiang X, Shen S, Cadwell CR, Berens P, Sinz F, Ecker AS, Patel S, Tolias AS (2015) Principles of connectivity among morphologically defined cell types in adult neocortex. *Science* 350:aac9462.

Jiang X, Wang G, Lee AJ, Stornetta RL, Zhu JJ (2013) The organization of two new cortical interneuronal circuits. *Nat Neurosci* 16:210–218.

Jouhanneau JS, Kremkow J, Dorrn AL, Poulet JFA (2015) In Vivo Monosynaptic Excitatory Transmission between Layer 2 Cortical Pyramidal Neurons. *Cell Rep* 13:2098–2106.

Kaila K (1994) Ionic basis of GABAA receptor channel function in the nervous system. *Prog Neurobiol* 42:489–537.

Kapfer C, Glickfeld LL, Atallah BV, Scanziani M (2007) Supralinear increase of recurrent inhibition during sparse activity in the somatosensory cortex. *Nat Neurosci* 10:743–753.

Karnani MM, Jackson J, Ayzenshtat I, Hamzehei Sichani A, Manoocheri K, Kim S, Yuste R (2016a) Opening Holes in the Blanket of Inhibition: Localized Lateral Disinhibition by VIP Interneurons. *J Neurosci* 36:3471–3480.

Karnani MM, Jackson J, Ayzenshtat I, Tucciarone J, Manoocheri K, Snider WG, Yuste R (2016b) Cooperative Subnetworks of Molecularly Similar Interneurons in Mouse Neocortex. *Neuron* 90:86–100.

Katona L, Lapray D, Viney TJ, Oulhaj A, Borhegyi Z, Micklem BR, Klausberger T, Somogyi P (2014) Sleep and Movement Differentiates Actions of Two Types of Somatostatin-Expressing GABAergic Interneuron in Rat Hippocampus. *Neuron* 82:872–886.

Kawaguchi Y, Katsumaru H, Kosaka T, Heizmann CW, Hama K (1987) Fast spiking cells in rat hippocampus (CA1 region) contain the calcium-binding protein parvalbumin. *Brain Res* 416:369–374.

Kawaguchi Y, Kubota Y (1996) Physiological and morphological identification of somatostatin- or vasoactive intestinal polypeptide-containing cells among GABAergic cell subtypes in rat frontal cortex. *J Neurosci* 16:2701–2715.

Kawaguchi Y, Kubota Y (1997) GABAergic cell subtypes and their synaptic connections in rat frontal cortex. *Cereb Cortex* 7:476–486.

Kepecs A, Fishell G (2014) Interneuron cell types are fit to function. *Nature* 505:318–326.

Kerlin AM, Andermann ML, Berezovskii VK, Reid RC (2010) Broadly tuned response properties of diverse inhibitory neuron subtypes in mouse visual cortex. *Neuron* 67:858–871.

Kirov SA, Sorra KE, Harris KM (1999) Slices have more synapses than perfusion-fixed hippocampus from both young and mature rats. *J Neurosci* 19:2876–2886.

Kitamura K, Judkewitz B, Kano M, Denk W, Häusser M (2008) Targeted patch-clamp recordings and single-cell electroporation of unlabeled neurons in vivo. *Nat Methods* 5:61–67.

Klausberger T, Somogyi P (2008) Neuronal diversity and temporal dynamics: the unity of hippocampal circuit operations. *Science* 321:53–57.

Ko H, Hofer SB, Pichler B, Buchanan KA, Sjöström PJ, Mrsic-Flogel TD (2011) Functional specificity of local synaptic connections in neocortical networks. *Nature* 473:87–91.

Kubota Y, Hattori R, Yui Y (1994) Three distinct subpopulations of GABAergic neurons in rat frontal agranular cortex. *Brain Res* 649:159–173.

Kuki T, Fujihara K, Miwa H, Tamamaki N, Yanagawa Y, Mushiake H (2015) Contribution of parvalbumin and somatostatin-expressing GABAergic neurons to slow oscillations and the balance in beta-gamma oscillations across cortical layers. *Front Neural Circuits* 9:6.

Kullmann DM (2000) Spillover and synaptic cross talk mediated by glutamate and GABA in the mammalian brain. *Prog Brain Res* 125:339–351.

Kullmann DM, Ruiz A, Rusakov DM, Scott R, Semyanov A, Walker MC (2005) Presynaptic, extrasynaptic and axonal GABAA receptors in the CNS: where and why? *Prog Biophys Mol Biol* 87:33–46.

Lee AK, Epsztein J, Brecht M (2009) Head-anchored whole-cell recordings in freely moving rats. *Nat Protoc* 4:385–392.

Lee SH, Kwan AC, Zhang S, Phoumthipphavong V, Flannery JG, Masmanidis SC, Taniguchi H, Huang ZJ, Zhang F, Boyden ES, Deisseroth K, Dan Y (2012) Activation of specific interneurons improves V1 feature selectivity and visual perception. *Nature* 488:379–383.

Lee S, Hjerling-Leffler J, Zagha E, Fishell G, Rudy B (2010) The largest group of superficial neocortical GABAergic interneurons expresses ionotropic serotonin receptors. *J Neurosci* 30:16796–16808.

Lee S, Kruglikov I, Huang ZJ, Fishell G, Rudy B (2013) A disinhibitory circuit mediates motor integration in the somatosensory cortex. *Nat Neurosci* 16:1662–1670.

Lefort S, Tomm C, Floyd Sarria J-C, Petersen CCH (2009) The excitatory neuronal network of the C2 barrel column in mouse primary somatosensory cortex. *Neuron* 61:301–316.

Letzkus JJ, Wolff SBE, Meyer EMM, Tovote P, Courtin J, Herry C, Lüthi A (2011) A disinhibitory microcircuit for associative fear learning in the auditory cortex. *Nature* 480:331–335.

London M, Roth A, Beeren L, Häusser M, Latham PE (2010) Sensitivity to perturbations in vivo implies high noise and suggests rate coding in cortex. *Nature* 466:123–127.

London M, Schreibman A, Häusser M, Larkum ME, Segev I (2002) The information efficacy of a synapse. *Nat Neurosci* 5:332–340.

Ma Y, Hu H, Berrebi AS, Mathers PH, Agmon A (2006) Distinct subtypes of somatostatin-containing neocortical interneurons revealed in transgenic mice. *J Neurosci* 26:5069–5082.

Madisen L, Zwingman TA, Sunkin SM, Oh SW, Zariwala HA, Gu H, Ng LL, Palmiter RD, Hawrylycz MJ, Jones AR, Lein ES, Zeng H (2010) A robust and high-throughput Cre reporting and characterization system for the whole mouse brain. *Nat Neurosci* 13:133–140.

Magistretti PJ (1990) VIP neurons in the cerebral cortex. *Trends Pharmacol Sci* 11:250–254.

Margrie TW, Brecht M, Sakmann B (2002) In vivo, low-resistance, whole-cell recordings from neurons in the anaesthetized and awake mammalian brain. *Pflugers Arch* 444:491–498.

Margrie TW, Meyer AH, Caputi A, Monyer H, Hasan MT, Schaefer AT, Denk W, Brecht M (2003) Targeted whole-cell recordings in the mammalian brain in vivo. *Neuron* 39:911–918.

Markram H, Muller E, Ramaswamy S, Reimann MW, Abdellah M, Sanchez CA, Ailamaki A, Alonso-Nanclares L, Antille N, Arsever S, Kahou GAA, Berger TK, Bilgili A, Buncic N, Chalimourda A, Chindemi G, Courcol JD, Delalondre F, Delattre V, Druckmann S, Dumusc R, Dynes J, Eilemann S, Gal E, Gevaert ME, Ghobril JP, Gidon A, Graham JW, Gupta A, Haenel V, Hay E, Heinis T, Hernando JB, Hines M, Kanari L, Keller D, Kenyon J, Khazen G, Kim Y, King JG, Kisvarday Z, Kumbhar P, Lasserre S, Le Bé JV, Magalhães BRC, Merchán-Pérez A, Meystre J, Morrice BR, Muller J, Muñoz-Céspedes A, Muralidhar S, Muthurasa K, Nachbaur D, Newton TH, Nolte M, Ovcharenko A, Palacios J, Pastor L, Perin R, Ranjan R, Riachi I, Rodríguez JR, Riquelme JL, Rössert C, Sfyrakis K, Shi Y, Shillcock JC, Silberberg G, Silva R, Tauheed F, Telefont M, Toledo-Rodriguez M, Tränkler T, Van Geit W, Díaz JV, Walker R, Wang Y, Zaninetta SM, DeFelipe J, Hill SL, Segev I, Schürmann F (2015) Reconstruction and Simulation of Neocortical Microcircuitry. *Cell* 163:456–492.

Markram H, Lübke J, Frotscher M, Sakmann B (1997) Regulation of synaptic efficacy by coincidence of postsynaptic APs and EPSPs. *Science* 275:213–215.

Markram H, Toledo-Rodriguez M, Wang Y, Gupta A, Silberberg G, Wu C (2004) Interneurons of the neocortical inhibitory system. *Nat Rev Neurosci* 5:793–807.

Martina M, Royer S, Paré D (2001) Cell-type-specific GABA responses and chloride homeostasis in the cortex and amygdala. *J Neurophysiol* 86:2887–2895.

Mateo C, Avermann M, Gentet LJ, Zhang F, Deisseroth K, Petersen CCH (2011) In Vivo Optogenetic Stimulation of Neocortical Excitatory Neurons Drives Brain-State-Dependent Inhibition. *Curr Biol* 21:1593–1602.

Matsumura M, Chen D, Sawaguchi T, Kubota K, Fetz EE (1996) Synaptic interactions between primate precentral cortex neurons revealed by spike-triggered averaging of intracellular membrane potentials in vivo. *J Neurosci* 16:7757–7767.

McGarry LM, Packer AM, Fino E, Nikolenko V, Sippy T, Yuste R (2010) Quantitative classification of somatostatin-positive neocortical interneurons identifies three interneuron subtypes. *Front Neural Circuits* 4:12.

McGinley MJ, David SV, McCormick DA (2015) Cortical Membrane Potential Signature of Optimal States for Sensory Signal Detection. *Neuron* 87:179–192.

Mesik L, Ma W-P, Li L-Y, Ibrahim LA, Huang ZJ, Zhang LI, Tao HW (2015) Functional response properties of VIP-expressing inhibitory neurons in mouse visual and auditory cortex. *Front Neural Circuits* 9:22.

Meyer HS, Schwarz D, Wimmer VC, Schmitt AC, Kerr JND, Sakmann B, Helmstaedter M (2011) Inhibitory interneurons in a cortical column form hot zones of inhibition in layers 2 and 5A. *Proc Natl Acad Sci USA* 108:16807–16812.

Miyoshi G, Butt SJB, Takebayashi H, Fishell G (2007) Physiologically distinct temporal cohorts of cortical interneurons arise from telencephalic Olig2-expressing precursors. *J Neurosci* 27:7786–7798.

Miyoshi G, Hjerling-Leffler J, Karayannis T, Sousa VH, Butt SJB, Battiste J, Johnson JE, Machold RP, Fishell G (2010) Genetic fate mapping reveals that the caudal ganglionic eminence produces a large and diverse population of superficial cortical interneurons. *J Neurosci* 30:1582–1594.

Mody I, De Koninck Y, Otis TS, Soltesz I (1994) Bridging the cleft at GABA synapses in the brain. *Trends Neurosci* 17:517–525.

Molnár G, Oláh S, Komlósi G, Füle M, Szabadics J, Varga C, Barzó P, Tamas G (2008) Complex events initiated by individual spikes in the human cerebral cortex. *PLoS Biol* 6:e222.

Neske GT, Patrick SL, Connors BW (2015) Contributions of diverse excitatory and inhibitory neurons to recurrent network activity in cerebral cortex. *J Neurosci* 35:1089–1105.

Niell CM, Stryker MP (2010) Modulation of visual responses by behavioral state in mouse visual cortex. *Neuron* 65:472–479.

Okun M, Lampl I (2008) Instantaneous correlation of excitation and inhibition during ongoing and sensory-evoked activities. *Nat Neurosci* 11:535–537.

Oláh S, Füle M, Komlósi G, Varga C, Báldi R, Barzó P, Tamas G (2009) Regulation of cortical microcircuits by unitary GABA-mediated volume transmission. *Nature* 461:1278–1281.

Oláh S, Komlósi G, Szabadics J, Varga C, Tóth E, Barzó P, Tamas G (2007) Output of neurogliaform cells to various neuron types in the human and rat cerebral cortex. *Front Neural Circuits* 1:4.

Oliva AA, Jiang M, Lam T, Smith KL, Swann JW (2000) Novel hippocampal interneuronal subtypes identified using transgenic mice that express green fluorescent protein in GABAergic interneurons. *J Neurosci* 20:3354–3368.

Ostojic S, Brunel N, Hakim V (2009a) Synchronization properties of networks of electrically coupled neurons in the presence of noise and heterogeneities. *J Comput Neurosci* 26:369–392.

Ostojic S, Brunel N, Hakim V (2009b) How connectivity, background activity, and synaptic properties shape the cross-correlation between spike trains. *J Neurosci* 29:10234–10253.

Otte S, Hasenstaub A, Callaway EM (2010) Cell type-specific control of neuronal responsiveness by gamma-band oscillatory inhibition. *J Neurosci* 30:2150–2159.

Overstreet-Wadiche L, McBain CJ (2015) Neurogliaform cells in cortical circuits. *Nat Rev Neurosci* 16:458–468.

Packer AM, Yuste R (2011) Dense, unspecific connectivity of neocortical parvalbumin-positive interneurons: a canonical microcircuit for inhibition? *J Neurosci* 31:13260–13271.

Pala A, Petersen CCH (2015) In vivo measurement of cell-type-specific synaptic connectivity and synaptic transmission in layer 2/3 mouse barrel cortex. *Neuron* 85:68–75.

Paulus W, Rothwell JC (2016) Membrane resistance and shunting inhibition: where biophysics meets state-dependant human neurophysiology. *J Physiol (Lond)* 594:2719–2728.

Paxinos G, Franklin KBJ (2013) The Mouse Brain in Stereotaxic Coordinates. *Elsevier Academic Press*.

Payne JA, Rivera C, Voipio J, Kaila K (2003) Cation-chloride co-transporters in neuronal communication, development and trauma. *Trends Neurosci* 26:199–206.

Pfeffer CK (2014) Inhibitory neurons: vip cells hit the brake on inhibition. *Curr Biol* 24:R18–R20.

Pfeffer CK, Xue M, He M, Huang ZJ, Scanziani M (2013) Inhibition of inhibition in visual cortex: the logic of connections between molecularly distinct interneurons. *Nat Neurosci* 16:1068–1076.

Pfeuty B, Golomb D, Mato G, Hansel D (2007) Inhibition potentiates the synchronizing action of electrical synapses. *Front Comput Neurosci* 1:8.

Pfeuty B, Mato G, Golomb D, Hansel D (2003) Electrical synapses and synchrony: the role of intrinsic currents. *J Neurosci* 23:6280–6294.

Pi HJ, Hangya B, Kvitsiani D, Sanders JI, Huang ZJ, Kepecs A (2013) Cortical interneurons that specialize in disinhibitory control. *Nature* 503:521–524.

Polack PO, Friedman J, Golshani P (2013) Cellular mechanisms of brain state-dependent gain modulation in visual cortex. *Nat Neurosci* 16:1331–1339.

Porter JT, Cauli B, Staiger JF, Lambolez B, Rossier J, Audinat E (1998) Properties of bipolar VIPergic interneurons and their excitation by pyramidal neurons in the rat neocortex. *Eur J Neurosci* 10:3617–3628.

Poulet JFA, Fernandez LMJ, Crochet S, Petersen CCH (2012) Thalamic control of cortical states. *Nat Neurosci* 15:370–372.

Poulet JFA, Petersen CCH (2008) Internal brain state regulates membrane potential synchrony in barrel cortex of behaving mice. *Nature* 454:881–885.

Price CJ, Cauli B, Kovacs ER, Kulik A, Lambolez B, Shigemoto R, Capogna M (2005) Neurogliaform neurons form a novel inhibitory network in the hippocampal CA1 area. *J Neurosci* 25:6775–6786.

Prönneke A, Scheuer B, Wagener RJ, Möck M, Witte M, Staiger JF (2015) Characterizing VIP Neurons in the Barrel Cortex of VIPcre/tdTomato Mice Reveals Layer-Specific Differences. *Cereb Cortex* 25:4854–4868.

Reig R, Zerlaut Y, Vergara R, Destexhe A, Sanchez-Vives MV (2015) Gain modulation of synaptic inputs by network state in auditory cortex in vivo. *J Neurosci* 35:2689–2702.

Reimer J, Froudarakis E, Cadwell CR, Yatsenko D (2014) Pupil Fluctuations Track Fast Switching of Cortical States during Quiet Wakefulness. *Neuron* 84:355–362.

Ren JQ, Aika Y, Heizmann CW, Kosaka T (1992) Quantitative analysis of neurons and glial cells in the rat somatosensory cortex, with special reference to GABAergic neurons and parvalbumin-containing neurons. *Exp Brain Res* 92:1–14.

Ringach DL (2009) Spontaneous and driven cortical activity: implications for computation. *Curr Opin Neurobiol* 19:439–444.

Rudy B, Fishell G, Lee S, Hjerling-Leffler J (2011) Three groups of interneurons account for nearly 100% of neocortical GABAergic neurons. *Dev Neurobiol* 71:45–61.

Sachidhanandam S, Sreenivasan V, Kyriakatos A, Kremer Y, Petersen CCH (2013) Membrane potential correlates of sensory perception in mouse barrel cortex. *Nat Neurosci* 16:1671–1677.

Sakaba T, Neher E (2003) Direct modulation of synaptic vesicle priming by GABA(B) receptor activation at a glutamatergic synapse. *Nature* 424:775–778.

Sakmann B, Neher E (1984) Patch clamp techniques for studying ionic channels in excitable membranes. *Annu Rev Physiol* 46:455–472.

Saleem AB, Ayaz A, Jeffery KJ, Harris KD, Carandini M (2013) Integration of visual motion and locomotion in mouse visual cortex. *Nat Neurosci* 16:1864–1869.

Sceniak MP, Maciver MB (2006) Cellular actions of urethane on rat visual cortical neurons in vitro. *J Neurophysiol* 95:3865–3874.

Seybold BA, Phillips EAK, Schreiner CE, Hasenstaub AR (2015) Inhibitory Actions Unified by Network Integration. *Neuron* 87:1181–1192.

Shu Y, Hasenstaub A, Duque A, Yu Y, McCormick DA (2006) Modulation of intracortical synaptic potentials by presynaptic somatic membrane potential. *Nature* 441:761–765.

Silberberg G, Markram H (2007) Disynaptic inhibition between neocortical pyramidal cells mediated by Martinotti cells. *Neuron* 53:735–746.

Simon A, Oláh S, Molnár G, Szabadics J, Tamas G (2005) Gap-junctional coupling between neurogliaform cells and various interneuron types in the neocortex. *J Neurosci* 25:6278–6285.

Sippy T, Yuste R (2013) Decorrelating action of inhibition in neocortical networks. *J Neurosci* 33:9813–9830.

Snider RK, Kabara JF, Roig BR, Bonds AB (1998) Burst firing and modulation of functional connectivity in cat striate cortex. *J Neurophysiol* 80:730–744.

Sohal VS, Zhang F, Yizhar O, Deisseroth K (2009) Parvalbumin neurons and gamma rhythms enhance cortical circuit performance. *Nature* 459:698–702.

Steriade M, Nuñez A, Amzica F (1993) A novel slow (< 1 Hz) oscillation of neocortical neurons in vivo: depolarizing and hyperpolarizing components. *J Neurosci* 13:3252–3265.

Suzuki N, Bekkers JM (2010) Inhibitory neurons in the anterior piriform cortex of the mouse: classification using molecular markers. *J Comp Neurol* 518:1670–1687.

Svoboda K, Yasuda R (2006) Principles of two-photon excitation microscopy and its applications to neuroscience. *Neuron* 50:823–839.

Szabadics J, Varga C, Molnár G, Oláh S, Barzó P, Tamás G (2006) Excitatory effect of GABAergic axo-axonic cells in cortical microcircuits. *Science* 311:233–235.

Tamamaki N, Yanagawa Y, Tomioka R, Miyazaki J-I, Obata K, Kaneko T (2003) Green fluorescent protein expression and colocalization with calretinin, parvalbumin, and somatostatin in the GAD67-GFP knock-in mouse. *J Comp Neurol* 467:60–79.

Tamás G, Buhl EH, Lörincz A, Somogyi P (2000) Proximally targeted GABAergic synapses and gap junctions synchronize cortical interneurons. *Nat Neurosci* 3:366–371.

Tamás G, Lorincz A, Simon A, Szabadics J (2003) Identified sources and targets of slow inhibition in the neocortex. *Science* 299:1902–1905.

Tan AYY, Chen Y, Scholl B, Seidemann E, Priebe NJ (2014) Sensory stimulation shifts visual cortex from synchronous to asynchronous states. *Nature* 509:226–229.

Taniguchi H, He M, Wu P, Kim S, Paik R, Sugino K, Kvitsiani D, Kvitsani D, Fu Y, Lu J, Lin Y, Miyoshi G, Shima Y, Fishell G, Nelson SB, Huang ZJ (2011) A resource of Cre driver lines for genetic targeting of GABAergic neurons in cerebral cortex. *Neuron* 71:995–1013.

Tricoire L, Pelkey KA, Daw MI, Sousa VH, Miyoshi G, Jeffries B, Cauli B, Fishell G, McBain CJ (2010) Common origins of hippocampal Ivy and nitric oxide synthase expressing neurogliaform cells. *J Neurosci* 30:2165–2176.

Ulrich D, Bettler B (2007) GABA(B) receptors: synaptic functions and mechanisms of diversity. *Curr Opin Neurobiol* 17:298–303.

Urban-Ciecko J, Fanselow EE, Barth AL (2015) Neocortical Somatostatin Neurons Reversibly Silence Excitatory Transmission via GABAb Receptors. *Curr Biol* 25:722–731.

van Welie I, Roth A, Ho SSN, Komai S, Häusser M (2016) Conditional Spike Transmission Mediated by Electrical Coupling Ensures Millisecond Precision-Correlated Activity among Interneurons In Vivo. *Neuron* 90:810–823.

Vervaeke K, Lorincz A, Gleeson P, Farinella M, Nusser Z, Silver RA (2010) Rapid desynchronization of an electrically coupled interneuron network with sparse excitatory synaptic input. *Neuron* 67:435–451.

Vida I, Bartos M, Jonas P (2006) Shunting inhibition improves robustness of gamma oscillations in hippocampal interneuron networks by homogenizing firing rates. *Neuron* 49:107–117.

Vucurovic K, Gallopin T, Férézou I, Rancillac A, Chameau P, van Hooft JA, Geoffroy H, Monyer H, Rossier J, Vitalis T (2010) Serotonin 3A receptor subtype as an early and protracted marker of cortical interneuron subpopulations. *Cereb Cortex* 20:2333–2347.

Wang Y, Gupta A, Toledo-Rodriguez M, Wu CZ, Markram H (2002) Anatomical, physiological, molecular and circuit properties of nest basket cells in the developing somatosensory cortex. *Cereb Cortex* 12:395–410.

Wang Y, Toledo-Rodriguez M, Gupta A, Wu C, Silberberg G, Luo J, Markram H (2004) Anatomical, physiological and molecular properties of Martinotti cells in the somatosensory cortex of the juvenile rat. *J Physiol* 561:65–90.

Waters J, Helmchen F (2006) Background synaptic activity is sparse in neocortex. *J Neurosci* 26:8267–8277.

Wehr M, Zador AM (2003) Balanced inhibition underlies tuning and sharpens spike timing in auditory cortex. *Nature* 426:442–446.

Wertz A, Trenholm S, Yonehara K, Hillier D, Raics Z, Leinweber M, Szalay G, Ghanem A, Keller G, Rózsa B, Conzelmann K-K, Roska B (2015) PRESYNAPTIC NETWORKS. Single-cell-initiated monosynaptic tracing reveals layer-specific cortical network modules. *Science* 349:70–74.

Wester JC, McBain CJ (2014) Behavioral state-dependent modulation of distinct interneuron subtypes and consequences for circuit function. *Curr Opin Neurobiol* 29:118–125.

Wickersham IR, Finke S, Conzelmann K-K, Callaway EM (2007a) Retrograde neuronal tracing with a deletion-mutant rabies virus. *Nat Methods* 4:47–49.

Wickersham IR, Lyon DC, Barnard RJO, Mori T, Finke S, Conzelmann K-K, Young JAT, Callaway EM (2007b) Monosynaptic restriction of transsynaptic tracing from single, genetically targeted neurons. *Neuron* 53:639–647.

Williams SR, Mitchell SJ (2008) Direct measurement of somatic voltage clamp errors in central neurons. *Nat Neurosci* 11:790–798.

Wilson CJ, Kawaguchi Y (1996) The origins of two-state spontaneous membrane potential fluctuations of neostriatal spiny neurons. *J Neurosci* 16:2397–2410.

Wilson NR, Runyan CA, Wang FL, Sur M (2012) Division and subtraction by distinct cortical inhibitory networks in vivo. *Nature* 488:343–348.

Wimmer VC, Bruno RM, de Kock CPJ, Kuner T, Sakmann B (2010) Dimensions of a projection column and architecture of VPM and POm axons in rat vibrissal cortex. *Cereb Cortex* 20:2265–2276.

Woodruff A, Xu Q, Anderson SA, Yuste R (2009) Depolarizing effect of neocortical chandelier neurons. *Front Neural Circuits* 3:15.

Wozny C, Williams SR (2011) Specificity of Synaptic Connectivity between Layer 1 Inhibitory Interneurons and Layer 2/3 Pyramidal Neurons in the Rat Neocortex. *Cereb Cortex* 21:1818–1826.

Xu X, Callaway EM (2009) Laminar specificity of functional input to distinct types of inhibitory cortical neurons. *J Neurosci* 29:70–85.

Xu X, Roby KD, Callaway EM (2006) Mouse cortical inhibitory neuron type that coexpresses somatostatin and calretinin. *J Comp Neurol* 499:144–160.

Xu X, Roby KD, Callaway EM (2010) Immunochemical characterization of inhibitory mouse cortical neurons: three chemically distinct classes of inhibitory cells. *J Comp Neurol* 518:389–404.

Yamashita T, Pala A, Pedrido L, Kremer Y, Welker E, Petersen CCH (2013) Membrane potential dynamics of neocortical projection neurons driving target-specific signals. *Neuron* 80:1477–1490.

Yoshimura Y, Callaway EM (2005) Fine-scale specificity of cortical networks depends on inhibitory cell type and connectivity. *Nat Neurosci* 8:1552–1559.

Yu J, Ferster D (2013) Functional coupling from simple to complex cells in the visually driven cortical circuit. *J Neurosci* 33:18855–18866.

Zagha E, McCormick DA (2014) Neural control of brain state. *Curr Opin Neurobiol* 29:178–186.

Zeisel A, Muñoz-Manchado AB, Codeluppi S, Lönnerberg P, La Manno G, Juréus A, Marques S, Munguba H, He L, Betsholtz C, Rolny C, Castelo-Branco G, Hjerling-Leffler J, Linnarsson S (2015) Brain structure. Cell types in the mouse cortex and hippocampus revealed by single-cell RNA-seq. *Science* 347:1138–1142.

Zhang SJ, Jackson MB (1993) GABA-activated chloride channels in secretory nerve endings. *Science* 259:531–534.

Zhang S, Xu M, Kamigaki T, Hoang Do JP, Chang W-C, Jenvay S, Miyamichi K, Luo L, Dan Y (2014) Selective attention. Long-range and local circuits for top-down modulation of visual cortex processing. *Science* 345:660–665.

Statement of contribution

Parts of the projects discussed in this thesis have been conducted in a collaborative approach. In the following, I will state the respective contributions to the data presented.

All experiments were designed by me and Dr. James Poulet. Experiments performed in GAD67-GFP animals were all done by myself. Dr. Jean-Sebastien Jouhanneau performed electrophysiological experiments in GIN-VIPcre-Ai9 mice, while I did the immunohistochemistry for these animals. I have analyzed all the data myself.

Publications

Articles in peer-reviewed journals

Jouhanneau J-S, Kremkow J, **Dorrn AL**, Poulet JFA (2015) In Vivo Monosynaptic Excitatory Transmission between Layer 2 Cortical Pyramidal Neurons. *Cell Rep* 13:2098–2106.

Maier N, Tejero-Cantero A, **Dorrn AL**, Winterer J, Beed PS, Morris G, Kempter R, Poulet JFA, Leibold C, Schmitz D (2011) Coherent Phasic Excitation during Hippocampal Ripples. *Neuron* 72:137–152.

Dorrn AL*, Yuan K*, Barker AJ, Schreiner CE, Froemke RC (2010) Developmental sensory experience balances cortical excitation and inhibition. *Nature* 465:932–936.
**equal contribution*

Selected Conference Contributions

Dorrn AL, Poulet JFA (2014) Monosynaptic inhibitory transmission between layer 2 GABA-ergic non-fast spiking interneurons in vivo. 44th Annual Meeting of the Society for Neuroscience. Washington DC, USA. *Poster.*

Dorrn AL, Poulet JFA (2013) In vivo monosynaptic transmission between layer 2 GABA-ergic interneurons in mouse forepaw primary somatosensory cortex. 43th Annual Meeting of the Society for Neuroscience. San Diego, CA, USA. *Poster.*

Dorrn AL, Poulet JFA (2013) In vivo monosynaptic transmission between layer 2 GABA-ergic interneurons in mouse forepaw primary somatosensory cortex. 26th Annual Barrels Meeting. La Jolla, CA, USA. *Poster.*

Dorrn AL, Poulet JFA (2012) Functional synaptic connectivity between layer 2 cortical excitatory and inhibitory neurons in vivo. EMBO workshop 'Cortical interneurons in health & disease'. Costa d'en Blanes, Mallorca, Spain. *Poster.*

Acknowledgements

First of all I would like to thank **Dr. James Poulet** for giving me the opportunity to work in his laboratory, where I found excellent research conditions and resources, which greatly helped to work on this thesis. I am grateful for his supervision and advice and appreciate his support that I enjoyed during various stages of my project.

I appreciate the effort of **Dr. Jean-Sebastien Jouhanneau**, who introduced me to the technique of two-photon targeted recordings. In addition I am extremely thankful for his collaboration on the SST-VIP-interneuron project.

Further I want to thank **Dr. Evgeny Bobrov**, who carefully read this manuscript and provided many helpful comments.

I am grateful for the excellent technical assistance of **Janett König**, regarding the organization of breeding the transgenic mouse lines and for her helpful advice on the immunohistochemistry.

Finally I want to say thank you to all past and present **members of the Poulet lab**: thanks for inspiring discussions on how to collect, analyze and interpret my data; thanks for helping hands in the lab and thanks for the entertaining company during numerous lunch and coffee breaks.